STUDY OF TURBULENT BOUNDARY LAYER IN A STEP CHANGE FROM SMOOTH TO ROUGH SURFACE

By

ALTAF HASAN
B.Sc.Engg. (Mech.)

Thesis submitted to the
Department of Mechanical Engineering in partial fulfilment of
the requirements for the degree of
Master of Science
in
Mechanical Engineering

December 1984

Bangladesh University of Engineering and Technology
Dhaka Bangladesh

STUDY OF TURBULENT BOUNDARY LAYER IN A STEP CHANGE FROM SMOOTH TO ROUGH SURFACE

A Thesis

by

Altaf Hasan

Approved as to style and content:

M. A. Taher Ali

Dr. M.A. Taher Ali — Chairman
Professor,
Dept. of Mechanical Engg.,
BUET, Dhaka.

Dr. A.M. Aziz-ul-Huq — Member
Professor and Head,
Dept. of Mechanical Engg.,
BUET, Dhaka.

Dr. Dipak K. Das — Member
Professor,
Dept. of Mechanical Engg.,
BUET, Dhaka.

Dr. S.M. Nazrul Islam — Member
Professor,
Dept. of Mechanical Engg.,
BUET, Dhaka.

Dr. M.A. Hannan — Member (External)
Professor,
Dept. of Water Resources Engg.,
BUET, Dhaka.

CERTIFICATE OF RESEARCH

This is to certify that the work presented in this thesis is the outcome of the investigation carried out by the candidate under the supervision of Dr. M.A. Taher Ali in the Department of Mechanical Engineering at Bangladesh University of Engineering & Technology, Dhaka.

M. A. Taher Ali
Supervisor

Candidate

CANDIDATE'S DECLARATION

It is hereby declared that neither this thesis nor any part thereof has been submitted or is being concurrently submitted anywhere for the award of any degree or diploma or for publication.

Candidate

ABSTRACT

Turbulent flows over flat surface undergoing transition due to a sudden increase in surface roughness were studied experimentally.

The experiment was carried out in an 18x18-in wind tunnel test section, the floor of which was used as the surface of interest. The surface was artificially roughened by stone chips of average size of 0.625 in. in a random manner. The measurements included both mean and turbulent quantities which made use of pitot-static tubes, boundary layer tube, yawmeter and hot-wire anemometer. The measurement of mean quantities were made at Reynolds numbers of 9.80×10^5, 7.20×10^5, 4.61×10^5 and 2.78×10^5, while those of turbulent intensities were done at a Reynolds number of 7.20×10^5 only.

The influence of roughness change on the boundary layer characteristics and flow resistance was quantified from the experimental results. At the beginning of the rough surface, the wall static pressure suddenly dropped from its smooth wall pressure gradient. Rough wall pressure gradient became linear after 2 hydraulic diameters downstream from the roughness change. Wall shear stress was found to increase more or less proportionately with the roughness height while the boundary layer thickness did not increase proportionately. Rough wall shear stress increased to about 10 times the smooth wall value, but the boundary layer thickness hardly doubled.

The flow close to the wall adjusted quickly to the new surface condition resulting the internal boundary layer, which was found to be proportional to $x^{0.46}$. At the smooth-rough junction, the roughness height caused the near wall flow to deflect upwards, resulting in the production of secondary current which died out quickly away from the wall. In the experimental range of Reynolds number, the distribution of mean velocity and secondary current remained nearly the same.

The longitudinal turbulence intensity over the rough wall increased from its value over smooth wall which preceded the rough surface. The effect of surface roughness on turbulence intensity was found to spread nearly upto the boundary layer height.

ACKNOWLEDGEMENTS

All praises are due to Almighty Allah.

The author expresses his deep sense of gratitude and acknowledges profound indebtedness to his supervisor Dr. M.A. Taher Ali, Professor, Department of Mechanical Engineering, Bangladesh University of Engineering & Technology, Dhaka without whose constant guidance, untiring help, invaluable suggestions and unceasing encouragement, this work would not have been possible.

The author feels highly grateful to Dr. A.M. Aziz-ul Huq, Professor and Head, Department of Mechanical Engineering, BUET who provided all necessary assistance in various ways at different stages of the work.

The helpful suggestions by Dr. Dipak K. Das and Dr. S.M. Nazrul Islam, Professors of Mechanical Engineering department are very much appreciated.

The inspiration and interest shown by Professor Musharrif H. Khan, Professor M. Anwar Hossain and Dr. M. Wahhaj Uddin of Mechanical Engineering department are gratefully acknowledged.

Sincere thanks are offered to Mr. Ahmad Ali Mollah, Chief Foreman Instructor, Machine Shop, BUET and Mr. Julfikar Ali Bhuiyan, Chief Supervisor, Welding and Sheet Metal Shop, BUET for their kind cooperation in the construction of the experimental set up. Thanks are also due to Messers Shahabuddin,

Razzaque and Bachchu of Fluid Mechanics Laboratory of Mechanical Engineering deptt. and the staff of Workshops of BUET for their cooperation in fabricating and assemblying different components of the experimental rig.

The author also wishes to thank Mr. Rabiul Islam, Chief Engineer of Central Instrumentation Shop, BUET for his help during operation of various instruments. The generous help extended by the Department of Electrical and Electronic Engineering, BUET in using some of their instruments is sincerely acknowledged.

The author thanks Mr. M.A. Malek for typing the thesis and Mr. M.A. Salam for drawing the figures with care.

Finally is offered a thank you to all of his colleagues in Mechanical Engineering Department and members of his family for their cooperation and inspiration during the work.

To my parents

TABLE OF CONTENTS

LIST OF TABLES

LIST OF NOMENCLATURE

Symbol	Meaning
Latin Letters:-	
A	constant in log law of the wall
A_1	constant in hot wire calibration eqn.
AR	aspect ratio
B	constant in log law of the wall
B_1	constant in hot wire calibration eqn.
c_p	specific heat of gas at constant pressure
C	constant
C_p	coefficient of pressure, $\frac{\Delta p}{\frac{1}{2}\rho U^2}$
C_f	coefficient of friction, $\frac{\tau_o}{\frac{1}{2}\rho U^2}$
d	diameter of hot-wire
D_t	depth of wind tunnel test section
D	diameter of a pipe
D_h	hydraulic diameter of a conduit
e	conversion factor in hot-wire heat balance
E	error in origin for rough surface
f	friction factor
F	velocity defect function
G	shear stress difference function
h	heat transfer coefficient from hot wire
H	shape factor of velocity profile

Symbol	Meaning
ID	Internal diameter
I	current through hot wire
k	absolute height of roughness
k_s	equivalent sand roughness height
k_1	thermal conductivity of gas
K	constant, eqn. (3.3.10)
ℓ	height of wake
L	length of hot-wire
m	slope of eqn. (A-2.4)
n	exponent in power law of velocity
Nu	Nusselt number. $\frac{hd}{k}$
OD	outer diameter
p	mean static pressure
P	total pressure
P_a	atmospheric pressure
Pr	Prandtl number, $\frac{\mu c_p}{k}$
$\bar{q}^2$	$\frac{1}{3}(\bar{u}^2 + \bar{v}^2 + \bar{w}^2)$
Q	heat transfer rate from hot wire
r	radius of a pipe
R_o	resistance of hot wire at reference temperature to
R_g	resistance of hot-wire at temperature t_g
R_w	resistance of hot-wire at temperature t_w
$R_{u'u'}$	auto correlation coefficient of u' and u'
$R_{u'v'}$	cross correlation coefficient of u' and v'

Symbol	Meaning
Re	Reyholds number , $\frac{ud}{\nu}$
Re_{D_t}	Reynolds number based on depth of test section, $\frac{uD_t}{\nu}$
Re_k	Roughness Reynolds number, $\frac{u^*k}{\nu}$
Re_δ	Reynolds number based on boundary layer thickness $\frac{u\delta}{\nu}$
$S(\gamma)$	Sensitivity of Yawmeter
t	temperature
t_w	temperature of hot wire
t_g	temperature of gas
T	absolute temperature
u	mean axial velocity
u'	longitudinal component of rms of fluctuation of velocity
u^*	friction velocity
u^+	non-dimensional velocity, $\frac{u}{u^*}$
U	axial free stream velocity
$\bar{U}$	spatial average axial velocity
v'	transverse component of rms of fluctuation of velocity
V	voltage across the hot-wire
w	roughness length scale, eqn. (3.3.12)
w'	transverse component of rms of fluctuation of velocity
W	width of a test section
x	axial distance measured from smooth rough junction
X	coordinate axis direction
y	vertical distance from the wall
y_r	corrected vertical distance from the rough wall

Symbol	Meaning
$\phi_{u'}$	spectral density of u' normalized by $\bar{u}'^2$
ψ	temperature coefficient of electric resistivity of hot-wire
ω	width of roughness elements
Δ	difference of argument

Subscripts:-

f	film temperature
fd	fully developed
g	gas
max	maximum
min	minimum
o	at surface
r	rough surface
s	smooth surface
x	axial distance measured from smooth-rough junction
w	hot-wire

C H A P T E R I

INTRODUCTION

1.1 General

All flows of fluid are broadly divided into two classes - laminar and turbulent. But turbulent flows far outstrip the laminar ones in respect of its occurrence in nature, and most of the engineering applications of fluid flows are also turbulent in nature.

1.1.1 Turbulence

Whereas laminar flows consist of motion of fluid particles in undisturbed uniform streams, turbulent flows are characterized by random, irregular fluctuating flows superimposed upon the main stream. These fluctuations are mainly responsible for the resistance experienced by turbulent flows in pipes or other closed conduits. These fluctuations are also responsible for the drag encountered by ships and airplanes and contribute chiefly to the losses in turbomachineries. On the other hand, it enables achievement of greater pressure rise in diffusers and airplane wings, compressor blades etc.

When a flow comes in contact with a surface, it involves the formation of a so called boundary layer in the most immediate vicinity of the contact zone. For turbulent flows,

there forms a turbulent boundary layer whenever the flow encounters a surface. The knowledge about the boundary layer is of prime importance for the study of any transport phenomenon, because transactions of shear, heat, momentum, kinetic energy etc. mainly take place within this zone.

For laminar flows, the problem is strictly mathematical, because the governing differential equations can be written exactly. So with the aid of high speed computers, much progress has been made in the calculation of laminar boundary layer, and satisfactory results have been obtained for many cases.

Inspite of its variety of occurrance and applications, not much is known about turbulent flow structures. The structure of turbulence is so complex in its detail that it seemed to be inaccessible to mathematical treatment. Because of the limited understanding of the turbulence process, the problem of turbulent flow is phenomological and exact formulation of boundary layer equations is not possible. The boundary layer equations for such flows contain extra terms involving the time mean of the product of two fluctuating velocities known as the Reynolds stress tensor. At present these terms have not been rigorously related to mean velocity distribution. Attempts have been made to create a mathematical basis for the investigation

of turbulent motion coupled with semi-empirical formulations. These range from simple mixing length hypothesis of Prandtl [57] to the solution of conservation equations for third order correlations by Launder and Spalding [43] , which envisaged properly dealing with the extra terms mentioned above. But none could succeed in analysing any turbulent flow in its full detail. The success in obtaining accurate turbulent flow predictions depends heavily, besides prescribing a closed set of equations adequately accounting for the flow process, on experimental means. For devising a suitable turbulence model for the complex correlations in the governing conservation equations, certain assumptions are to be made which need to be supplemented by theoretical reasoning and empirical facts which, if accurate enough within the range of interest , will lead to correct predictions of turbulent flows.

The experimental study of turbulent flow has long been handicapped by the complex and statistical nature of the flow and due to the lack of proper instrumentation to measure the turbulent quantities. Recently (ref. [30]) researches are being carried out to analyse turbulent flow structures experimentally with the aid of modern, sophisticated electronic equipments.

Though experimental study of turbulent flow is a sine qua non for its correct prediction, a full fledged experiment on turbulence is generally laborious, expensive

and very involved. So other methods of investigation are often looked for. After the inception of high speed digital computers, numerical solution coupled with semi-empirical results has become a useful way of dealing with turbulence. But till today, researchers have to embark upon experimental results as the sole way of acquiring an insight of turbulence process needed for its modelling.

1.1.2 Turbulent Flows over Rough Surfaces

In most engineering applications, turbulent fluid flows occur in contact with surfaces which are not hydraulically smooth. Flows through water or oil pipelines, chemical processing plants, air conditioning ducts, rotating machineries etc. are such common examples.

Again many engineering practice make use of flow with surface roughness for better performance. Heat exchangers, nuclear reactors, solar collectors generally employ artificially roughened surfaces of pipes and ducts for more heat transfer rate [47] .

Turbulent flows over open rough surfaces are very common in engineering arena and also in nature. Flows in dams, artificial canals etc. are a few important examples. The phenomenon of roughness change is of particular interest here. Sudden and frequent change in roughness is found in natural terrain where blowing wind encounters hills, ditches, meadows, forests, villages etc. All these surface configurations

lie within the atmospheric boundary layer of the earth. The influence of strong wind or storm on the earth surface is more severely felt in the boundary layer, and the effect depends on the nature of the boundary layer growth rather than the free stream of atmospheric air, which occurs high above the human habitation zone.

1.1.3 Surface Roughness

A great variety of surface roughness may be encountered above which flows may occur. These roughness vary in their shape, size, distribution and arrangement, microscopical surface property, characteristic behaviour with flow etc. But for engineering analysis, they may be broadly classified into groups as following.

Most general type of roughness is known as Sand Roughness which covers rough surfaces caused by irregular sand particles or stone chips. Nikuradse [52] was first to analyse the sand roughness in its proper technical perspective. His sand roughness may also include the inherent rough surface of a cast product. The average absolute protrusion height of the roughness elements or the relative roughness height with respect to some significant length are used to describe such roughness.

Rib roughness are employed by putting rectangular or cylindrical ribs on the surface transverse to the flow

direction. Depending on the ratio of the height of the roughness ribs and pitch, such roughnesses are again divided into d-type and k-type roughness [5,7,55,75] .

Also for certain technical purposes, specific geometric shaped roughness elements are attached to the surfaces. Amongst these cubical, spherical, conical, cylindrical, pyramid or diamond shaped elements, wire mesh roughness are often found in use [12,47,62] . These are characterized by their height, longitudinal, transverse and diagonal pitches.

After the sand roughness, another most common type of roughness which occurs in nature may be termed 'tuft roghness'. Grassy lands, green bushes, cornfields, green mosses grown in the ship hull may be cited as some of the examples of this type of roughness. This type of roughness differs from all the above type in the fact that its rougness characteristics vary with the flow velocity thus complicating the analysis of the flow behaviour. Further this type of roughness may have some sticking character due to the capillary action of narrow spaces present in between the fibres so far as the boundary layer is concerned. This type of rough surfaces may be useful in preventing or minimizing the phenomenon of flow separation in diffusers , curvedsurfaces etc.

All the above types of roughness again can be upstanding or depressed depending on how the change of surface

roughness comes about. If the crests of the roughness elements lie above the preceding smooth surface, it is an upstanding change of roughness. When the crests, on the other hand, lie below the level of preceding surface, it signifies a depressed-change of surface roughness.

All types of roughness, sand, rib or any other type, may be generally expressed in terms of an "equivalent sand grain roughness" for better comparison between different flows, as proposed by Nikuradse [51] and described by Schlichting [62] .

Surface roughness vis a vis fluid flow is completely a relative matter. The effect of the roughness on the flow and the boundary layer will be pronounced only when the surface is 'hydraulically rough' [62] . An apparently rough surface may well be hydraulically 'smooth' for one flow, but not for the other. This is indicated by the so called roughness Reynolds number $\frac{k_s u^*}{\nu}$. The values' spectrum determining the different roughness effect on flow is

$0 < \frac{k_s u^*}{\nu} < 5$ hydraulically smooth regime
-roughness protrusions are contained within the laminar sub-layer.

$5 < \frac{k_s u^*}{\nu} < 70$ hydraulically transition regime
-roughness protrusions are partly outside laminar sublayer.

$\frac{k_s u^*}{\nu} > 70$ hydraulically rough regime
-all roughness protrusions reach outside the laminar sublayer.

1.2 Motivation Behind Selection of Problem

It is now seen that study of turbulent flow with its relationship to surface roughness is important for many reasons. Many investigations have so far been made about turbulent boundary layer which is subjected to a change of surface roughness. The flow changes in the boundary layer have been the topics of many workers with an objective to predict related transport processes like heat and mass transfer etc., and their relation with the turbulent structure of the flow. Considerable works have been done on flow over smooth surface or rough surface alone both experimentally and analytically. But comparatively a little work is found to exist on flows over surfaces with sudden discontinuity in roughness pattern. Researches on turbulent flow characteristics due to surface roughness variation have been carried out in pipes with surface condition modified by fine sand roughness with $\frac{r}{k} \simeq 55$ [46] , $\frac{r}{k} \simeq 50$ [1,2] , or in ducts with surfaces fitted with uniform ribs with $\frac{D}{k} \simeq 72$ [7,75] , or surfaces fitted with other types of roughness [47,62,12] . But relatively less work has been done on turbulent flows in ducts or over plates with stone chip roughness creating the surface transition.

It is against this background the present research work has been embarked upon. It is aimed at studying the changes happening in the boundary layer undergoing a sudden

transition over a flat surface due to an upstanding intervention of natural stone roughness with comparatively high roughness ratio ($\frac{D}{k}t \simeq 28$). This is expected to be a new type of flow situation with strong relevance to the case of atmospheric boundary layer and comparability with some of the previous similar works. It is hoped to reveal some important flow characteristics valuable for greater understanding of turbulent boundary layer and turbulence structure in the context of varying surface condition in particular.

1.3 Objectives

The above discussion suggests a need for informations of the flow characteristics in the boundary layer over a sand roughenedflat surface. The objectives of the research program are accordingly set as follows:

(1) To measure the mean flow characteristics of the development of a turbulent boundary layer following a sudden increase in surface roughness brought about on the floor of the test section of a wind tunnel.

This includes the traversing of velocity profile, measurement of static pressure drop, calculation of shear stress and friction factor, investigation of the growth of internal boundary layer, which are intended to provide data for direct practical use in predicting meteorological

behaviour, open canal flows and designing of heat and mass transfer surfaces in possible cases.

(2) To measure turbulence characteristics in the same flow condition.

This includes the measurement of the longitudinal component of turbulence intensity inside the boundary layer. This is directed at providing insight into general turbulence structure and understanding of the related physical processes in the case of such a changing boundary conditions.

(3) To compare the results of present flow configuration with those of related cases.

1.4 Outline of Research

A detail experimental schedule was prepared to investigate the flow situation subjected to a discontinuity in boundary conditions. The flow was planned to be in a wind tunnel test section, the floor of which would offer the bed of varying roughness. In the experiment, the flow was tested to be fully developed before it encountered smooth-roughness junction. Flow development was checked by the universal log-law of velocity distribution near the wall. The flow was treated as a two dimensional one and the characteristics at the longitudinal mid section of the tunnel were measured for investigation. For the developed

flow, the dependent flow parameters, when suitably non dimensionalized, would be expectedly invariant in the mean flow direction. These dimensionless flow properties may, thus, be described as functions of one coordinate direction in a plane of the duct cross section.

In the experiment, change of roughness was created upstandingly by normal stone pieces with broken edges of average size of $\frac{5}{8}$ in (varying between $\frac{3}{4}$ in and $\frac{1}{2}$ in). For this type of change in surface roughness, the boundary layer was investigated employing different flow velocities with a view to correlate the results with Reynolds number.

The results obtained from the present investigations were compared with the other studies related to the problem under study, and possible interpretations of the experimental results were made to extend explanations of different characteristics of the present flow field.

CHAPTER II

LITERATURE REVIEW

2.1 Preview

History of works on turbulent flow dates back to the day Osborne Reynolds (ref. [30]) identified it distinctly different from the laminar one. Since then theoretical hypotheses, analytical methods and experimental researches have led to the gradual development of the knowledge about turbulent flow. In the following paragraphes, some of the important works which are pertinent to the present investigation of boundary layer flow are stated briefly.

2.2 Turbulent Flows Over Smooth Surfaces

In early stage of research on turbulent flows, the research workers devoted themselves mainly to the study of flows over smooth surfaces. The study of flows for different surface conditions was taken up later, and attempts have been made to find tbe correlation between the flow and the surface roughness.

The earliest investigators of turbulent flows through smooth pipes include Schiller (1923), Stanton and Panel (1915), Blasius (1913), Hermann (1930), Nikuradse (1932) and others (ref. [62]).

Reichard [60] made some of the earliest measurements of turbulence parameters. He measured longitudinal and transverse components of the fluctuating velocity, u' and v', in a wind tunnel with rectangular cross section test section measuring 1.0 m wide and 24.4 cm high. Rise of u' was found to be steep neer the wall where u' measured four times of v'.

Laufer [42] presented a detail exploration of the flow field of mean and fluctuating quantities in a two-dimensional channel flow. The measurements were performed at three Reynolds numbers, 1.23×10^4, 3.08×10^4 and 6.16×10^4 based on the half width of the channel and maximum mean velocity in a 5.0 in wide channel section with aspect ratio 12:1. He found distributions of u' and v' similar to those obtained by Reichard [60] .

Laufer [41] also reported investigation of all the three fluctuating components of velocity u', v', w' and of the correlation coefficient $R_{u'v'}$ in a two-dimensional smooth channel of high aspect ratio in presence of a favourable pressure gradient. He however, did not take into account of the effect of secondary velocity on the measurements. It was first Nikuradse [50] who detected presence of normal stress driven secondary current in rectangular duct flows.

Klebanoff [38] measured the three fluctuating components of velocity u', v', w' and the Reynolds shear stress $\tau_{u'v'}$

in a boundary layer along a smooth plate under zero pressure gradient. The experiment was carried out in an octagonal wind tunnel with a 12.0 ft long, 4.5 ft wide and 0.25 in thick aluminium test plate mounted vertically and centrally in the test section. He noticed isotropic behaviour of turbulence intensities near the free stream, but degree of anisotropy increased towards the wall.

In a significant extension of the work of Laufer [42], Clark [18] made en elaborate study of a turbulent boundary layer in a 25.0 ft long channel of 5.0 in wide section with aspect ratio 12:1. Measurements were done at Reynolds numbers ranging from 10,000 to 130,000 based on the channel half width and the centerline velocity. Mean velocity profiles were studied in every detail and all the three fluctuating components of velocity along with frequency spectral analysis were investigated.

Thomas and Easter [69] measured axial velocity, friction factor and wall shear stress in an 8.1 m long square cross section duct of size 101.6 mm. A DISA hot film pressure transducer was used to measure wall shear stress in order to correlate the friction factor with Reynolds number which was found to be

$$C_f = 0.079\ Re^{-0.25} \qquad (2.2.1)$$

The Reynolds number in the experiment varied from 0.43×10^5 to 1.90×10^5 based on the hydraulic diameter of the duct and

Table 2.1 Measurements of Turbulent Flows with Smooth Surfaces

Author	Flow Configuration	Measurements	Instrumentation	Comments
Reichard [60] 1938	Rectangular duct $W=1.0$ m $D=24.4$ cm	u', v' $\tau_{u'v'}$ u	Hot wire anemometer, Pitot tubes	Reynolds shear stress decreased to zero towards the center of the duct
Laufer [42] 1950	Rectangular duct $W=5.0$ in $\frac{D}{W} = 12$ $Re_{\frac{W}{2}}=1.23\times10^4-6.16\times10^4$	u', v'	Hot wire anemometer Pitot tubes	Distribution of u' similar to Reichard's but rise less steep near the wall
Laufer [41] 1951	Rectangular duct $W = 5.0$ in $\frac{D}{W} = 12$	u', v', w'	Hot wire anemometer	$R_{u'v'}$ varied linearly with y except near the wall
Klebanoff [38] 1954	Rectangular duct $W=4.5$ ft	u', v', w' $\tau_{u'v'}$	Hot wire anemometer static pressure tappings	u' highest near the wall at about $y^+=25$
Clark [18] 1968	Rectangular duct $W=5.0$ in $\frac{D}{W} =12$ $Re_{\frac{W}{2}}=10^4-13\times10^4$	u', v', w' u $\phi_{u'}, \phi_{v'}, \phi_{w'}$	Hot wire anemometer Pitot tubes, Wave analyser	Mean and turbulence quantities measured in the viscous sublayer
Thomas and Easter [69] 1972	Square duct $D=W=101.6$ mm $Re =0.43\times10^5$	τ_o u	Hot film instrument, static pressure tuppings, pitot tubes	Friction factor found to agree with Blasius' equation wall shear stress decreased towards the corner

the center line velocity.

2.3 Experimental Investigations of Turbulent Flows Over Rough Surfaces

Among the earliest workers who lent attention to the effects of surface roughness on turbulent flows were Schiller (1923), Nikuradse (1930), Streeter (1935), Moody (1944), whose works formed the basis of studying turbulent fluid motion in relation to the surface conditions (ref. [62]). The recapitulation of some of the related important research works are made below, dividing them into flows through pipes and flows through rectangular ducts or channels.

2.3.1 Turbulent Flows through Rough Pipes

Nikuradse [51] was pioneer in pointing out discrepancy in Blasius' formula for turbulent flows through pipes due to their dependence on surface roughness. He noted that velocity distributions in a rough pipe were progressively lowered from the smooth pipe relation as the Reynolds number increased. Later Nikuradse [52] performed existensive work on sand roughened pipe flow giving rise to a great volume of empirical results.

Following Nikuradse's findings, Clauser [20] presented a useful analysis of the effect of roughness on boundary layer

velocity profile, which was characterised by the velocity profile shift $\frac{\Delta u}{u^*}$, and proposed a velocity distribution near the rough wall as

$$\frac{u}{u^*} = 5.6 \log \frac{y u^*}{\nu} + 5.6 - \frac{\Delta u}{u^*} \qquad (2.3.1)$$

Robertson [61] gave a detailed analysis of the then existing results of turbulent flows through rough pipes. He used Nikuradse's data of natural sand roughness to put forward new informations on friction factor and pipe factor correlations. For fully rough region, he cited the relation

$$\frac{\Delta u}{u^*} = 5.6 \log \frac{k u^*}{\nu} - 2.7 \qquad (2.3.2)$$

giving $$\frac{u}{u^*} = 5.6 \log \frac{y}{k} + 8.3 \qquad (2.3.3)$$

Lawn and Hamlin [44] made detail measurements of velocity in an internally roughned pipe of diameter 13.16 cm using square rings of height 0.069 cm ($\frac{r}{k} \simeq 95$) with λ= 0.488 cm ($\frac{\lambda}{k} = 7.2$). They found that flow over a fully rough surface was very much influenced by viscosity, which was contrary to the above mentioned classic theory of Nikuradse.

Townes and Sebersky [73] gave informations about the behaviour of turbulent flows near a rough surface. Townes et al [74] presented some comprehensive results of turbulent

flows in sand-roughened pipes. They observed that within their experimental range of Reynolds number 5.0×10^4 to 48.0×10^4, the equation of representative mean velocity profiles for smooth pipe

$$\frac{U}{u_*} = 2.75 \ln \frac{yu_*}{\nu} + 4.55 \qquad (2.3.4)$$

best fitted their data for $\frac{yu_*}{\nu} > 70$.

Turbulent flow characteristics in a pipe following a transition of surface roughness condition was first, among others, studied by Logan and Jones [46] . They used an 8.0 in diameter pipe partly internally roughened by sand grains with $\frac{r}{k} = 55$. The flow was found not fully developed at 15 D downstream of the smooth to rough junction. They found the wall shear stress to increase abruptly to its final value after the change of surface condition and the pressure gradient more or less constant throughout the transition region.

Siuru and Logan [64] made detailed study of flow response characteristics in a pipe due to the change in surface roughness condition. They employed different roughness configurations after Nunner (1958) and measured mean velocity, static pressure, turbulence intensities and Reynolds shear stress. The spread of roughness effect was determined from the knee points in the semi-logarithmic plots of mean velocity profiles. The upper and lower layers in the internal boundary layer were

Table 2.2 Measurements of Turbulent Flows through Pipes with Roughness Change

Author	Flow configuration	Measurements	Instrumentation	Comments
Logan and Jones [46] 1963	D=8.0 in, $\frac{r}{k} \simeq 55$ Sand roughness $Re=4.0\times10^5$	u,p,u' $\tau_{u'v'}$	Pitot-static probes Static pressure probe, Hot-wire anemometer	Abrupt increase in roughness $(\frac{x}{D})_{fd} > 15$
Siuru and Logan [64] 1977	D=2.50 in, k=0.113 in ω=0.125 in, λ=0.25-2.9 in, Discrete rectangular ring roughness Re= 60,000	u,p,u'v',w' $\tau_{u'v'}$	Pitot-static probes, Static pressure probe, Hot-wire anemometer	Upstanding increase of roughness, $\delta_i \sim x^{0.5}$, $(\frac{x}{D})_{fd} \simeq 18$ extent of roughness effect determined by semi-logarithmic plot knee points.
Chang et al [17] 1979	D=101.6 mm, k=5.33 mm ω=5 mm, $\frac{\lambda}{k}$ = 30-240 Discrete rectangular ring roughness, $Re=5.0\times10^4$	u,u',v',w' $\tau_{u'v'}$	Pitot-static probes Hot-wire anemometer	Upstanding increase of roughness, roughness effect determined by knee-points of semi-logarithmic plots n for smoot section increase with λ
Ali and Islam [1], [2] 1982,1984	D=4.0 in $\frac{r}{k}$ = 50 Sand roughness $Re=2.4\times10^5$	u,p,u', τ	Pitot-static probes Static pressure tappings Hot-wire anemometer	Sudden decrease of roughness $\delta_i \sim x^{0.56}$, $(\frac{x}{D})_{fd} \simeq 17.5$ roughness effect determined by knee-points of semi-logarithmic plots.

identified on the basis of two knee points in the plots which were found to grow as $x^{0.5}$.

Chang et al [17] did similar investigations of the flow change in a pipe due to the presence of two rectangular cross section ring type roughness elements placed one after another at different intermediate distances. Measurements of mean and turbulent quantities were taken after both the first and the second elements and the two results were compared. They observed that the exponent of the power law of velocity profile increased with the reduction of spacing between the elements.

Ali and Islam [1,2] obtained measurements of turbulent pipe flow following a sudden reduction in surface roughness. They used a 4 in diameter partly sand roughened pipe in the experiment. It was found that the turbulent quantities needed more distance than the mean flow quantities to reach fully developed condition and that the mean and turbulent quantities responded immediately to the new surface condition near the wall.

2.3.2 Turbulent Flows through Rough Ducts and Channels

Jacobs [36] was the first to report investigations of turbulent flows over rough surfaces other than in circular pipes. He studied the transition which occurs in the turbulent boundary layer as it meets a sudden change in surface roughness. He measured velocity profiles in a

60 cm x 20 cm channel with its floor fitted with discrete rib type roughness of 1 mm height and 8.0 mm pitch. Shear stress was calculated from the measured velocity distribution using Prandtl's mixing length equation.

Clauser [19] obtained velocity profiles more or less similar to those of Jacobs as he studied the velocity distributions downstream from a sudden change in surface roughness on a flat plate in a constant pressure boundary layer.

Carper [16] measured turbulence intensities and correlation coefficients in turbulent flow of air in transition from a smooth to a rough wall in a two-dimensional channel of size 4.0 in x 46.5 in. Discrete rectangular ribs of height 0.281 in and width 0.437 in were placed each at 8 inches apart on both walls of the rough section. He observed that boundary layer developed rapidly after encountering the first roughness element.

Earlier J.K. Heilhecker (1962) performed experiments in the same channel and measured Reynolds shear stress in the transition region by a hot wire anemometer.

Islam [34] repeated the measurement of turbulence intensities in the channel used by Carper [16] , but with zero pressure gradient. Islam and Logan [35] reported that removal of pressure gradients in the rough channel section did not affect the growth rate of internal boundary layer

or that of the sublayer. But the modified pressure gradient was found to cause great reduction in the transitional overshoot of wall shear stress and turbulence intensities which were previously observed by other investigators.

Perry and Joubert [54] performed experiments on rough surfaces with adverse pressure gradients to compare the results of boundary layers with theory and with results of zero pressure gradient flow. They used wind tunnel test section measuring 5.5 ft x 4.25 ft at the downstream end. Discrete rib roughness of height 0.125 in and pitch 0.50 in were used. They proposed a method of finding out the position of origin of vertical distance for rough wall flow. They found that the roughness function was independent of imposed pressure gradient.

Perry et al [55] presented a detailed experimental study of turbulent boundary layer development over rough wall in both zero and adverse pressure gradients. The experiments were done in a wind tunnel test section of Perry and Joubert [54] . Roughness elements were of $\frac{1}{8}$ in, $\frac{1}{2}$ in and 1 in height and of k-and d-types. Velocity profiles were measured and wall function was determined. The skin friction was calculated from pressure gradient measured by tapping the roughness elements and considering their form drag. Roughness function was found to be a function of length of scale w. For k-type rough wall, w was proportional to roughness scale k and for d-type roughness it was postulated to be proportional to boundary layer thickness.

Antonia and Luxton [7] measured the flow field downstream of an upstanding k-type roughness just like that of Perry and Joubert [54] . Mean velocity profiles were taken to examine the growth of internal boundary layer from the plots of u versus $y^{\frac{1}{2}}$ (intersection or knee point of two straight portions of the curves marked the edge of internal boundary layer). Measurements also included longitudinal and transverse components of turbulence intensity, Reynolds shear stress, frequency spectral analysis of turbulence, auto- and cross-correlation coefficients of turbulence intensities.

The response of a turbulent boundary layer to a depressed change of surface roughness was measured by Antonia and Luxton [5] in a zero pressure gradient flow. They measured velocity profiles, shear stress, turbulence intensities and Reynolds stresses. They found the growth rate of internal boundary layer similar to that of zero pressure gradient boundary layer, whilst the level of turbulence inside the internal layer was high because of large energy production near the rough wall. The roughness geometry had the same values as that of Perry and Joubert [54].

Antonia and Luxton [6] also performed the experiment on the above mentioned configuration with a reversed flow direction, i.e. from rough to smooth surface. Detailed measurements of velocity profile, skin friction, turbulence

intensity, Reynolds shear stress were made and mixing length, turbulent energy balance and diffusion energy flux distributions were analysed. The rate of growth of internal boundary layer was found less than that for the smooth-to-rough change of surface roughness, and the flow could not be obtained self-preserving over the 8.0 ft long upstream smooth surface test section.

Schofield [63] made significant investigations in the turbulent boundary layers following a step change of surface roughness in strong adverse pressure gradient. The roughness used was of d-type as used by Perry et al [55] . Universal logarithmic distributions of mean velocity were found to be established shortly after the step. Only at a distance of two boundary layer thicknesses downstream of the step, the extent of wall similarity normal to the wall was comparable with that in a corresponding unperturbed layer. The shear stress implied by the logarithmic distributions adjusted quickly to the new wall conditions by attaining an equilibrium value with little overshooting in contrast to the cases of similar flows on flat plates or in ducts.

Wood and Antonia [75] conducted elaborate experiments on the turbulent boundary layer over a d-type surface roughness, similar to those used by Perry et al [55] , with $\frac{\lambda}{k} = 2$. The boundary layer was found to satisfy self-preservation characteristics after $\frac{x}{D_h} = 1.5$. The measurements included shear stress, turbulence intensities, turbulence frequency

spectra, and the analysis also included roughness function, dissipation of energy and flow visualization. Distribution of Reynolds normal and shear stresses across the boundary layer were found closely similar to those found over a smooth surface (excepting the region immediately above the grooves.

/Tani and Makita [65] measured for turbulent flows through a two-dimensional channel with the wall changing stepwise from smooth to rough and vice versa, and measurements included mean velocity, turbulence intensities and shear stress. The channel was 1.0 m wide and 10.0 cm high. The top and bottom surfaces of the rough section were fitted with 1.5 mm x 1.5 mm cross section ribs with pitch of 1.0 cm. Measurements were taken at Reynolds number = 3.8×10^4 based on channel half height and a reference velocity of 10 m/s. The flow near the wall was found to adjust rapidly to the change in surface roughness, while away from the wall, the response was slow. Adjustment to new equilibrium condition had set in the internal boundary layer shortly after the roughness change. The shear stress overshoot at the rough-smooth junction before returning towards the equilibrium value.

Table 2.3 Measurements of Turbulent Flows through Ducts and Channels with Roughness Change

Author	Flow configuration	Measurements	Instrumentation	Comments
Jacobs [36] 1939	60 mm x 20 mm channel 1 mm square ribs on floor with $\lambda/k=8$ to give sudden transition	$u; p; \tau$	Pitot-static tube	Shear stress calculated from Prandtl's mixing length equation.
Carper [16] 1962	4.0"x46.5" channel 0.437 in x 0.281 in descrete ribs on the walls with $\lambda=8$ in to give sudden change $Re_{\frac{w}{2}}=30,000$	$u; u', v', R_{u'v'}$ $\tau_s, \tau_r, \tau_{u'v'}$	Pitot-static tube, Hot-wire anemometer	Boundary layer developed rapidly following roughness
Islam and Logan [35] 1976	Same as above $Re_{\frac{w}{2}}=30,800$	p, u, u' τ_s, τ_r	Pitot-static tube, static pressure holes, Hot-wire anemometer	Flow with zero pressure gradient-reducing transitional overshoot of wall shear stress.
Perry and Joubert [54] 1963	5.5 ft x 4.25 ft duct discrete rib roughness, K=0.125 in, λ=0.50 in U=60 ft/s,122 ft/s	u, p	Pitot-static tube	Flow with adverse pressure gradient, roughness function independent of pressure gradient.
Perry et al [53] 1969	Wind tunnel section floor roughened by discrete ribs, K=1/8 in, $\frac{1}{2}$ in, 1 in, both k-and d-type	p, u	Pressure tapped pad roughness, Pitot-static tube	Flow with zero and adverse pressure gradients - roughness function was investigated for both types of flow

Table 2.3 Contd.

Author	Flow configuration	Measurements	Instrumentation	Comments
Antonia and Luxton [7] 1971	Upstanding k-type roughness as configuration of [54], smooth to rough, U=20 ft/s	$u, u', v', \tau_{u'v'}, R_{u'u'}, R_{u'v'}, \phi_{u'}, \phi_{v'}$	Pitot-static tube, Hot-wire anemometer	Internal boundary layers growth examined.
Antonia and Luxton [5] 1971	Depressed change of roughness configuration of [54] smooth to rough, $Re_{\delta} = 1.9\times10^4, 3.4\times10^4$	$u, u', v', \tau_{u'v'}$	Pitot-static tube. Hot-wire anemometer	Flow with zero pressure gradient-internal boundary layer's growth examined.
Antonia and Luxton [6] 1972	Depressed change of roughness, configuration of [54] Rough to smooth, $Re = 2.6\times10^4, 4.8\times10^4$	$u, u', v', \tau_{u'v'}$	Pitot-static tube, Hot-wire anemometer	Rate of growth of internal boundary layer less than that for smooth to rough case.
Schofield [63] 1975	Change of roughness of d-type, Configuration of [55]	u,p	Pitot-static tube	Flow in strong adverse pressure gradient, shear stress adjusted quickly to new equilibrium with little overshoot.
Wood and Antonia [75] 1975	Change of roughness of d-type, Configuration of [55]	u, u', v' $\tau_{u'v'}, \phi_{u'}, \phi_{v'}$	Pitot-static tube, Hot-wire anemometer	Flow visualization done, Dissipation of energy studied
Tani and Makita [65] 1971	1.0mx10cm channel Top and bottom surfaces fitted with 1.5mmx1.5mm ribs with λ =1.0 cm $Re=Uh/\nu = 3.8\times10^4$	u, u', v', p $\tau_{u'v'}$	Pitot-static tube, Static pressure hole, Hot-wire anemometer	Both smooth to rough and rough to smooth flows studied; shear stress overshoot at the transition

2.3.3 Turbulent Flows over Earth Surface

Compared to pipe and duct flows, relatively a smaller number of investigations have been carried out in the atmospheric flow field to study the effect of the changing terrain roughness on the boundary layer. This is mainly due to the practical difficulties and large cost involved in such measurements.

Elliot [23] was amongst the fore runners to concentrate attention on the growth of the atmospheric boundary layer in a change of surface roughness. He conducted experiments at Naval Air Station, Houma, Louisiana, USA and used the runway and surrounding grass field of average height of 1 m as the smooth and rough surfaces. Measurements included wind and temperature profiles using anemometers and thermistors. The height of internal boundary layer in which the flow adjusted to the new surface condition was found to grow as

$$\delta_i = 0.86\ x^{0.8}\ z_o^{0.2} \qquad (2.3.5)$$

The study was dovetailed with numerical computation of the growth of internal boundary layer assuming logarithmic wind velocity distribution and von Karman's integral method.

Panofsky and Townsend [53] further developed the-theory of Elliot and verified the results with different field observations, which included flows over a frozen lake fitted with bushel baskets (Lettau et al, 1962) and flow study

over cut and uncut grass of 50 cm height (Deacon,1953). Their theory was based upon the assumption of continuous variation of shear stress from the surface to the edge of the boundary where the stress was that in the original layer.

Bradley [12] undertook elaborate experiments in the lower atmosphere where the wind passed from one surface condition to another. The observation sight was an air field on the Jevis Bay peninsula of the south coast of New South Wales, Australia. The well maintained tarmac surface and the nearby trees and bushes offered the objects of interest. Surface shearing stress downwind of a surface roughness transition was measured using drag plates, and velocity profiles were measured for both ways transition (smooth to rough and rough to smooth) of flow using anemometers. The observed results were compared with theories put forward by Taylor (1962), Elliot [23] and Panofsky and Townsend [53] and good agreements were found with the latter one for the flow from smooth to rough surface; internal layer growth was found to follow $\frac{4}{5}$ th power law.

CHAPTER III

THEORY

3.1 General

The basic equations of boundary layer parameters and logarithmic velocity profile are introduced in this chapter. Different approaches of treating the log-law of the wall are described briefly and the method of 'locating the origin of rough wall distance is also dealt with.

3.2 Boundary Layer Parameters

The measure of the region of retarded flow in the vicinity of a surface is ideally the boundary layer. But as the velocity u within the boundary layer approaches the free-stream velocity U asymptotically, for practical purposes the boundary layer thickness δ is commonly defined as the distance from the boundary to the point where $u = 0.99\ U$.

The displacement thickness δ^* of the boundary layer is the distance the actual boundary would have to be displaced in order that the actual flow rate would be the same as that of an ideal fluid past the displaced boundary. Accordingly

$$U\,\delta^* = \int_0^{\delta} (U-u)\,dy$$

$$\delta^* = \int_0^{\delta} \left(1 - \frac{u}{U}\right) dy \qquad (3.2.1)$$

The momentum thickness θ of the boundary layer is the distance from the actual boundary such that the momentum flux through the distance θ is the same as the- deficit of momentum flux through the actual boundary layer. Thus

$$(\rho\theta\, U)\, U = \int_0^{\delta} \rho(U-u)u\, dy$$

$$\theta = \int_0^{\delta} \frac{u}{U}\left(1 - \frac{u}{U}\right) dy \qquad (3.2.2)$$

The ratio of the displacement thickness and momentum thickness gives the shape factor of the boundary layer.

$$H = \frac{\delta^*}{\theta} \qquad (3.2.3)$$

The average mean velocity at any cross section is found from

$$\bar{U} = \frac{U}{A} \int (u/U)\,dA \qquad (3.2.4)$$

3.3 Log-Law of Wall for Rough Surfaces

For constant shear region close to a smooth wall, the wall shear stress and velocity profile obey the universal logarithmic distribution well known as the log-law of the wall:

$$u_s^+ = A_s \log y^+ + B_s \qquad (3.3.1)$$

where

$$u_s^+ = \frac{u}{u_s^*} \qquad (3.3.2)$$

$$y^+ = \frac{y\, u_s^*}{\nu} \qquad (3.3.3)$$

$$u_s^* = \sqrt{\frac{\tau_{os}}{\rho}} \qquad (3.3.4)$$

aand A_s and B_s are constants. A_s is related to von Karman constant by the relation

$$A_s = \frac{\ln 10}{\kappa} \qquad (3.3.5)$$

If the wall is rough and the flow is fully turbulent, the velocity in the vicinity of the rough wall is independent of viscosity and the velocity distribution has been shown to be [62]

$$u_r^+ = \frac{1}{\kappa} \ln \frac{y}{k} + B_r \qquad (3.3.6)$$

where $$u_r^+ = \frac{u}{u_r^*} \qquad (3.3.7)$$

$$u_r^* = \sqrt{\frac{\tau_{or}}{\rho}} \qquad (3.3.8)$$

The velocity gradient near the rough wall is less steep than that near the smooth wall and the log-law region shifts outward from the wall than the region for the smooth wall. Further, the log-law profile of the mean velocity gets a parallel shfit downward from that of the smooth wall with the same flow. To account for the parallel shift of the rough wall profile from the smooth wall one , the log-law equation for rough walls can be written in the form

$$\frac{u}{u^*} = \frac{1}{\kappa} \ln \frac{yu^*}{\nu} + B_s - \frac{\Delta u}{u^*} \qquad (3.3.9)$$

where $\Delta u/u^*$ is called the wall function or roughness function measuring the vertical shift of the rough wall profile from the smooth wall one and it is universally a function of roughness Reynolds number $\frac{ku^*}{\nu}$ for the particular roughness configuration. Many investigators including Hama (1954) and Robertson [61] have put the functional relationship in

the form (for high Re_k, say $Re_k > 50$)

$$\frac{\Delta u}{u^*} = \frac{1}{\kappa} \ln \frac{k u^*}{\nu} + K \qquad (3.3.10)$$

substitution of which in eqn. (3.3.9) generates the eqn. (3.3.6). Here K is a constant depending on the roughness characters and flow conditions. For a wide range of Re_k, $\kappa \simeq 0.41$. For high values of Re_k, the first term of the right hand side of eqn. (3.3.10) becomes predominant yielding

$$\frac{\Delta u}{u^*} = \frac{1}{\kappa} \ln \frac{k u^*}{\nu} \qquad (3.3.11)$$

Wood and Antonia [75] treated the log-law for the rough wall putting it in the form

$$\frac{u}{u^*} = \frac{1}{\kappa} \ln \frac{y}{w} \qquad (3.3.12)$$

where w, the roughness length scale is given by

$$w = \frac{\nu}{u^*} \exp [\kappa (\Delta u/u^* - B_s)] \qquad (3.3.13)$$

3.4 Determination of Origin for Rough Surfaces

In the eqn. (3.3.6) the measurement of wall distance for rough wall is critical. This is because of the fact that the rate of change of velocity increases very rapidly with the decrease ofwall distance. So the determination of wall distance is very important to analyse the characteristics of a boundary layer in relation to its surface and other parameters. In the case of 'smooth' wall, its measurement is straight forward. The wall distance is measured from the upper surface of the wall by some suitable measurement methods and the origin of the universal log-law is taken at the surface where velocity is zero. But in the case of rough wall, selection of origin for the log-law equation is difficult and controversial. This is mainly because of irregular nature of the rough surface.

In analysing the boundary layer over rough surfaces, different researchers adopted different methods of finding origin to suit their requirements. From different experimental results, it is clear that the origin of the rough wall log-law occurs neither at the crests nor at the roots of the roughness elements. It is somewhere above the roots but below the crests as reported by Perry and Joubert [54], Lin et al (1966), Betterman (1966) and others. The rough wall log-law origin has been reported to be situated even below the roots of the roughness elements by Hanjalic and Launder (1972), Lawn (1971), Berger and Whitehead (1977).

It was discussed in the last article that wall roughness displaces the smooth wall log-law profile downward and rightward keeping its slope unchanged. In determining the error of rough wall origin, Perry and Joubert [54] considered this fact of rough wall influence on smooth wall profile. Using the rough-wall property, Perry and Joubert started adding and subtracting an amount E, known as the 'error in origin' from the roughness crest until the experimental points (u^+, y^+) lied on a straight line parallel to the smooth wall profile under the identical flow conditions. In the present investigation, the above method was adopted in locating the rough wall origin.

CHAPTER IV

EXPERIMENTAL SET UP AND METHODS OF MEASUREMENT

4.1 Experimental Program

The experimental program comprised measurements of mean and turbulent characteristics of developing flows over a stone-roughened flat surface following a smooth surface. For the purpose of comparison as well as for preliminary test of the flow through the wind tunnel test section with all smooth surfaces, mean axial velocities and wall static pressures were measured with particular attention to the flow over the floor which was later roughened with stone chips (Plate 4.1).

After roughening the floor of the test section, the mean axial velocities, wall static pressures were measured and the wall shear stress was calculated from the axial pressure gradient. Amongst the turbulent fluctuating quantities, longitudinal and transverse turbulent intensities were considered. The whole set of experiments was performed for four different Reynolds numbers.

Mean velocities were sensed by a pitot-static tube and velocity gradient "very near" to the smooth surface by a boundary layer tube. Measurements of turbulent parameters were obtained with the help of single hot-wire probes normal to the direction of flow. All the measured

quantities were recorded by appropriate recording instruments.

A brief description of the main flow system appears in the next section and the calibration facility is described in section 4.3. The traversing mechanism and probe setting arrangements are described in section 4.4. A short discussion on the possible sources of error is given in section 4.5.

4.2 The Flow System : Wind Tunnel

The basic experimental facility used in this work was a 53 feet long open circuit subsonic wind tunnel with a test section of 1.5 ft x 1.5 ft cross section.

The wind tunnel was originally designed by Islam [33] as a closed circuit one. Subsequently the design was modified by Khalil [37] to an open circuit wind tunnel. For the present work the wind tunnel was further modified and some imporovements were made by incorporating a filter cum settling chamber, a flow straightener, a flow controlling valve, a silencer and an additional 5 feet long 1.5 ft x 1.5 ft size section.

The schematic diagram of the wind tunnel is shown in Figure 4.1. Different views of the tunnel are given in Plates 4.2 and 4.3. The wind tunnel broadly consists of a filter cum settling chamber, a bell mouth entry, an eddy

breaker, a flow straightener, a uniform upstream section, a test section, a diverging section, two counter rotary axial flow fans, a flow controlling valve and a silencer.

The diverging part and the fan section of the wind tunnel used by Khalil [37] were kept intact and the rest of the wind tunnel was fabricated or modified.

The filter cum settling chamber measuring 100 in x 60 in was made with wooden frames covered with double layer of $\frac{1}{4}$ in thick foam sheets. A cloth cover for the settling chamber was used in order to keep the foam clean and to prevent external damages. This chamber immunized the flow inside the tunnel against all outside disturbances and foreign particles.

The 60 in long converging nozzle was made of 15 SWG black sheet. The inlet and outlet dimensions of the nozzle were 40 in x 40 in and 18 in x 18 in respectively, resulting a contraction ratio of 5:1.

A honeycomb like flow straightener was made using 1 in diameter PVC pipes. As per suggestion of Bradshaw [13], $9\frac{1}{2}$ in long PVC pipe pieces were stacked at the entry of the tunnel section, the pipes being fastened to one another and fixed to the tunnel wall with the help of Aica glue (No. 601). This honeycomb made the flow sufficiently straight and parallel to the axis of the duct.

A wire net with 4 holes/inch was fitted at the entrance of the nozzle. This together with the flow-straightener helped

in breaking large scale turbulent eddies and reducing lateral components of disturbance in the test section.

The wind tunnel section comprised five 18 in x 18 in sections. The first two were made of $\frac{1}{4}$ in thick perspex sheet reinforced with araldite glued aluminium angles. The first perspex section partly accommodated the honeycomb straightner. The latter three sections were made of wood. Roughness elements were provided in the 4th and 5th sections, which formed the main test section for the present experimental work. The upstream length of 7 feet ensured achievement of a fully developed flow over smooth surface before if reached the working section.

Two holes were made at $12\frac{1}{2}$ in and 25 in from the entrance end of the tunnel section at the center line of the ceiling of the section - one for monitoring the temperature and the other for that of wall static pressure. Temperature was recorded by a mercury thermometer and pressure by an Ellison Company(U.S.A),inclined draft gage. A continuous $\frac{1}{2}$ in slot was provided at the mid section ceiling of the test section to facilitate traversing of pitot-static tubes and hot-wire probes vertically at different longitudinal positions of the tunnel. During experiment, the slot was kept closed with wooden blocks which flushed with the inside surface of the ceiling. The probe insertion arrangement is shown in Fig. 4.2.

The test section was followed by the diverging section. It was $15\frac{1}{2}$ ft long and made of 15 SWG black sheet. The angle of divergence of the duct was 6^{o}, which envisaged minimizing the expansion loss and reducing greatly the possibility of flow separation.

The flow producing fan unit was placed next to the diverging section. It was a two-stage contra-rotating axial flow fan (Woods of Colchester Ltd. England, Type 38 JTE) of capacity 30,000 cfm at the head of 6 in of water. The blades were L-type aerofoil of diameter 38 in and the speed was 1475 rpm (motor 3 ph/50 hz/400 a). The position of the fan downstream of the tunnel section produced an induced flow through it providing a more uniform, stable and undisturbed flow through the test section.

The flow controlling butterfly type valve was used to control the flow through the test section. It was fabricated from $\frac{1}{8}$ in mild steel sheet and was placed at delivery end of the fan unit. A screw thread mechanism was used to actuate the valve.

Finally the silencer was fitted at the end of the tunnel to reduce noise of the system.

All the sections were connected with each other with the help of C-clamps and nuts and bolts. Duct surfaces were matched properly at the joints so that the stream lines were not disturbed while passing from one section to another.

Rubber gaskets were used between adjacent ducts and foam with musking tape was applied to prevent any possible leakage of air. Special care was taken to ensure proper alignments of the ducts so that a straight horizontal flow could be obtained in the test section. The central longitudinal axis of the wind tunnel was maintained at a constant height from floor (viz. 4 ft 3 in).

All the component ducts of the wind tunnel were mounted on 20 pairs of stands made of galvanised iron pipe. The base-plate of each stand was bolted to the floor of the laboratory. Wood and rubber pad packing were given between the ducts and the stand platforms to damp out vibration. A foam made isolator was placed between the fan unit and the diverging part so that the vibration of the rotating fan could not proceed towards the test section. The fan section was mounted on a special foundation isolated from the remaining floor by an air gap, insulating the test section against possible transmission of vibration of fan through the foundation.

4.3 Calibration Rig

The calibration rig was a low turbulence round jet issuing from a 31 mm nozzle. The flow was produced by a centrifugal blower run by an $1\frac{1}{2}$ hp, 1420 rpm induction motor. The blower discharged air into a 4 in diameter 5 feet long PVC pipe holding the nozzle at its end. A cylindrical

filter was fitted at the suction of the blower to get dust free air at nozzle delivery. A hand operated butterfly valve was installed just after the discharge of the blower. The flow could be varied both by controlling the valve and by changingthe speed of the blower. A flow straightener made of 1 in diameter PVC pipes was fitted before the nozzle along with a wire net to work as an eddy breaker. The air stream finally emerged as a smooth, turbulence free jet from the exit of the nozzle. The core of the jet offered the bed for calibration of both the hot-wire and the transducer. The velocity of the calibration jet could be varied from 10 ft/s to 160 ft/s, which covered well the required range of the experiment.

4.4 Traversing Mechanism and Probe Setting

The pitot-static tube and the hot-wire probe were traversed in the air stream with the help of a Mitutoyo (Japan) Coordinate Measuring Machine (Type CX 652 Code 198-402) with ranges X coordinate 24 in, Y coordinate 20 in and Z coordinate 10 in (Plate 4.6). The mechanism was actuated by a wheel through a rack and pinion arrangement. A position could be fixed upto an accuracy of 0.0005 in with the help of it, thus enabling the probes to be placed with a great precision. The traversing mechanism was kept over a rigid table made of mild steel angle with a view to prevent external vibration.

The boundary-layer tube was traversed with the help of an Eberbach (U.S.A) traversing gear during checking of the velocity profiles of the side walls, as shown in Plate 4.7.

In order to prevent undue vibration of the sensing probe, the pitot-static tube was supported by a stepped aluminium rod of diameter $\frac{3}{8}$ in as shown in Fig. 4.4(a). The pitot tube was placed inside a groove cut throughout the length of the rod and fastened with it. The rod was rigidly fixed to the holder, Fig. 4.4(b), which was again fixed with the traversing gear. The sensing point was kept 3 inches beyond the end of the smaller diameter step of the rod to ensure that no major disturbance was caused to the flow near the sensor by the presence of the supporting rod.

The boundary layer tube and the hot-wire probe were fitted with a DISA holder tube, which gave them enough rigidity against any vibration.

Great care was taken to set the probes as correctly as possible with respect to the flow direction and wall proximity.

For calibration of hot-wire or transducer, two rigid probe holders with heavy bases were used (Plate 4.8). The hot-wire probe holder was provided with the facility of angular adjustment upto an accuracy of 0.5^{o}.

For sensing static pressures inside the duct, 15 static pressure holes were made in the lateral wall of the test section through brass nipples as shown in Fig. 4.5 and Plate 4.9. Connections to the pressure transducer were made through a multiple channel selector valve shown in Plate 4.10, facilitating rapid recording of the pressure drop.

4.5 Error Analysis

In this section a brief account of errors and uncertainties associated with different stages of measurements are given. The errors that crept into the analyses are also discussed. The uncertainties were introduced in the system of measurements during the calibration of the sensing elements and were later cumulated to those during the final measurements. The analyses of uncertainties involved in different measurements are given in Appendix-C.

The error in the measurement of wall distance was critical for those properties whose gradient near the wall was greatest and prominent. As indicated in section 4.4, the sensing probes could be placed in the duct with an uncertainty of $\pm$ 0.00025 in. This could result in errors of upto 0.50% in the mean velocity measurements near the wall. The error was partially accounted for as discussed in section 3.1.2. Error in the measurement of distance between successive points beyond the wall was negligible.

In case of measurements over rough surface, the distance of probe was measured with great accuracy with the help of telescope. However, the initial error in aligning the probe with the datum mark had relative and cumulative effects on the subsequent distance measurements.

During the experimental measurements, flow in the tunnel varied for a particular valve setting due to the variation of fan speed for transient motor core resistance characteristics and changes in the atmospheric conditions. To minimize the first effect, the fan was kept running for half an hour before taking actual measurements. The flow was monitored continuously by recording the static pressure at the reference section of the wind tunnel. The flow was found to vary within 0.01 in of H_2O of static pressure in one experimental run and the flow reproducibility between different runs was also maintained within the same range.

In all pressure measurements, static or total, the maximum transducer error was 0.75% of the measured value. This is smaller than the experimental scatter which can be seen in the plots of mean velocity profiles and the static pressure gradients

In the experiments, the effects of secondary currents were not considered. Due to the presence of secondary currents in the duct cross section, the wall shear stress decreased continuously towards the corner, as reported by Ali [3] . So the shear stress calculated from the pressure

gradient was not the true one but an approximate value. However, as the decrease of wall shear stress is prominent only near the corner, the effect of secondary current in the present case, has little influence on wall shear stress because of the comparatively large duct dimension.

In the measurements of turbulence properties, the possible sources of errors were related to probe setting, probe's proximity to wall, level of turbulence etc. The misalignment of the probe wire with respect to the flow direction was within $\pm 3^{o}$. Also for the same alignment of the wire, the response to the turbulence property would vary due to the variation in the flow field. For example, flow direction other than the true axial one would cause to record a longitudinal turbulence quantity different from the designated one. The secondary flow due to wall proximity caused such deviations of the measurement of longitudinal turbulence intensity. Also the hot wire system used was meant for a typical turbulence level 15%. So for turbulence level above 15%, the values became inaccurate. However this effect would be only secondary compared to those of other external error sources mentioned above in the measurement of turbulence

4.6 Preliminary Tests of Wind Tunnel

In order to test the flow in the wind tunnel and the reliability of measuring techniques, preliminary measurements

were made before starting the actual experiments. Mean velocity and mean static pressure were measured at section $\frac{x}{D_t} = 0$ for different flow rates. From the Figure 4.6, the flow was found to be almost symmetric about the centerline of the test section. The mean velocity was found stable within 1% of its value. The small discrepency between the velocity profiles on the floor and on the ceiling of the test section is attributed to the difference in surface finishes of the wooden walls.

The flow in the test section of the wind tunnel was found almost absolutely free from any transverse pressure gradient, as evident from Figure 4.7.

The smooth-wall flow was found to be fully developed at the station $\frac{x}{D_t} = 0$, where from the roughness elements were added afterwards. The mean velocity profiles at different axial positions ($\frac{x}{D_t} = 0.0, 0.25, 0.5, 0.75$) would coalesce to a single curve justifying the attainment of a fully developed flow condition on the smooth surface. To avoid overcrowding of experimental points, however, the profiles are drawn shifting their origin upwards, as shown in Figs.5.1a-d . The straight line nature of the semilogarithmic plots of mean velocity also serve as strong evidence of a fully developed flow condition (Fig. 5.3). These plots are discussed in chapter V in the context of smooth wall characteristics.

The reproducibility of measurements by pressure transducer was checked by repeating the same set of readings several times distributed over a fortnight. Also the reproducibility of a flow condition in the test section was verified by adjusting the flow controlling valve to achieve a few certain flow rates repeatedly over a period of one month. All the tests showed satisfactory evidence of reproduction of flow conditions within 3% of mean center line velocity and of measurements by the instrument within 1% of a measured value. And these variations were allowed during the period of measurements.

4.7 Measurement of Mean Quantities

Measurement of mean quantities include those of mean velocity, mean static pressure and different total pressure of yawmeter holes.

4.7.1 Instrumentation for Velocity and Pressure Measurements

For measurement of axial mean velocity, a 1/16 in OD, 18 in long United Sensor pitot-static tube was used (Fig.4.8a). Before measurements, the holes were checked for any burrs and were cleaned carefully by compressed air.

The head of the pitot-static tube was hemispherical. According to Huston [32] , for a hemispherical head pitot-static tube, misalignments of the tip of the tube by $\pm 10^{o}$ from the flow direction have little effect on the measured value of total pressure. In the experiment, the misalignment of the tube with flow direction was kept within $\pm 2^{o}$.

For determining wall velocity gradient, a thin boundary layer tube (Fig.4.8b) was used. Velocity was found from the recorded total pressure and wall static pressure. The wall static pressures were measured through static pressure tappings made in the side walls of the tunnel.

Due to the small tip height of the pitot tube used in the measurements, McMillan [48] correction factor for the effective displacement of the pitot tube center towards the region of higher velocities was negligible and so it was not considered. The low Reynolds number correction described in Bryer and Pankherst [15] was applied when pitot tube or boundary layer tube Reynolds number $\frac{hU}{\nu}$ were less than 200, where h is the internal dimension of the tube. In addition to this, the wall proximity correction was applied for total pressure readings near the smooth wall as suggested by McMillan [48] . The wall distance was ascertained from the mirror image of the probe on highly polished floor.

The mean velocities were inferred from the total and static pressure data with the aid of incompressible Bernoulli's equation

$$u = \sqrt{\frac{2}{\rho}(P_o - p)} \qquad (4.7.1)$$

where p and P_o are the wall static pressure and stagnation pressure respectively.

For determination of secondary flow direction in the longitudinal mid-section of the tunnel, a three-tube Yawmeter was employed, which is dealt in detail in Appendix B.

4.7.2 Recording of Pressure

For measurements of different pressures, the pressure signals were transmitted to a transducer through a narrow

(1.4 mm bore) flexible plastic tubing to get a good pressure response characteristic of the system. A Furness Controls Ltd. (U.K.) pressure transducer (Model MDC FC 001) was used for recording the pressures. To check the calibration of the transducer, its readings were compared with those of a liquid micromanometer of Flow Corporation (Model MM3) and some internal electrical circuit adjustments were made to give correct readings in different scale ranges.

The pressure transducer was also calibrated against its output voltage which varied linearly with the pressure. The output voltage of the transducer was recorded with the help of a Bruel & Kajaer (Denmark) autoranging time-domain voltmeter (Model 2426) to get the ultimate signal of the pressure. For measurement of all pressures, an integration period of 3 seconds was used.

4.8 Measurement of Turbulent Quantities

For the experimental investigations of fluid flow, quite a large number of methods, techniques and instruments have been developed and used. Majority of these methods are, however, for measurement of mean velocity and outher parameters in fluid flows. Only a few techniques are in use for measuring turbulent quantities for the last 2 or 3 decades.

In the measurement of turbulent flows, distinction between measurement of mean flow parameters and measurement of turbulence is important. The problems connected with these two types of measurement are to certain extent related, but the required criteria of the instruments to measure the two

are different. The measurement of mean velocity is more or less affected by the turbulence present in the flow, and it is necessary to know only what correction should be made in the reading of measuring instrument, but in measuring the turbulence itself, any influence of the mean velocity that produces an error in the reading of turbulence measuring instrument can not be tolerated. Consequently provisions are to be made to correct this error in the instrument.

Methods and techniques used for flow investigation can be broadly divided into two groups.

In the first group, use is made of a tracer or other indicator which is introduced into the fluid to make the flow pattern visible (by photographic recording) or observable (by a suitable detecting apparatus) outside the field of flow. Due to very rapid flow change with respect to time and place, this method is not very suitable for the measurement of turbulence for want of appropriate instrument of instantaneous and frequent recording.

In the second group, a detecting element is introduced into the flowing fluid, and the turbulence is measured by the change in mechanical, physical or chemical nature that occur in this element due to the flow. In measuring these changes to get the value of turbulence parameters, the detecting element and the connected recording apparatus must satisfy a number of requirements, which are enumerated in ref. [30] . Hot-wire

anemometers, hot-film apparatus and laser-doppler anemometers are the major techniques that are now widely used for turbulence measurements, because they satisfy, most of the above mentioned requirements. Of these, the development and application of the hot wire anemometer in surveying turbulent flow have far outstripped those of other instruments meant for the same purpose.

4.8.1 The Hot-Wire Anemometer

The hot-wire anemometer is used to study fluid velocities and turbulence through measuring the heat loss rate from a very fine wire introduced into the stream as the sensing element. The wire is generally of diameter of the order of micron and made of platinum, tungsten or platinum-iridium. The wire is heated by passing small electrical current (usually 30 ma to 300 ma) through it. The heated wire is cooled by the flowing stream of fluid across it causing its temperature to decrease. Consequently the electrical resistance of the wire is diminished. Then the different electrical parameters can be used as the signal of turbulence quantities. For example, if the current through the wire is kept constant, the electrical resistance serves as a convenient measure of stream velocity. Alternatively, for a constant wire resistance maintained by a constant wire temperature, the heating current or the voltage across the wire may indicate the velocity.

4.8.2 Hot-Wire Instrumentation

For constant current hot-wire anemometry, the basic circuit principle is shown in Figure 4.13a, where the wire current is adjusted with the help of the variable resistance connected in series with the wire. The wire resistance ascertained by the ammeter and voltmeter serves as the measure of average stream velocity that produces the change in temperature and subsequently the resistance of the wire.

In practice the value of the wire resistance is found by incorporating it in a Wheatstone bridge arm as shown schemetically in Figure 4.13b. For a given current, the bridge is balanced by varying the resistance of one arm (R_3), and the current through the wire is measured to get an idea about the stream velocity.

For measuring mean velocity, the wire was calibrated against velocities recorded by a pitot-static tube. The wire and the pitot-static tube were placed side by side in the core of the jet of calibrating nozzle and the velocity and the wire current were noted simultaneously. This tantamounted to the experimental determination of the constants A_1 and B_1 of eqn. (D-9) thus providing the correlation between wire current and cooling stream velocity (Fig. 4.15).

For measurements of fluctuation in velocity, the fluctuation of wire temperature or resistance has to be recorded in the best possible manner. Here the measuring

criterion is the fluctuating voltage across the wire. To account for different frequency of fluctuation, generally a linear combination of the voltage and rate of change of the voltage is considered. Since the fluctions are random in nature, the voltage signals are measured with the help of a root-mean-square voltmeter. Since the relative magnitudes of the fluctuations of velocity are generally very small, the voltage signals are sent to the voltmeter after sufficient amplification and appropriate compensation to get the value at a measurable level.

In the present experiment, a Flow Corporation Hot-Wire Anemometer (Model HWB 3) was used. The model comprised the basic hot-wire bridge, a square wave calibrator for signal compensation and an amplifier for signal amplification. The voltage output signal was measured with the help of a Flow Corporation Random Signal Voltmeter (Model 12A1) after filtering the signals through an electric filter of the external and system noises. The instrument set up is given in schemetic diagram form in Figure 4.14.

CHAPTER V

RESULTS AND DISCUSSIONS

5.1 Introduction

Turbulent flows over smooth surface and in transition from smooth to rough surface have been experimentally studied. The varnished wooden floor of the wind tunnel test section was taken as the smooth surface and the mean flow properties over this surface were studied. Later the mean and turbulent properties were investigated for flows over the same surface roughened by stone chips.

Results for flows over smooth surfaces are discussed with some important aspects of the flow elaborated.

This investigation was concerned with the measurements in the smooth-rough transition zone for flow over a flat surface. For presenting the flow characteristics the duct hydraulic diameter was used as the characteristic length. At each section of the duct, its centerline velocity was taken as the characteristic velocity, and was looked upon as the free stream velocity for the flat surface. To represent the flows near the wall, smooth or rough, friction velocity u^* was used as the characteristic velocity and ν/u^* as the characteristic length for smooth surface while the roughness height, k, as the characteristic length for rough surface. For the purpose of comparison, boundary layer thickness was also used as length scale.

Measurements of this investigation are also compared with some of the comparable measurements of transition boundary layer flows presented by previous researchers.

5.2 Measurements of Smooth Wall

The measurements of flow over smooth wall included mean axial velocity profile, pressure gradient along the wall, and calculation of wall shear stress, boundary layer parameters and log-law parameters. The whole set of measurements was done at four different Reynolds numbers, viz. $Re_{Dt} = 9.80 \times 10^5$, 7.20×10^5, 4.61×10^5, 2.78×10^5, based on hydraulic diameter of the duct and mean center line axial velocity.

5.2.1 Mean Velocity Profiles

Figs.5.1a-d display the mean axial velocity profiles measured over the 'smooth' wooden floor of the test section for different Reynolds numbers. Since only the flow over the floor is of prime concern in the present study, the profiles are shown upto the centerline of the duct. The velocity profiles at four axial positions $\frac{x}{D_t} = 0.0, 0.25, 0.50, 0.75$ clearly show the self-preservation of flow velocity attained at the first station.

From the velocity profiles, the smooth wall boundary layer characteristics are found out. The boundary layer

thickness is determined from the profiles based on the 99% of the free stream velocity. The average velocity, the displacement thickness, the momentum thickness and the shape factor of the boundary layers are calculated using the following formulas:

$$\bar{U} = \frac{U}{A} \int f\left(\frac{u}{U}\right) dA \qquad (3.2.4)$$

$$\delta^* = \int_0^{\delta} \left(1 - \frac{u}{U}\right) dy \qquad (3.2.1)$$

$$\theta = \int_0^{\delta} \frac{u}{U} \left(1 - \frac{u}{U}\right) dy \qquad (3.2.2)$$

$$H = \frac{\delta^*}{\theta} \qquad (3.2.3)$$

The values of the parameters for the different Reynolds numbers are given in Table 5.1.

Table 5.1 Smooth Wall Boundary Layer Characteristics

U ft/s	$Re_{Dt} \times 10^5$	$\bar{U}$ ft/s	δ in	δ/D_t	δ^* in	θ in	H
113.0	9.80	109.5	1.75	0.0972	0.250	0.200	1.250
84.0	7.20	81.4	1.78	0.0989	0.252	0.203	1.242
55.0	4.61	52.5	1.85	0.1028	0.260	0.211	1.232
33.0	2.78	31.6	1.90	0.1055	0.287	0.216	1.329

The values of the boundary layer indicate that boundary layer thickness is less for higher Reynolds numbers, which agree with the findings of Antonia and Luxton [5] , Antonia and Wood [8], Faruque [29] .

5.2.2 Axial Pressure Gradient

Axial pressure gradients of the duct for different Reynolds number are shown in Fig. 5.2 and are found to be constant throughout the length of the duct. The constant pressure gradients conform to the general trend of flow behaviour in uniform cross section ducts as reported by Ali [3], Logan and Jones [46] and others.

5.2.3 Wall Shear Stresses and Friction Factors

The wall shear stresses for the smooth surface are calculated by different independent methods as enunciated in Appendix A. Axial pressure gradients, smooth wall resistance coefficient and velocity gradients near the wall yield different sets of values for shear stress, of which Schiller's (1923) resistance coefficient data gave a lower side value. This is attributed to the difference in 'smoothness' in Schiller's ducts and the present case. The surface velocity gradients are taken from the velocity profiles (Fig. 5.4) measured by the boundary layer tube. The average wall shear stresses calculated for different Reynolds numbers are shown in Table 5.2.

Table 5.2 Friction Ceofficients for Smooth Wall

$Re_{Dt} \times 10^{-5}$	τ_{os} lb/ft^2 (eqn.A-1.4)	$C_f \times 10^3$	u^* ft/s
9.80	0.0545	3.806	4.929
7.20	0.0317	4.006	3.759
4.61	0.0159	4.687	2.662
2.78	0.0068	5.568	1.741

Fig. 5.5 represents the variation of friction coefficient C_f with Reynolds number. The friction coefficient is calculated from the relation

$$C_f = \frac{2\tau_{os}}{\rho U^2} \qquad (5.2.5)$$

The exponential relationship of C_f with Reynolds number is found for the present case as

$$C_f = 0.156\ Re^{-0.27} \qquad (5.2.6)$$

This is on the higher side of the commonly known friction factor equation of Clauser [20] which is expressed as

$$C_f = 0.079\ Re^{-0.25} \qquad (5.2.7)$$

Later Thomas and Easter [69] in their measurements in smooth square duct verified the result of Clauser. The higher values of C_f as found in the present case is due to the fact that the results of Clauser or Thomas and Easter were for flows through square ducts made of perspex sheet while in the present study polished wood was used for duct walls. The difference in the surface condition caused the difference in shear stress variation patterns between the two cases.

The variation of friction velocity with Reynolds number is shown in Fig. 5.6. It shows a decreasing tendency with Reynolds number as was reported by Clark [18] . However, the friction velocities are found to lie above those obtained by Clark because of the reasons mentioned above.

The universal velocity profiles over the smooth surface at different positions (x/D_t = 0.0, 0.25, 0.50, 0.75) are given in Figure 5.3. The mean velocity and wall distance are normalized by u^* and ν/u^* respectively. The straight line patterns the graphes testify the attainment of fully developed flow condition at or before the station x/D_t=0. In the plots, the experimental values of u^* were used.

5.3 Measurements of Rough Wall

After roughening the floor of the test section by stone chips, the mean and turbulence chararacteristics of the flow were measured. The mean quantities were measured for four Reynolds numbers as used for smooth surface measurements (section 5.2.1). The mean quantities included mean axial velocity profiles, pressure drop along the duct axis, wall shear stress etc. Secondary flow characteristics in the mid-longitudinal section of the duct were studied for Reynolds numbers of 7.20×10^5 and 2.78×10^5. The measurements of longitudinal turbulence intensities were made at a Reynolds number of 7.20×10^5.

In the following sections, the measurements over rough surface are presented and the results thus obtained are discussed.

5.3.1 Mean Velocity Profiles

Mean velocity profiles measured over the rough surface at different stations for the four Reynolds numbers are given

in Figs. 5.7. The vertical distances for all the velocity profiles are measured from the smooth wall surface and the mean velocities are non-dimensionalized by the free stream velocities of the respective sections. The profiles show the gradual development of boundary layer thickness with axial distance and the trend indicates that the flow was not fully developed at $x/D_t = 4.0$, the last station of the present research setup . The profiles for different Reynolds numbers suggest that the rate of growth of boundary layer and its thicknaess over the rough surface are almost independependent of Reynolds number of the present experimental range while, those over smooth surface decreased with Reynolds number as discussed in section 5.2.1.

Comparing the velocity profiles of Figs. 5.1, 5.7 and those of previous researchers, viz. Khalil [37] , Perry et al [55] and others, it is found that the boundary layer thickness increases with increase in surface roughness, but at a decreasing rate. The inflation of boundary layer is most pronounced for small initial increase of surface roughness from smooth surface. The rate of growth of boundary layer decreases progressively as the roughness height increases to higher and higher values as evident from the following table.

Table 5.3 Boundary Layer Thickness for Different Surfaces

Auther	Surface Type	$Re_{Dt} \times 10^{-5}$	δ in
Khalil [37]	Perspex	5.83	0.80
Present study	Wood (Polished)	7.20	1.79
Present study	Stone Roughened	7.20	3.50

The velocity profiles over the rough surface show very shy points of inflexions which signify the edge of the internal boundary layer. Close observation of the profiles shows that these inflexion points progressively move away from the wall with increase in axial distance. The growth of internal boundary layer is more clearly demonstrated in the semi-logarithmic plots of velocity, which is discussed in section 5.3.4.

Comparing the velocity profiles at $x/D_t = -0.25$ in Figs. 5.1 and 5.7, it is observed that the boundary layer thickness over the same smooth surface increases from 1.73 in to 5.0 in due to the presence of roughness in the downstream position, Secondary flow angle results of section 5.3.6 show the deflection of mean flow away from the wall. Due to the presence of secondary component of velocity in the upward direction, lower momentum fluid from near the surface moves away from the surface, reducing the velocity in the neighbourhood, and thus thickens the boundary layer there.

The patterns of velocity variation in axial direction are given in Figs. 5.8. Mean axial velocities non-dimensionalized by the local free stream velocity are plotted with axial distance, x, for different wall distances. These velocity distributions also seem apathetic to Reynolds number. The effect of surface roughness on the velocity distribution is more pronounced near the surface and distortions fade away

as one goes away from the surface. The transitional behaviour of the profiles persists mainly upto x/D_t = 3.0 after which they look forward to attaining development of flow.

As the stone chips protrude above smooth surface, the flow area decreases from the smooth-rough junction. Due to the reduction of flow area, fluid particles are accelerated at the junction to satisfy the continuity equation. To show this effect, axial distribution of actual mean velocity (non-dimensionalized by smooth section free stream velocity) are shown in Fig. 5.8e. It shows that the accelerated state of flow persists only near the junction point and that the condition dies out gradually in axial direction to attain a fully developed flow condition.

5.3.2 Pressure Gradient along the Duct Axis

Wall static pressures measured through the pressure tappings at the side wall are plotted in Fig. 5.9. There are visibly three major regions in static pressure variation. The first straight line portion represents the smooth wall pressure gradient, the next part shows a sharp pressure drop starting from the smooth rough junction. This pressure drop is associated with the accelerated flow in transition zone as discussed previously in section 5.3.1. The nose dive of pressure is more pronounced at higher Reynolds numbers because the same relative acceleration of flow demands more

velocity increase for higher Reynolds numbers. After about $2D_t$ downstream of the junction, the pressure gradient approaches a new equilibrium value for the rough surface overcoming the transition.

5.3.3 Friction Coefficient and Wall Function

The average wall shear stress for the rough surface is calculated on the basis of near equilibrium value of the pressure gradient, as described in Appendix A. The rough surface friction coefficient is plotted against Reynolds number in Fig. 5.11. The correlation between the two quantities is estimated to be

$$C_f = 0.1357\ Re^{-0.08} \qquad (5.3.1)$$

which shows weak dependence of C_f on Reynolds number for the present case of high roughness.

The friction coefficient for the duct as a whole is also presented in Fig. 5.11. The duct resistance coefficient is found to obey the relation

$$C_f = 0.065\ Re^{-0.11} \qquad (5.3.2)$$

The resistance is found to be on the higher side of the values found by Fujita [25] and Ali [3] . It shows that the frictional resistance increases considerably with the increase of surface roughness, because roughness elements used by Ali [3] and Fujita [25] were much smaller compared to those of the present.

5.3.4 Log-Law Profiles and Wall Function

The logarithmic velocity profiles for different Reynolds numbers are shown in Fig. 5.10. Velocities are normalized by the friction velocity u^* and distances by ν/u^*. The wall distance is measured from an origin determined by the method put forward by Perry and Joubert [54] , and Perry et al [55] . The origin of the universal velocity profiles was found to be at 0.025 in from the roots of the stones or 0.6 in below the average crest height. The log law profiles for the rough surface thus plotted shows the vertical shift from the smooth wall profiles for the same flow situation. This vertical shift is called the 'wall function' of the rough surface and is seen in the Table 5.4 to increase with the roughness Reynolds number $\frac{ku^*}{\nu}$.

Table 5.4 Rough Wall Log-Law Characteristics

$Re_{Dt} \times 10^{-5}$	u^* ft/s	$\frac{ku^*}{\nu}$	B_r	$\frac{\Delta u}{u^*}$
9.80	17.90	1485	-14.95	17.82
7.20	13.35	1130	-14.45	17.25
4.61	8.22	800	-13.63	16.19
2.78	5.98	525	-12.60	14.75

Fig. 5.12 shows the wall function's correlation with the roughness Reynolds number. The wall function is determined from the definition

$$\frac{\Delta u}{u^*} = \left(\frac{u}{u^*}\right)_s - \left(\frac{u}{u^*}\right)_r \qquad (5.3.2)$$

using the experimental values of the right hand side terms. The wall function dependence on roughness Reynolds number is found to be

$$\frac{\Delta u}{u^*} = 5.91 \log \frac{u^* k}{\nu} - 1.0 \qquad (5.3.3)$$

which implies $\kappa = 0.39$. In the light of Hinze's [30] discussion, the intercept portion is sufficiently small to be neglected for the present range of Re_k and the wall function may be taken to be directly proportional to $\log \frac{u^* k}{\nu}$. The slopes of the similar relations obtained by Moore (1951) and Hama (1954) are the same as that of present investigation and Moore's relation is very close to the present one. The roughness of Moore was rib type with small equivalent sand roughness compared to the present case, which suggests that wall function's variation with roughness Reynolds number is not very dependent on roughness height. The data of Furuya and Fujita [26] shows a similar trend for wall function but at a lower range of Re_k. Nikuradse's (1933) sand roughness, on the other hand, exhibits a higher slope than those obtained by others. Clauser [19] dealt with this issue in detail and attributed the variation in different results to the choice of length scale of Re_k - either absolute roughness height or equivalent sand roughness.

5.3.5 Growth of Internal Boundary Layer

Near the smooth-rough junction, the mean velocity profiles of Figs. 5.7 show points of inflexion which move away from the wall in the flow direction. These inflexion points are clearly seen in their semi-log plots in Figs.5.13a-d where these are termed as 'knee points'. In the figure the 'knee points' of each profile are marked. The locus of the outer 'knee points' indicates the growth of inner layer while that of the lower knee points identifies the inner sublayer and they are shown in Fig. 5.15 on logarithmic scale. The lines joining the outer 'knee points' and inner 'knee points' indicate the presence of transition zone which is clearly seen for profile at $x/D_t = 0.75$. Both the growth rates have a nominal slope of 0.46 ($\delta_i \propto x^{0.46}$). For comparison results of Ali and Islam [2], Islam and Logan [35], Antonia and Luxton [5,7] are also shown in Fig. 5.15. Results of sand roughened pipe flow of Ali and Islam [2] coincides with present results, though the scale of roughness in the present study is about 15 times of Ali and Islam's value. Results of Islam and Logan [35] and Antonia and Luxton [7] for upstanding rib type roughness show nearly the same rate of growth ($\delta_i \propto x^{0.50}$) which is higher than the present findings. Results of depressed rib type roughness of Antonia and Luxton [5] show still higher rate ofogrowth ($\delta_i \propto x^{0.79}$) of internal boundary layer. The above analysis indicates that upstanding roughness

initially thickens the boundary layer more than the depressed type of roughness as the flow encounters the roughness change but have lower growth rate than the later type. It is also found that its growth rate is independent of Reynolds number within the experimental range (Re_{Dt} = 9.80×10^5-2.78×10^5) as found by Antonia and Luxton [5] (Re_δ= 1.9×10^4-3.4×10^4).

Islam and Logan [35] tried to correlate the growth rate of different flow conditions. Their correlation successfully predicted the inner layer growth of channel flow measurements, but the pipe flow measurements of Siuru and Logan [64] showed a higher value than the prediction. The discrepencies of Islam and Logan's correlation are thought to be due to the improper selection of length scale, i.e. radius of the pipe or half height of the channel, for normalization.

The growth of inner layer is independent of the outer flow condition and depends mainly on the adjoining surface condition. So instead of using the length scale representative of the broad flow geometry, some length scale representative of the surface itself may be useful in normalizing the inner layer. For this purpose, equation (3.3.9) may be rewritten in the form:

$$\frac{U}{U^*} = \frac{1}{\kappa} \ln \frac{y}{w} \qquad (5.3.4)$$

where w is the length scale representative of the surface and can be expressed by comparing equation (6.3.9) with

eqn. (5.3.4)

$$w = \frac{\nu}{u^*} \exp\left[\kappa\left(\frac{\Delta u}{u^*} - A\right)\right] \qquad (5.3.5)$$

For smooth wall $\frac{\Delta u}{u^*} = 0$, so

$$w = \nu / \left[u^* \exp(\kappa A)\right] \qquad (5.3.6)$$

The present results of inner layer are normalized with w and plotted in Fig. 5.16 with those of Antonia and Luxton [5,7] and Schofield [63] . Within the experimental scatter, all the results seem to lie on a single curve represented by:

$$\frac{\delta_i}{w} = 0.085 \left(\frac{x}{w}\right)^{1.037} \qquad (5.3.7)$$

To indicate the relative roughness change of different experiments, the meteorological parameter M is indicated in the figure where $M = \ln \frac{w_2}{w_1}$, the suffixes 1 and 2 refer to upstream and downstream of the junction respectively.

5.3.6 Axial Distribution of Wall Shear Stress

Mean axial velocities are plotted semilogarithmically in Figs.5.13a-d. The slopes of these graphes near the surface shear stress from the log-law of wall, as described in Appendix A. The shear stress variation in the axial direction is shown in Fig. 5.14. The curve shows that immediately after the junction, there is a steep overshoot of surface shear stress, and shortly afterwards the shear stress gives

a nose dive to a lower value. Then the shear stress moves towards an equilibrium value, which issseen to agree well with the-average value of shear stress obtained from the rough wall pressure gradient as shown in the figure.

The overshoot of wall shear stress in the transition region were also observed by Tani and Makita [65] and Islam and Logan [35] . The reason of this overshoot is thought to be due to the upstanding obstruction to the flow, which offers a sudden high resistance. The pressure gradients are also found to be very steep at the junction (Fig.5.9), justifying this large variation of shear stress. Determination of wall shear stress in the way, as done here, is controversial as the von Karman constant's value is not necessarily the same in all of the flow region.

5.3.7 Secondary Velocity in Mid-Longitudinal Section

Viewing the flow as a two-dimensional one, the vertical components of the mean velocity were measured in the boundary layer undergoing a smooth-rough transition. The angles made by the mean velocity in the mid-longitudinal section of the duct with the axial direction are plotted in Figs. 5.17. The flows are found to have head up direction from the surfaces as they encounter the surface obstacles. The deviation of flow from the axial direction is seen to start at or before 0.25 D_t upstream of the smooth rough junction. The angles are maximum at the junction ($x/D_t=0$) and near the surface. The angles, then, gradually decrease along the flow direction as well as

away from the wall. Only close to the rough wall (y/D_t=0.083), the flow directions are seen to be towards the wall, which is probably due to the local vortices produced around the crests of the big stone chips.

The resultant mean velocity in the mid-longitudinal section is found from the relation

$$u^r = \frac{u}{\cos \gamma} \qquad (5.3.8)$$

where γ is the angle made by the resultant velocity with the axial direction. To show the flow field, the velocity vectors are drawn in Fig. 5.18. The pictorial representation demonstrates the expected pattern of mean flow field. The effect of surface roughness on flow direction is found to die down as the distance from the rough surface increases. The effect of roughness on the flow direction is noticed to be less for higher Reynolds number as one goes away from the wall.

5.3.8 Turbulence Intensity

The longitudinal turbulence intensity of the flow field measured over the rough surface following the smooth-rough junction is presented in Figures 5.19 and 5.20. The ratio between the rms value of the longitudinal component of the fluctuating velocity and local mean axial velocity is plotted against vertical distance from the wall for different axial locations in Fig. 5.19. The plots show that turbulence

intensity is maximum near the surface, both smooth and rough, and reduces as the wall distance increases. The fact is also demonstrated of by the oscillograms of the turbulent fluctuations at different wall distances for x/D_t = 1.0 in Plates 5.1. The turbulence intensity decreases gradually with vertical distance for smooth surface and at smooth-rough junction, but the decrease is sharp and sudden over the rough surface in transition region. Then as one goes in the downstream direction, the rate of decrease of the turbulence intensity away from the wall becomes lower.

Fig. 5.20 shows the pattern of variation of turbulence intensity with x for different wall distances. It is seen from the graphes that the turbulence intensity rises sharply as the flow encounters the roughness, and the rise is more severe near the wall. The same trend was observed by Logan and Jones [46] for the flow in a pipe undergoing a smooth to rough transition. Also it is found that the magnitude of turbulent intensity over the present rough surface is not significantly different from that over the rough surface of Logan and Jones who used very small roughness compared to the present case. This suggests that rough surface turbulence intensity is weakly dependent upon roughness dimensions. After the erratic behaviour in the transition region, the turbulence intensity is seen to proceed towards an equilibrium value approximately from x/D_t = 3.0 downstream from the junction.

A reference is here made to the comment of Hinze [30] that the ratio between the turbulence intensities of rough and smooth surfaces should be 'roughly' equal to the ratio between the rough and smooth wall shear stresses. The two ratios for a few studies are tabulated below.

Table 5.5 Ratios Between Rough Wall and Smooth Wall Shear Stresses and Turbulence Intensities

Author	Roughness	k_s in	τ_r/τ_s	u'_r/u'_s
Logan and Jones [46]	Sand	0.073	3.33	2.33
Ali [4]	Sand	0.040	3.0	2.0
Carper [16]	Rib	0.150	3.0	2.0
Present study	Stone	0.625	10.0	5.0

The table shows that Hinze's contention is crudely true for small wall roughness only and the divergence between the two ratios is higher for high roughness.

CHAPTER VI

CONCLUSIONS

6.1 Introduction

The present research objectives have been achieved and the findings are discussed in chapters V and VI. The important points are again emphasized and summarized in this chapter and possible extension of the present work is underscored.

6.2 Achievements of the Present Work

The measurements of the flow structure over a flat surface following an increase in surface roughness revealed both well-known as well as not-so-known features. To the best of the author's knowledge, this study is the first of its kind in the field of rough wall flow, because no other previous laboratory research used the big size stone chips (k_s = 0.625) as in the present case. The study of the turbulent boundary layer over the stone roughened surface showed that increased surface roughness increases the wall shear stress proportional to the roughness scale while other important flow parameters such as boundary layer thickness, rate of growth of internal boundary layer, wall function, longitudinal turbulence intensity are not proportionately

responsive to the roughness scale for its higher values. In the present measurement, determination of actual flow direction which is away from the wall, explains the fact of boundary layer growth overtthe smooth surface even at the upstream position of the roughened surface.

6.3 Conclusions

The following conclusions are drawn as consequence of the present research work:

1. The boundary layer thickness increases with the increase of surface roughness, but the rate of increase decreases progressively as the roughness height increases.

2. The wall shear stress is greatly dependent upon the surface roghness and increases as the roughness he-ght increases.

3. The static pressure falls suddenly at the smooth-rough junction caused by the flow acceleration due to the reduced flow area.

4. The rough-wall shear stress exhibits a sharp shoot up immediately after the roughness change.

5. For the roughness used in the present research, the flow does not develop 4 hydraulic diameters downstream of the smooth-rough junction.

6. The deviation of mean flow from the axial direction starts before the flow encounters the roughness and dies down as the wall distance increases. This deviation in the upper region is lower for higher Reynolds numbers.

7. The semi-logarithmic velocity profiles show two knee points immediately after the transition but after a distance of $x = 2D_t$, the knee points are not clear.

8. The internal boundary layer thickness is found to be proportional to 0.46 th power of the axial distance from the smooth-rough junction.

9. A length scale based on the surface roughness is competent in predicting the growth rate of internal boundary layer.

10. The wall function, $\Delta u/u^*$, does not considerably depend on the roughness height.

11. The turbulence intensity is maximum near the rough wall and quickly decreases with wall distance. The rough surface turbulence intensity is about six times of the value of the smooth surface.

12. Magnitude of turbulence intensity does not increase proportionately with the roughness height.

6.4 Extension of the Present Work

The study of turbulent flow in the transition region of the surface roughness change has been undertaken by a few workers in the past and has been presented in this thesis. Due to relatively limited amount of measurements performedffor flows over surface with high roughness change, several questions, as regards the turbulence parameters and secondary velocity, are yet to be solved. As a direct extension of the present work, the following suggestions may be made for continuation of the research in the similar flow fields.

1. The same roughness configuration can be used with a longer rough section to allow for the fully developed flow condition after the transition and the flow characteristics in that condition may be studied.

2. Reynolds' shear stress, correlation coefficients, turbulence frequency spectra can be measured on the same type of surface in order to get a greater insight into turbulence structure of the flow field.

3. Roughness elements of size even bigger than those used in the present work may be employed and the work may be repeated to see the effect of roughness size on mean and turbulent quantities.

4. Secondary flow in the boundary layer over the rough surface in the transition region can be studied in more detail by measuring the flow angles in the plane perpendicular to the flow.

5. The effect of roughness change from one small roughness to another larger roughness on the flow may be studied rather than the flow from a smooth to a rough surface.

6. Measurements of flow in sections other than the mid-longitudinal section can be done in the same flow condition.

APPENDICES

APPENDIX A

DETERMINATION OF WALL SHEAR STRESSES

A-1 Shear Stress for Smooth Wall

The wall shear stress for smooth wall is obtained by several independent methods.

The first method calculates smooth wall shear stress from its basic definition, following the method of Preston [58] , which is

$$\tau_{os} = \mu\left(\frac{du}{dy}\right)_o \qquad (A\text{-}1.1)$$

The velocity gradient near the surface is found from the velocity profiles obtained by the measurement with the boundary layer tube. Velocity profiles for different Reynolds numbers were measured both for the smooth wooden floor and the side perspex wall and their respective shear stress are listed in Table A-1.

Table A-1 Wall Shear Stresses Calculated From Velocity Gradients

$Re_{Dt} \times 10^{-5}$	SMOOTH WOODEN FLOOR		SIDE PERSPEX WALL	
	$\left(\frac{du}{dy}\right)_o$ /s	τ_{os} lb/ft^2	$\left(\frac{du}{dy}\right)_o$ /s	τ_{os} lb/ft^2
9.80	150,000	0.0582	93,000	0.0361
7.20	96,000	0.0372	56,000	0.02173
4.61	43,000	0.01668	27,000	0.0105
2.78	21,000	0.0081	12,000	0.00465

Secondly the smooth wall shear stress for the duct calculated from the data of resistance coefficient of Schiller (1923). As described by Schlichting [62] , the smooth duct shear stress is given by

$$\tau_s = \frac{1}{8} \lambda \rho \bar{U}^2 \qquad \text{(A-1.2)}$$

where λ is the resistance coefficient. The values obtained from this equation are given in Table A-2.

The shear stress for smooth surfaces is again determined from the axial pressure gradient of the duct. If the wall shear stres is assumed uniform throughout the perimeter of the duct, then a simple force balance provides

$$\tau_s = \left(\frac{dp}{dx} \right)_s \frac{D_t}{4} \qquad \text{(A-1.3)}$$

where $\frac{dp}{dx}$ is the pressure gradient assessed from the wall static pressures measured by the wall tapings.

However if the difference in wall shear stresses for wooden floor, wall, ceiling and perspex wall is taken into account, then the force balance gives

$$3D_t dx\, \tau_{os} + D_t\, dx\, \tau'_{os} = dp.D_t^2$$

$$\tau_{os} = \left(\frac{dp}{dx}\right)_s \frac{D_t}{3} - \frac{\tau'_{os}}{3} \qquad \text{(A-1.4)}$$

where τ'_{os} is the wall shear stress for perspex wall known from the knowledge of velocity gradient. The values of wall

shear stress obtained by both the eqns. (A-1.3) and (A-1.4) are to be found in Table A-2.

Table A-2 Wall Shear Stresses Calculated from Resistance Coefficient and Pressure Gradient

$Re_{D_t} \times 10^5$	Eqn. (A-1.2) $\lambda_{1} \times 10^2$	τ_s lb/ft^2	$\frac{dp}{dx}$ lb/ft^2-ft	Eqn.(A-1.3) τ_s lb/ft^2	Eqn.(A-1.4) τ_{os} lb/ft^2
9.80	1.06	0.0356	0.1331	0.0499	0.0545
7.20	1.18	0.0220	0.0779	0.0292	0.0317
4.61	1.45	0.0112	0.0388	0.01455	0.0159
2.78	1.65	0.00465	0.0167	0.00626	0.0068

A-2 Shear Stress for Rough Wall

The wall shear stress for rough wall is obtained by two independent methods.

Firstly the axial pressure gradient is employed to calculate rough wall shear stress, the pressure-gradient being found from the measurements of the wall static pressure tappings. A force balance gives

$$D_t dx \, \tau_r + 2D_t dx \, \tau_{os} + D_t \, dx \, \tau'_{os} = dp. \, D_t^2$$

$$\tau_r = \left(\frac{dp}{dx} \right)_r D_t - 2 \tau_{os} - \tau'_{os} \qquad \text{(A-2.1)}$$

where the smooth wall values are those obtained from the velocity gradients. The values of rough wall shear stresses

are listed in Table A-3. The shear stress for the duct as a whole is also calculated using the relation

$$\tau_r = \left(\frac{dp}{dx} \right)_r \frac{D_t}{4} \qquad (A\text{-}2.2)$$

Another method to find out the rough wall shear stress is the use of logarithmic velocity profile over the rough wall

$$\frac{u}{u^*} = \frac{1}{K} \ln \frac{y}{K} + B_r \qquad (A\text{-}2.3)$$

which can be written in the form

$$u = \frac{u^*}{K} \ln y + B_r' \qquad (A\text{-}2.4)$$

Assuming the value of Nikaradse [52] for K to be 0.4 the eqn. (A-2.4) becomes

$$u = 5.75\, u^* \log y + B_r' \qquad (A\text{-}2.5)$$

which is a straight line with slope $m = 5.75\, u^*$. By knowing the slope m from the actual plot of eqn. (A-2.5), m can be obtained to give

$$u^* = \frac{m}{5.75} \qquad (A\text{-}2.6)$$

As by definition

$$u^* = \sqrt{\tau_r/\rho} \qquad (A\text{-}2.6)$$

so finally it is found

$$\tau_r = \frac{\rho m^2}{33.1} \qquad (A\text{-}2.7)$$

APPENDIX B

YAWMETER: A PRESSURE PROBE METHOD OF DETERMINING FLOW DIRECTION

B-1 The Yawmeter

There are two ways by which flow direction can be measured with the help of pressure probes. In the first method a symmetrical arrangement of sensing holes is used. Here the probe system's orientation is adjusted to a position for which the same pressure is sensed at each hole and the flow direction is then found from a correlation with the geometry of the probe. This method is known as 'null-reading' or equibalanced method (Lewkowicz, 1976).

The second method of determination of flow direction is based on the fact that the fraction of total pressure of the flow field sensed by the pressure probe depends on the angle of incidence of the flow with the plane of the probe hole. It is a maximum when the flow is normal to the plane of the probe hole and a minimum when parallel to it. Based on this philosophy a multi-tube probe with holes of different angles of inclination with flow direction is employed to measure the flow angle, which is called 'Yawmeter'. The pressure recovery characteristic or the sensitivity of the probe to 'Yaw' depends on the probe's apex angle. The sensitivity of the yawmeter in incompressible flow can be

expressed as

$$S(\gamma) = \frac{P_1 - P_2}{(P_3 - P_a)\gamma} \qquad (B\text{-}1.1)$$

where P_1 and P_2 are the pressures recorded in the camphered tubes (Fig. 3.2), P_3 is the total pressure recorded by the total head tube of the yawmeter, P_a is the atmospheric pressure and γ is the 'angle of the yawmeter' with respeet to the flow direction. The most important thing is the magnitude of the pressure difference $\Delta P = P_1 - P_2$ which can be detected by the probe and the accuracy with which it can be measured, as these together determine the resolution attainable in the measurement of flow direction. The smallest change of the flow angle which can be detected by a yawmeter system can be expressed by the equation

$$\Delta\gamma = \frac{\Delta P_{min}}{S(\gamma) \times \frac{1}{2}\rho u^2} \qquad (B\text{-}1.2)$$

where ΔP_{min} is the minimum pressure difference that can be read on the manometer and $S(\gamma)$ is the yawmeter sensitivity.

In the present investigation, a multitube (3-tube) yawmeter made from stainless steel tubes of 0.81 mm OD and 0.5 mm ID, with an apex angle of 70^o was used. This value was used by Bryer et al (1958) and gave satisfactory results. The sensitivity of the yawmeter was calculated to be $S(\gamma) = 0.057$. The Furness Co. pressure transducer used in the measurements could read pressure upto an accuracy of

0.5 mm of water in the experimental range. The yawmeters in the present system, thus, could read upto an angle better than 0.2^{o} at an air speed of 85 ft/s. This lower limit of resolution is adequate for the present measurements.

B-2 Calibration of Yawmeter

When a yawmeter is placed in a flow field, the pressures recorded by the different sensing tubes varies with the flow direction. If P_1, P_2 and P_3 are the pressures recorded by the two camphered tubes and the total head tube respectively (Fig. 3.2), then the ratio $(P_1-P_2)\div\{P_3-(P_1+P_2)/2\}$ is a function of flow angle γ . According to Bryer and Pankhurst [15] , within the limit of γ between $\pm 20^{o}$, the variation is linear in the form

$$\frac{P_1 - P_2}{P_3-(P_1+P_2)/2} = C\gamma \qquad \text{(B-2.1)}$$

where C is a constant to be found out experimentally.

During the process of calibration, the yawmeter was placed in the calibration rig at certain angles ($<20^{o}$) with the flow direction. The velocity of the flow was maintained constant, yawmeter's angular position was varied. For each angular position of the yawmeter, the pressures of the three tubes were recorded with the help of a selector valve. The pressure ratio $(p_1-p_2)/[p_3-(p_1+p_2)/2]$ was plotted against the angular position γ on a plane graph paper as shown in Fig.3.3.

The calibration curve obtained showed a small deviation from the pattern of eqn. (B-2.1) that the straight line did not pass through the origin but made a negative intercept on the vertical axis. This was attributed to the assymetry of the placement of the camphered tubes during fabrication.

APPENDIX C

UNCERTAINTY ANALYSIS FOR MEAN QUANTITY MEASUREMENTS

In the present investigation, measurements were taken with great care to minimise the possible sources of error. But the inherent limitations of the sensing transducers and the measuring instruments, the atmospheric changes and the probe settings introduced some error in the process of measurements. Uncertainties thus crept into the measurements of velocity and pressure is analysed in the way as suggested by Kline and McClintock [39] .

C-1 Uncertainty in Mean Velocity Measurements

When air was flowing with a velocity u (ft/s) and a pitot-static was placed parallel to the flow, the velocity was found from the dynamic head h_w(ft) of water recorded by the pressure transducer from the relation

$$u = \sqrt{\frac{2gh_w\gamma_w}{\gamma_a}} \qquad \text{(C-1.1)}$$

where γ_w and γ_a were the specific weights of water and air respectively. If the sensing point of the pitot-static had a misalignment of θ from the direction of flow due to adjustment error, then the measured velocity would be

$$u = \sqrt{\frac{2gh_w\gamma_w}{\gamma_a}} \cos\theta \qquad \text{(C-1.2)}$$

Using $P = \gamma_a RT$ (C-1.3)

where P, R and T are pressure, gas constant and absolute temperature of air respectively, velocity becomes

$$u = \sqrt{2gh_w\gamma_w RT/P}\cos\theta$$

$$u = \sqrt{2g\gamma_w R/(25.4\times12)}\sqrt{h_w T/P}\cos\theta \qquad (C\text{-}1.4)$$

where transducer reading is in mm of water.

Now the question of variation of specific weight of water during measurements does not arise as pressure transducer was used for measurements. The small variation of density of the micromanometer liquid during the short period of calibration of the transducer has negligible effect on the final reading.

The uncertainty in velocity measurement can thus be expressed as

$$U_u = \left[\left(\frac{\partial u}{\partial p}U_p\right)^2 + \left(\frac{\partial u}{\partial T}U_T\right)^2 + \left(\frac{\partial u}{\partial h_w}U_{hw}\right)^2 + \left(\frac{\partial u}{\partial \theta}U_\theta\right)^2\right]^{\frac{1}{2}} \qquad (C\text{-}1.5)$$

where U_p, U_T, U_{hw} and U_θ are uncertainties associated with pressure, temperature, transducer reading and alignment of the probe with flow direction.

To get the uncertainties involved in the different variables the respective partial derivatives are now found out. Rewriting eqn. (C.1.4) in the form

$$u = C\sqrt{h_w T/P}\cos\theta \qquad (C\text{-}1.6)$$

where $C = \sqrt{2g\gamma_w R}/304.8$ (C-1.7)

the partial derivatives of u are found to be

$$\frac{\partial u}{\partial p} = -\frac{C}{2}\sqrt{h_w T/P^3}\cos\theta \qquad \text{(C-1.8)}$$

$$\frac{\partial u}{\partial T} = \frac{C}{2}\sqrt{h_w/(TP)}\cos\theta \qquad \text{(C-1.9)}$$

$$\frac{\partial u}{\partial h_w} = \frac{C}{2}\sqrt{T/(h_w P)}\cos\theta \qquad \text{(C-1.10)}$$

$$\frac{\partial u}{\partial \theta} = -C\sqrt{h_w T/P}\sin\theta \qquad \text{(C-1.11)}$$

Combining these equations with eqn. (C-1.5) we get

$$U_u = \frac{C}{2}\cos\theta\left[\left(\frac{h_w T}{P^3}\right)U_p^2 + \left(\frac{h_w}{TP}\right)U_T^2 + \left(\frac{T}{h_w P}\right)U_{hw}^2 + 4\left(\frac{hT}{P}\right)U_\theta^2\tan^2\theta\right]^{\frac{1}{2}} \qquad \text{(C-1.12)}$$

From eqns. (C.1.5) and (C.1.12), the uncertainty in velocity measurement takes the form

$$\frac{U_u}{u} = \frac{1}{2}\left[\frac{U_p^2}{p^2} + \frac{U_T^2}{T^2} + \frac{U_{hw}^2}{h_w^2} + 4\,U_\theta^2\tan^2\theta\right]^{\frac{1}{2}} \qquad \text{(C-1.13)}$$

Now during an experimental run, the following conditions were observed:

$P = 29.98 \pm 0.05$ in of Hg

$T = 90^o \pm 2^o$ F

$h_w = 80 \pm 0.5$ mm of H_2O

$\theta = 0^o \pm 2^o$

The corresponding uncertainty in velocity measurement becomes $\frac{U_u}{U} = 0.0116$ or 1.16% .

C-2 Uncertainty in Static Pressure Measurement

The wall static pressures measured from the wall tappingswere the gage pressures below atmospheric pressure. If p be the absolute static pressure and P_a be the atmospheric pressure, then the recorded pressure would be

$$P_r = P_a - p \qquad (C\text{-}2.1)$$

and the absolute static pressure

$$p = P_a - P_r \qquad (C\text{-}2.2)$$

The recorded pressure is nothing but $\gamma_w h_w$, so that

$$p = P_a - \gamma_w h_w \qquad (C\text{-}2.3)$$

Since change of density of water is irrelevant in transducer, the uncertainty in wall static pressure measurement is

$$U_p = \left[\left(\frac{\partial p}{\partial P_a} U_{P_a} \right)^2 + \left(\frac{\partial p}{\partial h_w} U_{hw} \right)^2 \right]^{\frac{1}{2}} \qquad (C\text{-}2.4)$$

Now $$\frac{\partial p}{\partial P_a} = 1 \qquad (C\text{-}2.5)$$

$$\frac{\partial p}{\partial h_w} = -\gamma_w \qquad (C\text{-}2.6)$$

Since for a short interval, $U_p = 0$ and for an experiment, p = 14.55 psi (2095 psf), U_{hw} = 0.5 mm of H_2O, the uncertainty becomes

$$\frac{U_p}{p} = \frac{62.4}{2095} \times \frac{0.5}{25.4 \times 12} = 5 \times 10^{-5} \text{ i.e. } 0.005\%$$

However the static pressure recording was greatly prone to the deviation from the squareness of the static pressure holes.

When static pressure was measured by pitot-static tube, the recorded static pressure was subjected to error of misalignment. If h was the transducer reading, then the recorded pressure would be

$$p_r = \gamma_w h_w - \frac{\gamma_a}{2g} u^2 \cos^2(90^o - \theta) \qquad \text{(C-2.7)}$$

which can be reduced to the form

$$p_r = \frac{\gamma_w}{25.4 \times 12} h_w - \frac{p_a u^2}{2gRT} \sin^2\theta \qquad \text{(C-2.8)}$$

h being measured in mm of water.

Eqn. (C.2.8) is now looked upon as

$$p_r = p_1 + p_2 \qquad \text{(C-2.9)}$$

where $p_1 = \frac{\gamma_w}{304.8} h_w \equiv C_1 h_w$ (C-2.10)

$$\text{and} \quad p_2 = -\frac{p_a u^2}{2gRT}\sin^2\theta \equiv C_2 \frac{p_a u^2}{T}\sin^2\theta \qquad (C\text{-}2.11)$$

If U_{p_1} and U_{p_2} are uncertainties in p_1 and p_2 respectively, then accordingly

$$U_{p_1} = \left(\frac{\partial p_1}{\partial h}\right) U_{h_w} \qquad (C\text{-}2.12)$$

$$\text{or} \quad \frac{U_{p_1}}{p_1} = \frac{U_{hw}}{h_w} \qquad (C\text{-}2.13)$$

$$\text{and } U_{p_2} = \left[\left(\frac{\partial p_2}{\partial p} U_p\right)^2 + \left(\frac{\partial p_2}{\partial T} U_T\right)^2 + \left(\frac{\partial p_2}{\partial u} U_u\right)^2 + \left(\frac{\partial p_2}{\partial \theta} U_\theta\right)^2\right]^{\frac{1}{2}} \qquad (C\text{-}2.14)$$

Evaluating the partial derivatives as

$$\frac{\partial p_2}{\partial p_a} = C_2 \frac{u^2}{T}\sin^2\theta \qquad (C\text{-}2.15)$$

$$\frac{\partial p_2}{\partial T} = -\frac{C_2 p_a u^2}{T^2}\sin^2\theta \qquad (C\text{-}2.16)$$

$$\frac{\partial p_2}{\partial u} = \frac{2C_2 p_a u}{T}\sin\theta \qquad (C\text{-}2.17)$$

$$\frac{\partial p_2}{\partial \theta} = \frac{2C_2 p_a u^2}{T}\sin\theta\cos\theta \qquad (C\text{-}2.18)$$

the uncertainty of p_2 can be written, with the help of eqn. (C.2.11), as

$$\frac{U_{p_2}}{p_2} = \left[\left(\frac{U_{p_a}}{p_a}\right)^2 + \left(\frac{2U_u}{u}\right)^2 + \left(\frac{U_T}{T}\right)^2 + \left(\frac{2U}{\tan\theta}\right)^2\right]^{\frac{1}{2}} \qquad (C\text{-}2.19)$$

Now from eqn. (C.2.9), the uncertainty in measurement of p_r is

$$U_{p_r} = \left[\left(\frac{\partial p_r}{\partial p_1} U_{p_1}\right)^2 + \left(\frac{\partial p_r}{\partial p_2} U_{p_2}\right)^2\right]^{\frac{1}{2}}$$

$$= \left[U_{p_1}^2 + U_{p_2}^2\right]^{\frac{1}{2}}$$

For an experimental situation, the following values are taken:

$p_a = 29.98 \pm 0.05$ in of H_g

$T = 90^o \pm 2^o$ F

$h_w = 95 \pm 0.5$ mm of H_2O

$u = 112 \pm 1.23$ ft/s

$\theta = 0^o \pm 2^o$

From eqns. (C.2.10), (C.1.11), (C.2.13), (C.19) and (C.2.20)

$p_1 = 19.45$

$p_2 = 0.206$

$\frac{U_{p_1}}{p_1} = 0.0053$

$\frac{U_{p_2}}{p_2} = 1.999$

$U_{p_r} = 0.4245$

$\frac{U_{p_r}}{p_r} = 0.022$ i.e uncertainty is 2.2%.

APPENDIX D

BASIC PRINCIPLE OF HOT-WIRE ANEMOMETRY

In the hot-wire anemometry, the amount of heat loss from the electrically heated wire filament inside the flow field is the measuring criterion. The total amount of heat transfer from the wire to the fluid depends on several factors viz. the flow velocity, the temperature difference between the wire and the fluid, the physical properties of the fluid and the physical properties and dimensions of the wire filament. Of these factors, all are generally known except the flow velocity, which can be measured.

The hot wire is cooled by the heat conduction to the fluid and the supports, forced convection and free convection, and radiation. A brief account of conduction to the supports is given in ref. [14] . The effect of radiation is generally neglected and that of free convection may also be neglected for a wide range of application, e.g. when $Re_d > 0.50$.

For cases in which the effects of compressibility and free convection can be neglected, and without accounting for any conduction to the supports, many investigators have collected data on heat transfer from a right circular cylinder to either a gas or a liquid. The emperical relation

$$Nu = 0.42\ Pr^{0.20} + 0.57\ Pr^{0.33}\ Re^{0.50} \qquad (D\text{-}1)$$

$$0.71 < Pr \leq 1000$$

as suggested by Kramers [40] and supported by van der Hegge Zijnen (ref. [30]) gives very satisfactory results for most gases and liquids. For air, it has proved to be valid in the range

$$0.01 < Re < 10{,}000,$$

Re based on the diameter of the wire, which covers the major range of all applications. Another relation

$$Nu = 0.75\ Pr^{0.20} + 0.67\ Pr^{0.90}\ Re^{0.50} \qquad (D\text{-}2)$$
$$0.85 < Pr < 1.6$$

adopted by Bourke et al. [11] appears to include the heat conduction to the supports along with the forced convection, but has very limited applicability.

The heat flow rate to the ambient fluid from heated wire of length L and uniform temperature t_w is

$$Q = \pi d L h\ (t_w - t_g) \qquad (D\text{-}3)$$

With the aid of Kramer's correlation, equation (D-1) and using $Nu = \frac{hd}{k_f}$, the heat flow rate becomes

$$Q = \pi k_f L (t_w - t_g)\ [0.42(Pr)_f^{0.20} + 0.57(Pr)_f^{0.33}\ (Re)_f^{0.50}] \qquad (D\text{-}4)$$

the subscript f refers to the so called film temperature $(t_w + t_g)/2$.

For steady thermal equilibrium conditions, this heat loss rate must be equal to the heat generation rate by the

electric current passing through the wire, which is given by

$$Q = I^2 R_w \qquad (D\text{-}5)$$

I being the heating current and R_w the total electric resistance of the wire. Thus we have

$$I^2 R_w = e\,\pi k_f L (t_w - t_g)\,[0.42(Pr)_f^{0.20} + 0.57(Pr)_f^{0.33}(Re)_f^{0.50}] \qquad (D\text{-}6)$$

where e is a suitable conversion factor.

The temperature dependence of the wire resistance may be expressed as

$$R_w = R_o\,[1 + \psi(t_w - t_g)] \qquad (D\text{-}7)$$

where R_o is wire resistance at a reference temperature t_o and ψ is the temperature coefficient of the electric resistivity of the wire.

Substituting the value of $(t_w - t_g)$ from equation (D-7) into equation (D-6)

$$I^2 R_w = \frac{e\,\pi k_f L}{\psi} \cdot \frac{R_w - R_g}{R_o}\,[0.42(Pr)_f^{0.20} + 0.57(Pr)_f^{0.33}(Re)_f^{0.50}] \qquad (D\text{-}8)$$

which can be reduced to the form

$$I^2 = \frac{(R_w - R_g)}{R_w}\,[A_1 + B_1\sqrt{U}] \qquad (D\text{-}9)$$

where $A_1 = 0.42 \frac{\pi k_f L}{\psi R_o} (Pr)_f^{0.20}$ (D-10)

and $B_1 = 0.57 \frac{\pi k_f L}{\psi R_o} (Pr)^{0.33} \left(\frac{\rho_f d}{\mu_f} \right)^{0.50}$ (D-11)

and A and B are essentially constant.

Equation (D-9) is the fundamental and most useful equation in constant current hot-wire anemotnetry. Originally, the relation used for describing cooling of the wire by gas flow was not equation (D-1) , but was of the form

$$Nu = f\ (Pr, Re)$$

as suggested by King (ref. [30]) on the assumption of potential flow around the wire. Then the final equation takes the form

$$I^2 = \frac{R_w - R_g}{R_w} [A_1 - B_1 \sqrt{Re}] \quad \text{(D-12)}$$

where A_1 and B_1 are constants.

In equation (D-9) and (D-12) , the expressions for A_1 and B_1 differ appreciably. But the general practice of hot-wire anemometry is to determine the constants experimentally rather than calculating them out.

In constant current anemometry, the current through the wire is kept at a fixed level and the velocity is estimated from the knowledge of the current, as shown above.

In constant temperature anemometry, on the contrary, the temperature or in other words, the electric resistance of

the wire is maintained at a constant value with the help of a feed-back system. The flow velocity is estimated from the knowledge of the voltage across the wire. Using the relation $V = I R_w$, it is found from equation (D-9)

$$V^2 = R_w(R_w - R_g) [A_1 + B_1\sqrt{U}] \qquad (D\text{-}13)$$

which is the basic equation of constant temperature hot-wire anemometry.

PRESSURE TRANSDUCER

In place of the conventional liquid column manometer, pressure transducers are quickly coming up in use for pressure measurements which convert the pressures into some equivalent electrical signals. Transducer's electronic circuits respond to pressure variations by the change of some resistance, capacitance or inductance which is recorded in the form voltage or current. The magnitude of the pressure is obtained from the calibrated pattern of the output signal of the transducer.

The basic construction of a pressure transducer consists of two closed chambers separated by a common diaphragm. A pressure differential created between the chambers deflect the diaphragm. The deflection or strain thus produced is exploited to generate a suitable output signal.

In the electrical resistance type pressure transducer, a strain gage is fitted to the diaphragm to sense the pressure (Fig.4.11a). The corresponding change in resistance in the gage due to the strain in the diaphragm is recorded by a galvanometer through the use of a Wheatstone type of bridge, which gives the information about the applied pressure.

In capacitance type pressure transducer, the deflection of the diaphragm is utilized to vary a closed space thus to cause the change of capacitance in a circuit as shown in Fig.4.11b. The capacitor's response is picked up by a suitable output device via a suitable bridge circuit, giving a measure of the pressure.

The deflection of the diaphragm is used to impart movement to a magnetic core, in the inductance type pressure transducer. Here the device consists of a primary and a secondary coil. An alternating input voltage is impressed upon in the primary coil. The output voltage of the secondary coil depends on the inductive coupling between the core and the coils, which is, in turn dependent on the relative position of the core and the coils. Thus, the output voltage gives an indication of the pressure applied at the diaphragm (Fig.4.11c).

The Furness Controls Ltd. pressure transducer used in the present experiments was a capacitance type one, in which the output signal was obtained on a voltmeter dial graduated directly in mm of H_2O. There were six different ranges of the scale (0 - 30 mm, 0 - 10 mm, 0 - 30 mm, 0 - 100 mm, 0 - 300 mm, 0 - 1000 mm) and the output voltage was to vary linearly with pressure, being 1.0 volt for full scale deflections.

REFERENCES

1. Ali, M.A.T., and Islam, O., "Development of a turbulent flow in a smooth pipe following a rough pipe", *J. Institution of Engineers Bangladesh*, Vol. 10, No.2, p. 19, 1982.

2. Ali, M.A.T., and Islam, O., "Flow in a pipe following an abrupt decrease in surface roughness", *Proc. 12th South-eastern Conference on Theoretical and Applied Mechanics, Auburn University*, 1984.

3. Ali, M.A.T., "Flow through square ducts with rough ribs", *Ph.D. Thesis, Imperial College, London*, 1980.

4. Ali, M.A.T., "Flow in a pipe following an abrupt decrease in surface roughness", *M.Sc. Thesis, Bangladesh University of Engineering & Technology*, 1973.

5. Antonia, R.A., and Luxton, R.E., "The response of a turbulent boundary layer to a step change in surface roughness. Part 1. Smooth to rough", *J. Fluid Mechanics*, Vol. 48, Part 4, p. 721, 1971.

6. Antonia, R.A., and Luxton, R.E., "The response of a turbulent boundary layer to a step change in surface roughness. Part 2. Rough to smooth", *J. Fluid Mechanics*, Vol. 53, Part 4, p. 737, 1972.

7. Antonia, R.A., and Luxton, R.E., "The response of a turbulent boundary layer to an upstanding step change in surface roughness", *Transactions of the ASME, J. Basic Engineering*, p. 22, March 1971.

8. Antonia, R.A., and Wood, D.H., "Calculation of a turbulent boundary layer downstream of a small step change in surface roughness", *Aeronautical Quarterly*, Vol. , p. 202, 1975.

9. Asano, Y., "Friction coefficient of flow through square ducts with different rough surfaces", *Transactions of JSME*, Vol. 38, p. 3223, 1972.

10. Aytekin, A., and Berger, F.P., "Turbulent flow in rectangular ducts with low aspect ratios having one rough wall", *Dept. of Nuclear Eng.; Queen Mary College, University of London*, (Unpublished Report),1980.

11. Bourke, P.J., Paulling, D.J., Gill, L.E., and Denton, W.H., "The measurement of turbulent velocity fluctuations and turbulent temperature fluctuations in the supercritical region by a hot-wire anemometer and a "cold" wire resistance thermometer", *Proc. Instn. Mech. Engrs.*, Part 31, p. 182, 1968.

12. Bradley, E.F., "A micrometeorological study of velocity profiles and surface drag in the region modified by a change in surface roughness", *Quarterly J.R. Met. Soc.*, Vol. 94, p. 361, 1968.

13. Bradshaw, P., "Experimental Fluid Mechanics", 2nd edition, *Pergamon Press, Oxford*, 1970.

14. Bradshaw, P., "An Introduction to Turbulence and its Measurement", *Pergamon Press, Oxford*, 1975.

15. Bryer, D.W., and Pankhurst, R.C., "Pressure-probe Methods for Determining Wind Speed and Flow Direction", *Her Majesty's Stationery Office*, London, 1971.

16. Carper, H.J., "A study of the turbulent intensities and correlation coefficients in the incompressible flow of air in transition from a smooth to rough wall in a two-dimensional channel", *M.S. Thesis, The Agricultural and Mechanical College of Texas*, 1972.

17. Chang, J.E., Logan, E., Alexander, M.B., and Camp, D.W., "The response of a disturbed pipe flow to an upstanding roughness element", *Proc. 2nd Symposium on Turbulent Shear Flows, Imperial College, London*, p. 618, 1979.

18. Clark, J.A., "A study of incompressible turbulent boundary layers in channel flow", *Transactions of the ASME, J. Basic Eng.*, p. 455, Dec. 1968.

19. Clauser, F.H., "The turbulent boundary layer", *Advances in Applied Mechanics*, Vol. IV, Academic Press, 1956.

20. Clauser, F.H., "Turbulent boundary layer in adverse pressure gradient", *J. Aero. Science*, Vol. 21, p.91, 1954.

21. Coles, D., "The law of the wake in the turbulent boundary layer", *J. Fluid Mechanics*, Vol. 1, p. 191,1956.

22. Corrsin, S., "Turbulence: experimental methods", *Handkuchden Physik*, Vol.8, Part 2, Springer, Berlin, 1963.

23. Elliott, W.P., "The growth of the atmospheric internal boundary layer", *Transactions, American Geophysical Union*, Vol. 39, No. 6, p. 1048, 1958.

24. Estoque, M.A., "A numerical model of the atmospheric boundary layer", *J. Geophysical Research*, Vol. 68, No. 4, p. 1103, 1963.

25. Fujita, H., "Turbulent flows in square ducts consisting of smooth and rough planes", *Research Reports of Faculty of Engg., Mie University*, Vol. 3, 1978.

26. Furuya, Y., and Fujita, H., "Turbulent boundary layers on wire-screen roughness", *Bulletin of JSME*, Vol. 10, No. 37, p. 77-86, 1967.

27. Furuya, Y., Miyata, M., and Fujita, H., "Turbulent boundary layer and flow resistance on plates roughened by wires", *Transactions of ASME, J. Fluid Engineering*, Vol. 98, p. 635, 1976.

28. Furuya, Y., and Fujita, H., "Effect of surface roughness on velocity defect law", *The Physics of Fluids Supplement*, p. S155, 1967.

29. Faruque, P.M.O., "Experimental investigation of two dimensional wakes behind flat plates", *M.Sc. Thesis, Bangladesh University of Engineering & Technology*, 1983.

30. Hinze, J.O., "Turbulence", 2nd edition, *McGraw-Hill Book Co.*, 1975.

31. Holman, J.P., "Experimental Methods for Engineers", 3rd edition, *McGraw-Hill Book Co.*, 1978.

32. Huston, W.B., "Accuracy of airspeed measurements and flight calibration procedures", *NACA Technical Report* No. 919, 1948.

33. Islam, S.M.N., "Design and construction of a closed circuit wind tunnel", *M.Sc. Thesis, Bangladesh University of Engineering & Technology*, 1975.

34. Islam, O., "The determination of the turbulent intensities in a transitional flow from a smooth to a rough wall with zero pressure gradient in a two-dimensional channel", *M.S. Thesis, The Agricultural and Mechanical College of Texas*, 1963.

35. Islam, O., and Logan, E., "Channel flow over a smooth-to-rough surface discontinuity with zero pressure gradient", *Transactions of the ASME, J. Fluids Engg.*, p. 626, Dec. 1976.

36. Jacobs, V.W., "Umformung eines turbulenten geschwindigkeitsprofiles", *Z. Angew. Math. Mech.*, Vol. 19, p. 87, 1939.

37. Khalil, G.M. "The initial region of a plane turbulent mixing layer", *Ph.D. Thesis, Bangladesh University of Engineering & Technology*, 1982.

38. Klebanoff, P.S., "Characteristics of turbulence in a boundary layer with zero pressure gradient", *NACA Technical Report* No. 3187, 1954.

39. Kline, S.J., and McClintock, F.A., "Describing uncertainties in single-sample experiments", *Mechanical Engg.*, Vol. 75, No. 1, p.3, 1958.

40. Kramers, H. *Physica*, Vol. 12, p. 61, 1946.

41. Laufer, J., "Investigation of turbulent flow in a two-dimensional channel", *NACA Report* No. 1053, 1951.

42. Laufer, J., "Two-dimensional turbulent channel flow", *NACA Technical Report* No. 2123, 1950.

43. Launder, B.E., and Spalding, D.B., "Mathematical models of turbulence", *Academic Press, London*, 1972.

44. Lawn, C.J., and Hamlin, M.J., "Velocity measurements in an internally roughened pipe", *Central Electricity Generating Board, Research & Development Deptt, Berkley Nuclear Laboratories*, RD/B/N 1156, Sept. 1968.

45. Logan, E., and Fichtl, G.H., "Rough-to-smooth transition of an equilibrium neutral constant stress layer", *NASA Technical Memorandum*, NASA TM X-3322, Dec.1965.

46. Logan, E., and Jones, J.B., "Flow in a pipe following an abrupt increase in surface roughness", *Transactions of the ASME, J. Basic Engineering*, p. 1, March 1963.

47. Mantle, P.L., "A new type roughened heat transfer surface selected by flow visualization techniques", *Proc. 3rd International Heat Transfer Conference*, Vol. 1, p. 45.

48. McMillan, F.A., "Experiments on pitot tubes in shear flow", *Report Memor. Aeronautical Research Council, London*, No. 3028, 1956.

49. Miyata, M., and Ram, V.V., "A study of the scales involved in the adjustment of turbulent channel flow to a step change in wall roughness", *Proc. 1st Asian Congress of Fluid Mechanics, IIS, Bangalore*, p. 1, 1980.

50. Nikuradse, J., Untersuchungen uber die geschwindigkeitsverteilung in turbulenten stromungen", VD 1, *Forschungsheft*, Vol. 70, p. 1229, 1926.

51. Nikuradse, J., "Gesetzmabigkeiten der turbulenten stromung in glatten rohren", VD 1, *Forschungsheft*, p. 356, 1932.

52. Nikuradse, J., "Laws for flow in rough pipes", *NACA Technical Memorandum* p.1292, 1950.

53. Panofsky, H.A., and Townsend, A.A., "Change of terrain roughness and the wind profile", *Quart. J. Royal Met. Society*, Vol. 90, p. 147, 1964.

54. Perry, A.E., and Joubert, P.N., "Rough-wall boundary layers in adverse pressure gradients", *J. Fluid Mechanics*, Vo. 17, Part 2, p. 193, 1963.

55. Perry, A.E., Schofield, W.H., and Joubert, P.N., "Rough wall turbulent boundary layers", *J. Fluid Mechanics*, Vol. 37, Part 2, p. 383, 1969.

56. Peterson, E.W., "Modification of mean flow and turbulent energy by a change in surface roughness under conditions of neutral stability", *Quart. J.R. Met. Soc.*, Vol. 95, p. 561, 1969.

57. Prandtl, L., "Bericht uber untersuchungen zur ausgebildeten turbulenz", *ZAMM 5*, p. 136, 1925.

58. Preston J.H., "The determination of turbulent skin friction by means of pitot tubes", *J.R. Aeronautical Society*, Vol. 58, 1954.

59. Rao, K.S., Wyngaard, J.C., and Cote, O.R., "The structure of the two-dimensional internal boundary layer over a sudden change of surface roughness", *J. Atmospheric Science*, Vol. 31, p. 738, 1974.

60. Reichard, H., "Messungen turbulenten schwankungen", *Naturwissenschaften*, p. 404, 1938.

61. Robertson, J.M., "The turbulent velocity distribution in rough pipe", *5th Mid Western Conference on Fluid Mechanics*, p. 67, 1957.

62. Schlichting, H., "Boundary-Layer Theory", 6th edition, *McGraw-Hill Book Co., New York*, 1968.

63. Schofield, W.H., "Measurements in adverse-pressure-gradient turbulent boundary layers with a step change in surface roughness', *J. Fluid Mechanics*, Vol. 70, Part 3, p. 573, 1975.

64. Siuru, W.D., and Logan, E., "Response of a turbulent pipe flow to a change in roughness", *Transactions of the ASME, J. Fluids Engg.*, p. 548, Sept. 1977.

65. Tani, I., and Makita, H., "Response of a turbulent shear flow to a step wise change in wall roughness", *Z. Flugwiss*, Vol. 19, 8/9, p. 335, 1971.

66. Taylor, P.A., "On wind and shear stress profiles above a change in surface roughness", *Quart., J. Royal Met. Soc.*, Vol. 95, p. 77, 1969.

67. Taylor, P.A., "The planetary boundary layer above a change in surface roughness", *J. Atmospheric Sciences*, Vol. 26, p. 432, 1969.

68. Taylor, J.R., "An Introduction to Error Analysis", *University Science Books, Mill Valley, California*, 1980.

69. Thomas, D.L., and Easter, P.G., "Measurement of wall shear stress in a duct of square cross section", *CEGB Report, Berkeley Nuclear Laboratories, R & D Dept.* RD/B/N 2477, 1972.

70. Townsend, A.A., "The response of a turbulent boundary layer to abrupt changes in surface conditions", *J. Fluid Mechanics*, Vol. 22, Part 4 , p. 799, 1965.

71. Townsend, A.A., "The flow in a turbulent boundary layer after a change in surface roughness", *J. Fluid Mechanics*, Vol. 26, Part 2, p. 255, 1966.

72. Townsend, A.A., "Self-preserving flow inside a turbulent boundary layer", *J. Fluid Mechanics*, Vol. 22, Part 4, p. 773, 1965.

73. Townes, H.W., and Sebersky, R.H., "Experiments on the flow over rough surface", *International J. Heat and Mass Transfer*, Vol. 9, p. 729, 1966.

74. Townes, H.W., Glow, J.L., Powe, R.E., and Weber, N., "Turbulent flow in smooth and rough pipes", *Transactions of the ASME, J. Basic Engg.*, p. 353, 1972.

75. Wood, D.H., and Antonia, R.A., "Measurements in turbulent boundary layer over a d-type surface roughness", *Transactions of the ASME, J. Applied Mechanics*, p. 591, Sept. 1975.

76. Whitehead, A.W., "The effects of surface roughening on fluid flow and heat ransfer", *Ph.D. Thesis, University of London*, 1976.

77. Wilkie, D., "Calculation of heat transfer and flow resistance of-rough and smooth surfaces contained in a single passage", *Proc. 3rd International Heat Transfer Conference*, Vol. 1, p.20, 1966.

ADDITIONAL REFERENCES

1. Berger, F.P. and Whitehead, A.W., "Fluid flow and heat transfer in tubes with integral square rib roughening", *J. British Nuclear Energy Society*, Vol. 16, p. 153, 1977.

2. Betterman, D., "Contribution a l'etude de la convection force turbulente le long de plaques ruguses", *International J. Heat and Mass Transfer.* Vol. 9, p. 153,1966.

3. Blasius, H., "Das ahnlichkeitsgesetz bei reibungs-vorgangen in flussigkeiten", *Forschg. Arb. Ing.-Wes., Berlin*, No. 131, 1913.

4. Bradshaw, P., Ferris, D.H., and Atwell, A.N., "Calculation of turbulent boundary layer development using the turbulent energy equation", *J. Fluid Mechanics*, Vol.28, p. 593, 1967.

5. Bryer, D.W., Walshe, D.E., and Garner, H.C., "Pressure probes selected for three-dimensional flow measurements", *Aero. Research Council, RM 3037*,1958.

6. Deacon, E.L., "Vertical profiles of mean wind in the surface layers of the atmosphere", *Meteorological Office, London, Geophys. Memo.*, Vol. 11, No.91, 1953.

7. Hama, F.R., "Boundary layer characteristics for smooth aand rough surfaces", *Trans. Soc. Naval Archit & Marine Engr.*, NY 62, p. 333, 1954.

8. Hanjalic, K. and Launder, B.E., "Fully developed asymmetric flow in plane channel", *J. Fluid Mechanics*, Vol. 52, p. 301, 1972.

9. Heilhecker, J.K., "The determination of the Reynolds shear stress distribution in the transition region resulting from a change in wall roughness in a two dimensional channel", *M.S. Thesis, Agricultural and Mechanical College of Texas, 1962.*

10. Hermann, R., "Experimentelle untersuchungen zum widerstandsgesetz des kreisrohres bei hohen Reynoldsschen zahlen and groben anlauflangen", *Diss Leipzig Akad Verlagsgesselschaft, Leipzig,* 1930.

11. Launder, B.E., and Ying, W.M., "Prediction of flow and heat transfer in ducts of square cross section", *Proc. Institute of Mechanical Engineers,* Vol.187, p. 73, 1973.

12. Lawn, C.J., "The use of eddy viscosity model to predict the heat transfer and pressure drop performance of roughened surface", *CEGB Report,* RR/B/N 1287, 1971.

13. Lettau, H.H., et al, "Studies of the three-dimensiona structure of the planetary boundary layer", *Annual Report, U.S. Army Electronic Proving Ground,* DA 36-039-SC, 80282, 1962.

14. Lewkowicz, A.K., "Review of the pitot/static methods in incompressible and compressible flows", *Bulletin, Dept. of Mechanical Engineering,University of Liverpool,* 1976.

15. Lin, C.K. and others, "An experimental study of turbulent boundary layer on rough walls", *Thermosciences Division, Stanford University,* Report no. MD-15, 1966.

16. Moody, L.F., "Friction factors for pipe flow", *Transactions of ASME* Vol. 66, p. 671, 1944.

17. Moore, W.L., "An experimental investigation of the boundary layer development along a rough surface", *Ph.D. Thesis, Iowa State University*, 1951.

18. Nikuradse, J. "Turbulente stromung in nicht kreisformigen rohren", *Ing. Arch.*, Vol.1, p.306, 1930.

19. Nikuradse J. "Gesetzmabigkeit der turbulenten stromung in glatten rohren", *Forsch. Arb. Ing.-Wes.*, No. 356, 1932.

20. Nunner, W., "Warmeubergang und druckabfall in rauhen rohren", *VDI-Forschungsheft 455*, Vol.22, p.5, 1958.

21. Patel, V.C., "Calibration of Preston tube and limitation on its use in pressure gradients", *J. Fluid Mechanics*, Vol. 44, Part 4, p. 721, 1965.

22. Schiller, L., "Uber den stromungswiderstand von rohren verschiedenen querschnitts -und rauhigkeitesgrades", *ZAMM*. Vol.3, p.2, 1923.

23. Stanton, T.E., and Pannel, J.R., "Similarity of motion in relation of the surface friction of fluids", *Phil. Trans. Roy. Soc., London*, Vol. A91, p. 46,1915.

24. Streeter, V.L., "Frictional resistance in artificially roughened pipes", *Proc. American Soc. Civil Engineers*, Vol.61, p.163,1935.

25. Taylor, R.J., "Small-scale advection and the neutral wind profile", *J. Fluid Mechanics*, Vol.13, p.529,1962.

26. Taylor, P.A., "On turbulent wall flows above a change in surface roughness", *Ph.D. Thesis, University of Bristol*, 1967.

LIST OF FIGURES

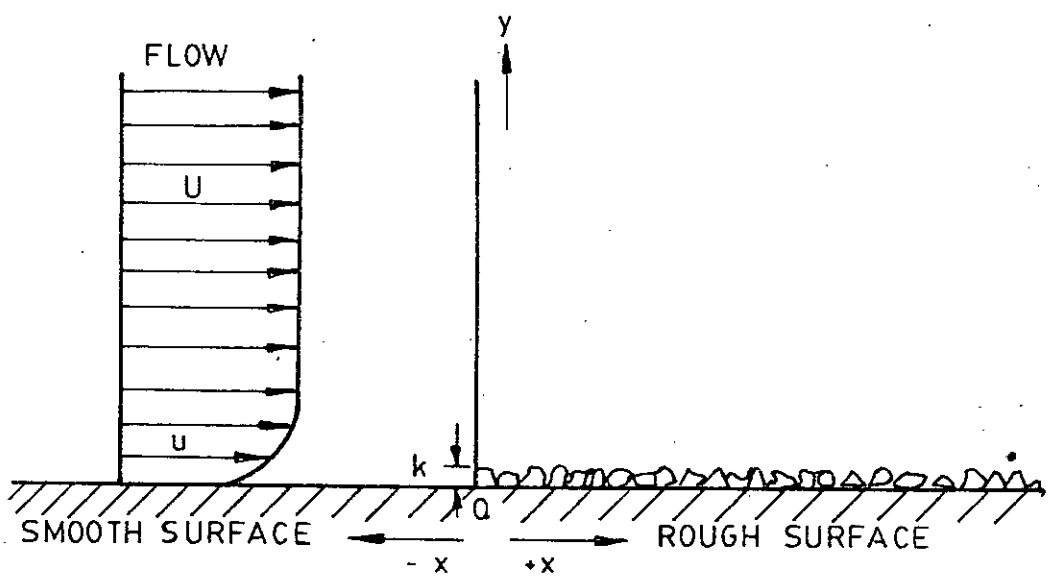

FIG. 1.1 FLOW GEOMETRY AND COORDINATE SYSTEM

1 SETTLING CHAMBER
2 CONVERGING MOUTH
3 PERSPEX SECTION WITH HONEYCOMB
4 PERSPEX SECTION
5 WOOD SECTION
6 WOOD SECTION
7 WOOD SECTION
8 DIVERGING SECTION
9 FAN SECTION
10 FAN SECTION
11 BUTTERFLY SECTION
12 SILENCER

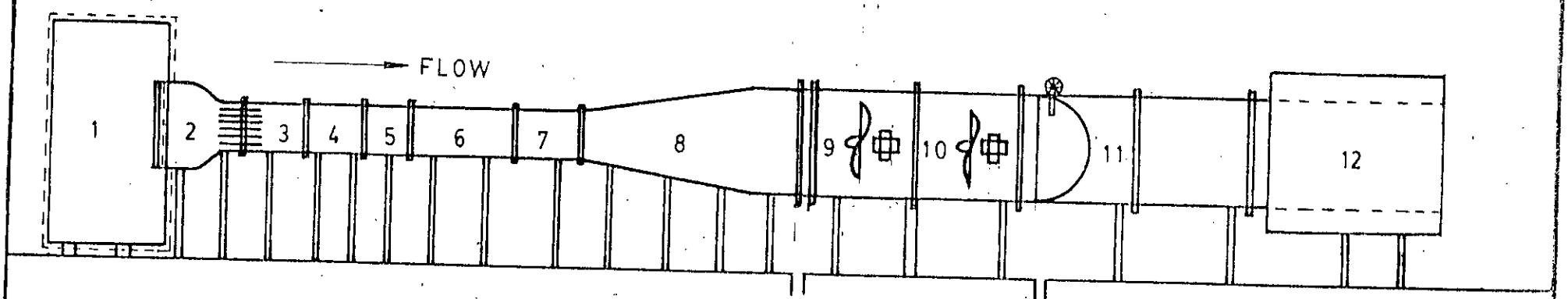

FIG. 4·1 SCHEMATIC DIAGRAM OF WIND TUNNEL

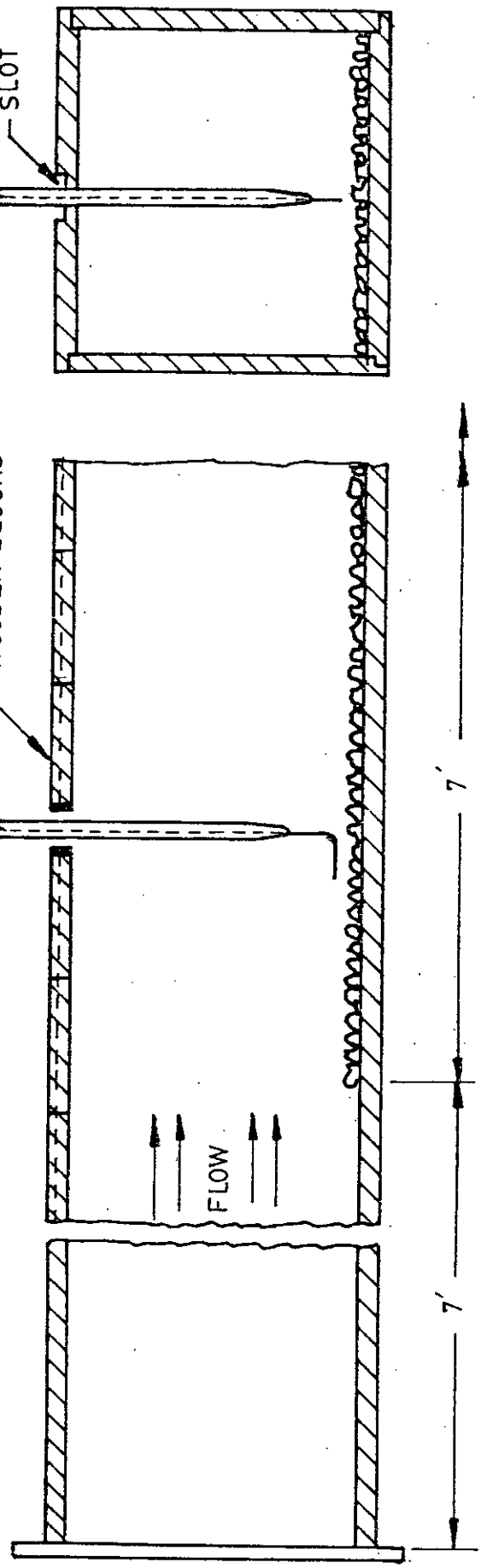

FIG. 4.2 TEST SECTION WITH SENSING PROBE

1 MOTOR
2 BLOWER
3 FILTER
4 FLOW CONTROLLING VALVE
5 CIRCULAR PIPE
6 FLOW STRAIGHT ENER
7 NOZZLE

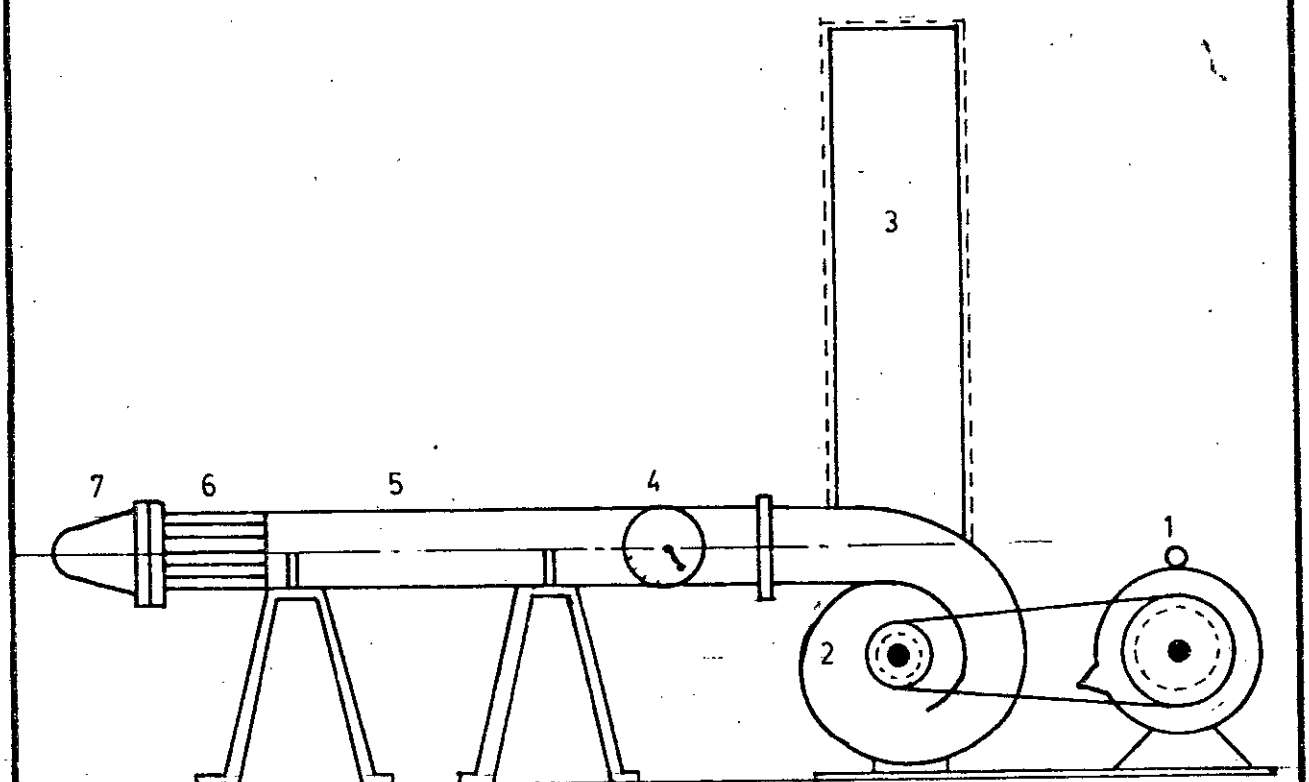

FIG. 4·3 SCHEMATIC DIAGRAM OF CALIBRATION RIG

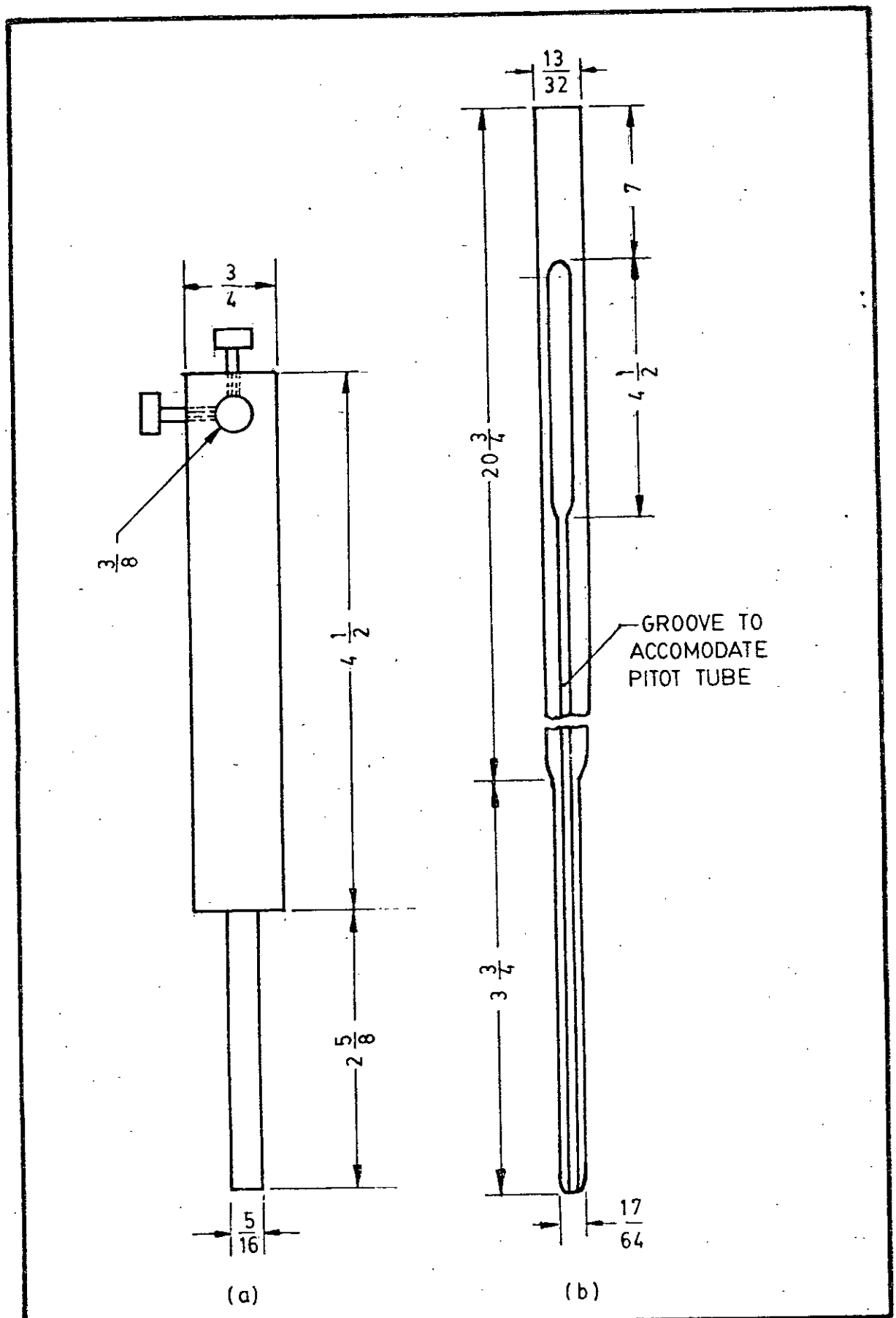

FIG.4.4 a. PITOT STATIC TUBE HOLDER

FIG.4.4 b PITOT TUBE AND HOT WIRE SUPPORT HANGER

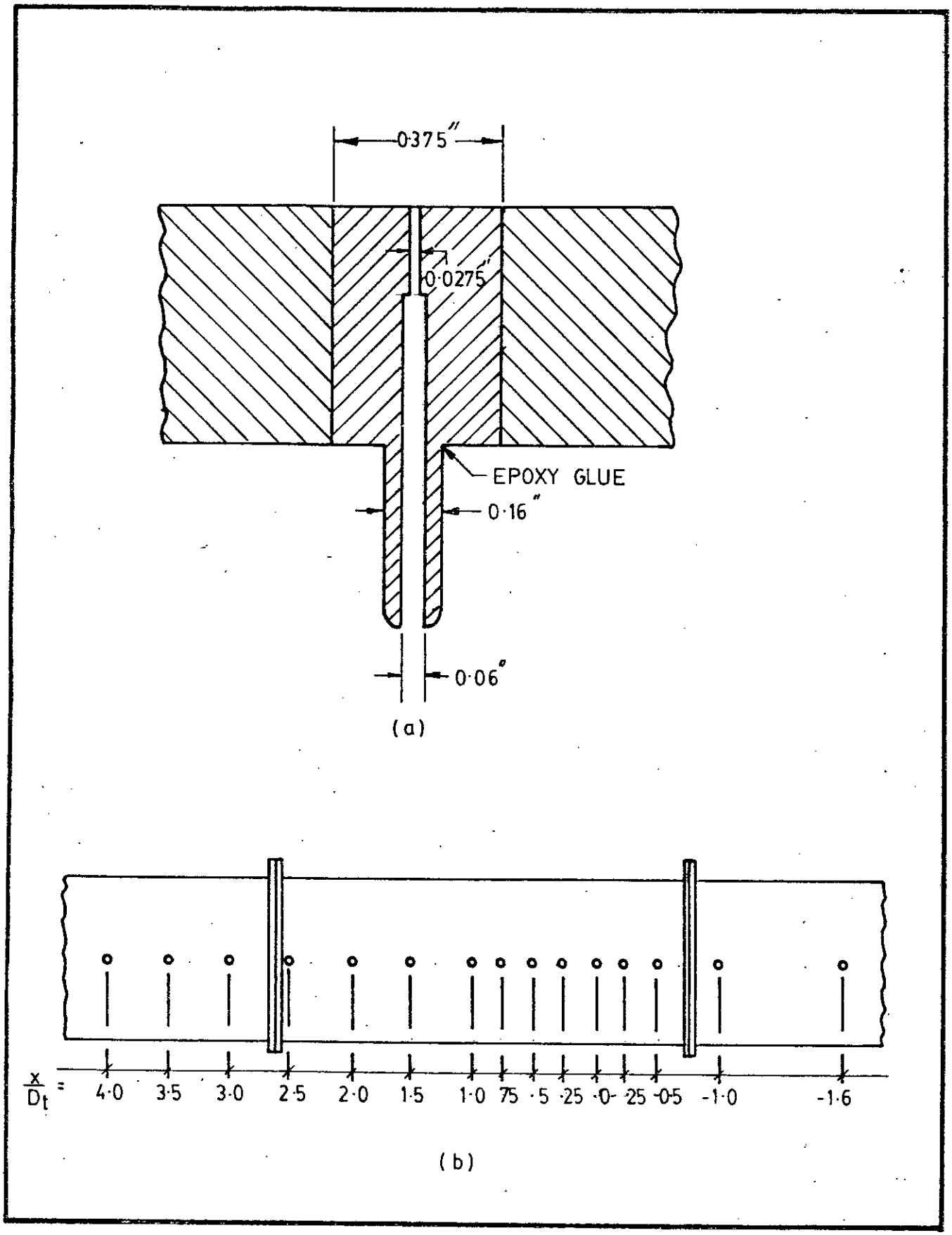

FIG. 4·5a SECTIONAL VIEW OF STATIC PRESSORE HOLE

FIG. 4·5b STATIC PRESSURE HOLES IN THE WALL OF THE TEST SECTION

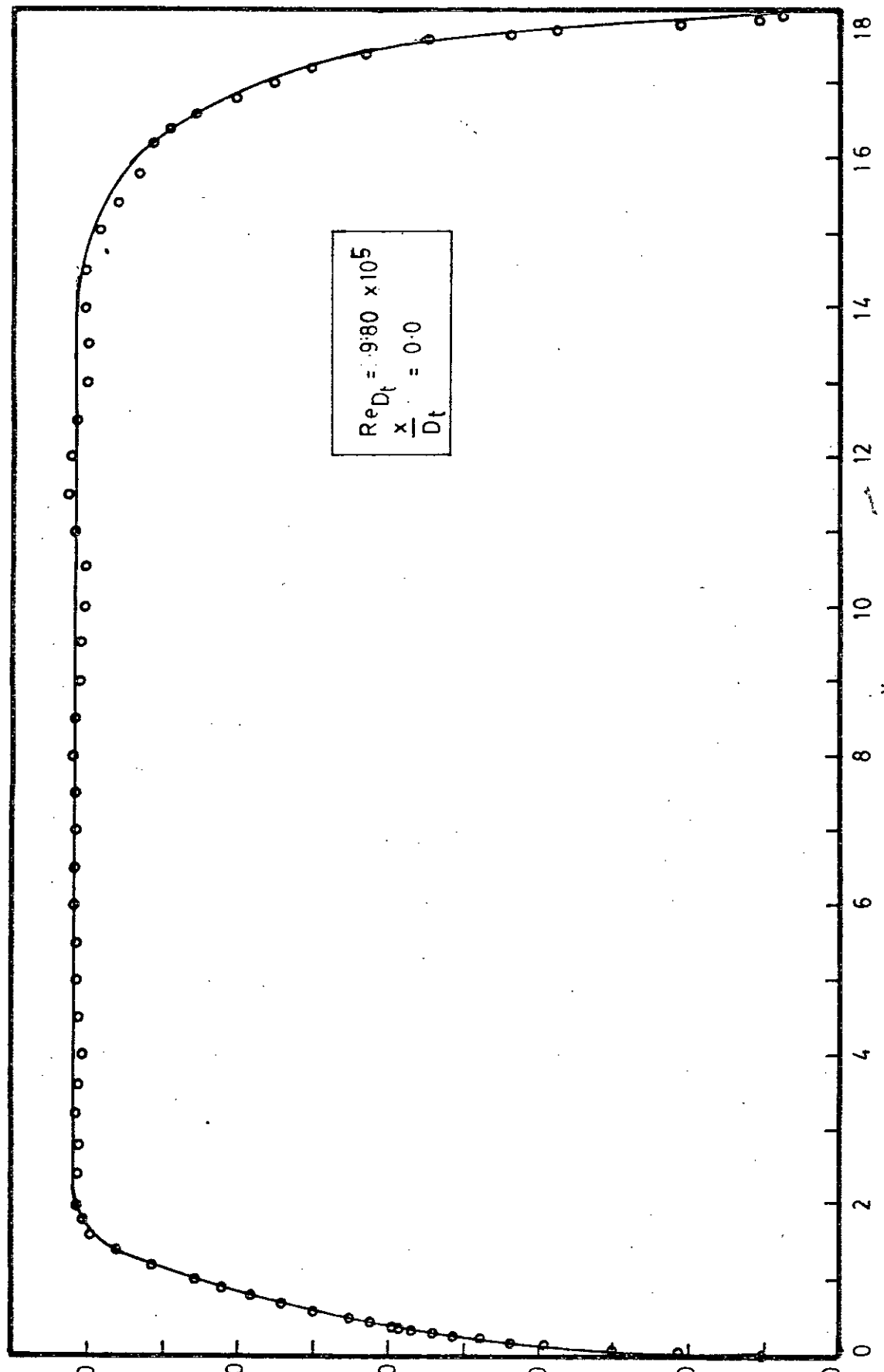

FIG. 4·6 MEAN VELOCITY PROFILE OVER SMOOTH SURFACE IN THE TEST SECTION

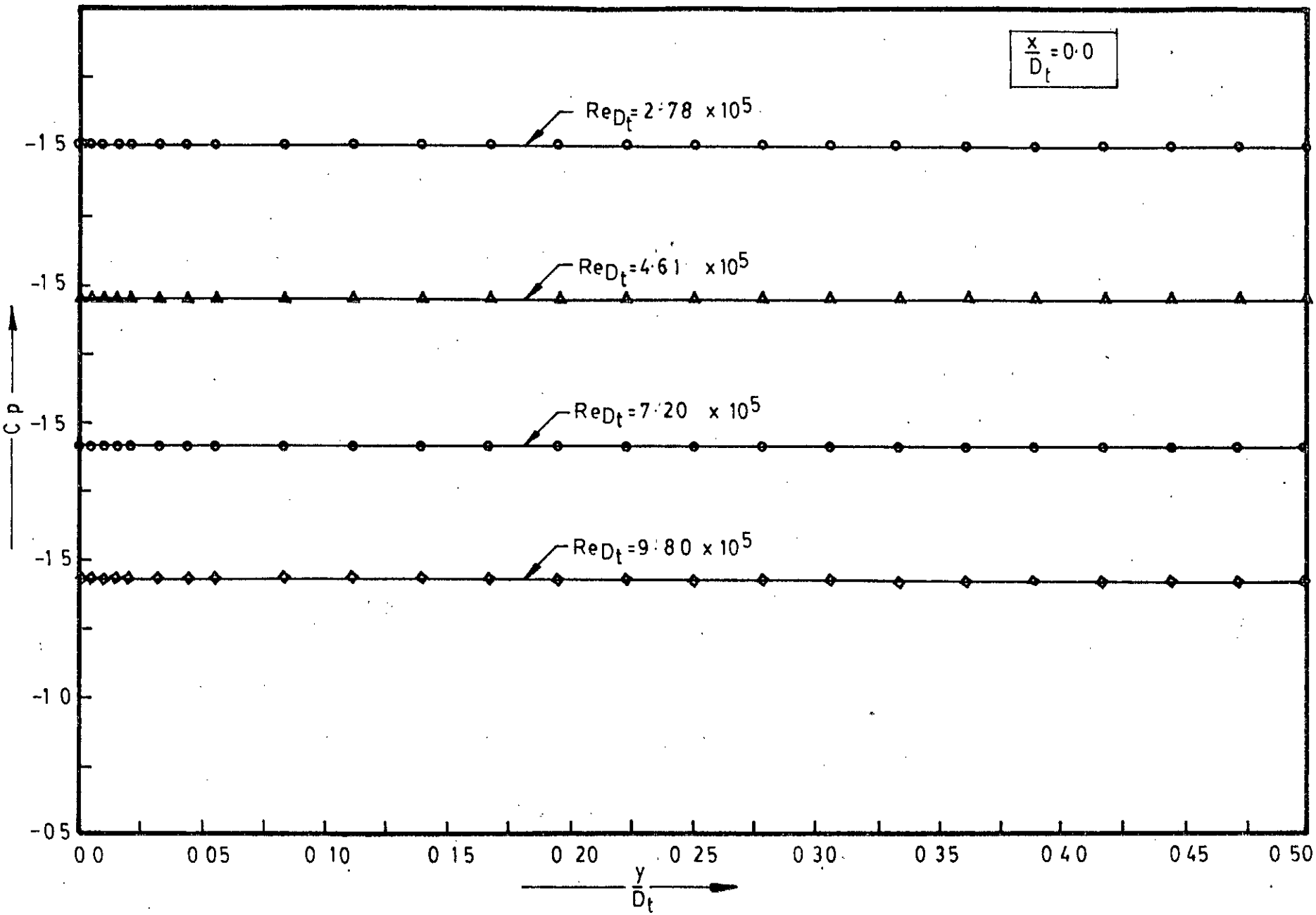

FIG. 4-7 TRANVERSE PRESSURE DISTRIBUTION IN THE TEST SECTION WITH SMOOTH SURFACE

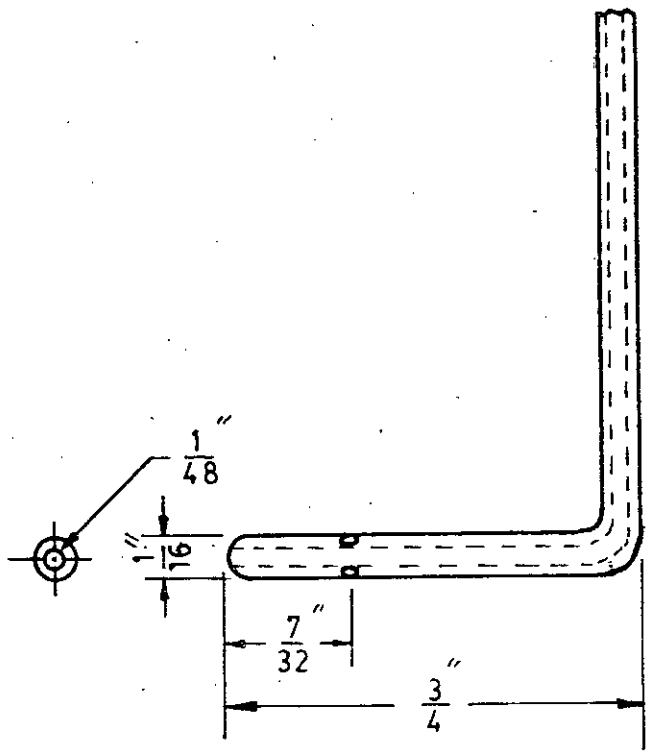

FIG. 4.8 a PITOT STATIC TUBE (UNITED SENSOR)

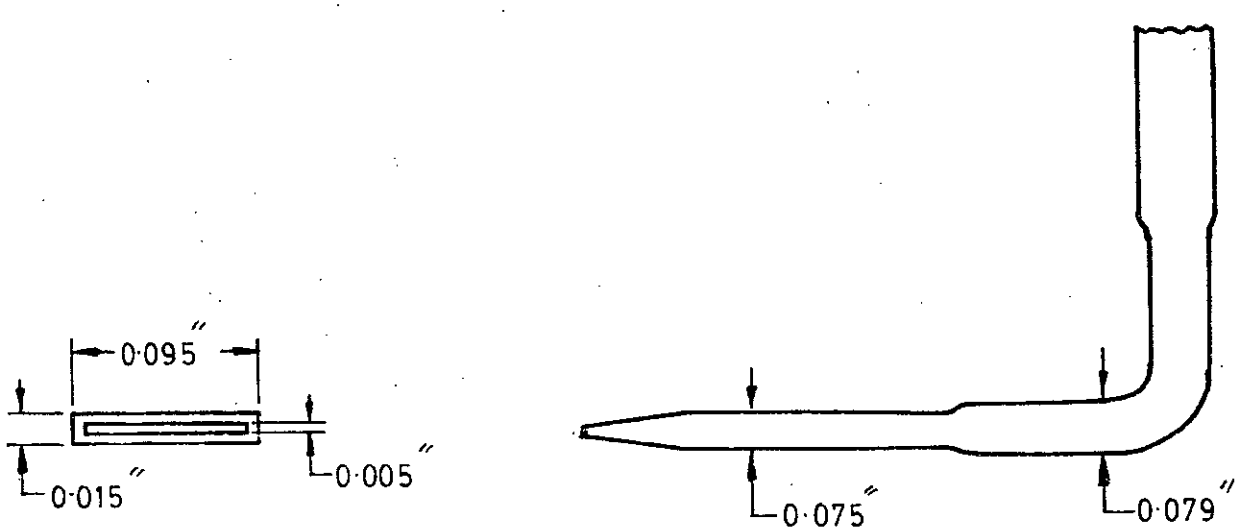

FIG. 4·8 b BOUNDARY LAYER TUBE

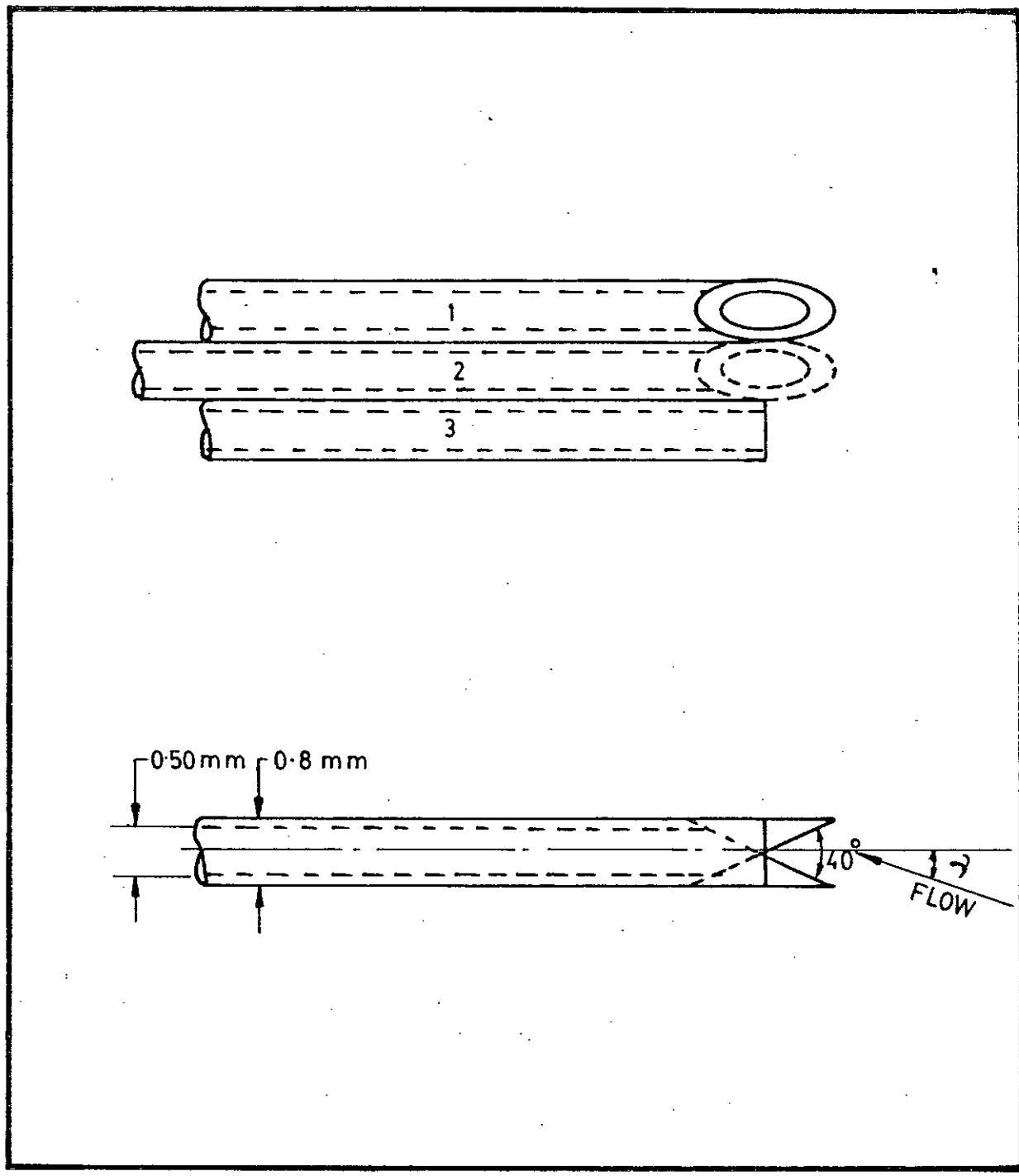

FIG. 4·9 YAWMETER USED TO MEASURE RESULTANT VELOCITY ANGLE

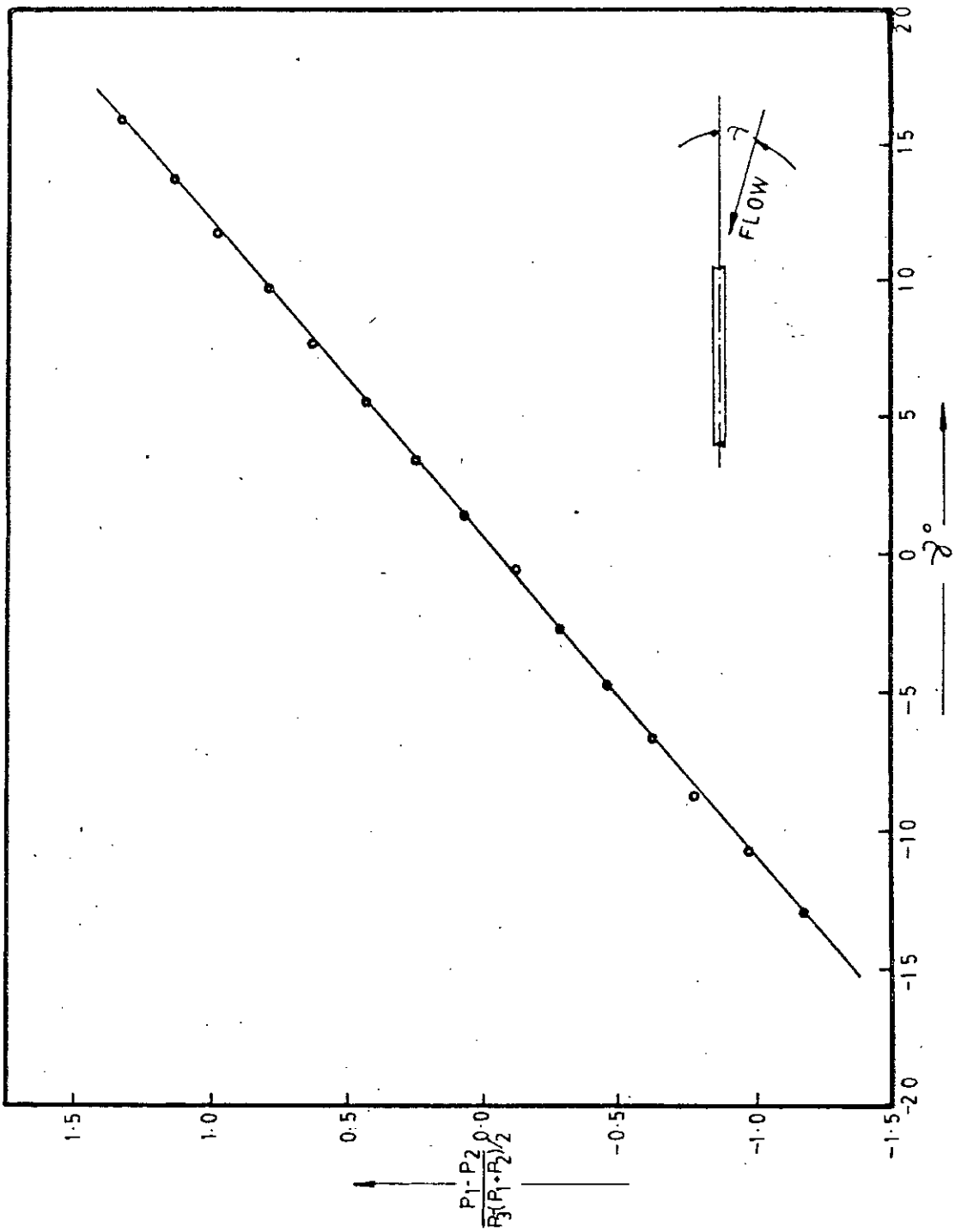

FIG. 4.10 CALIBRATION CURVE FOR THE YAWMETER

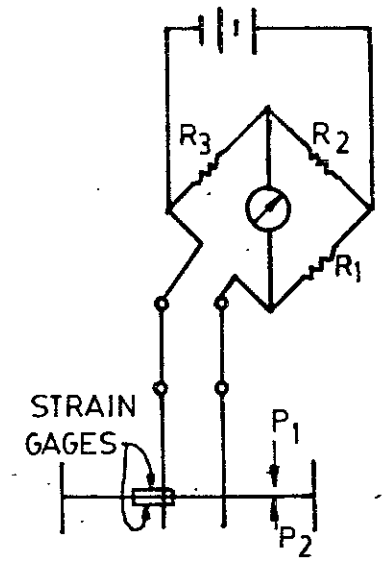

(a) REGISTANCE TYPE

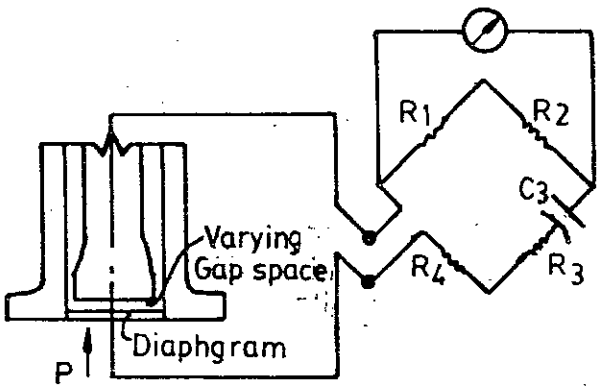

(b) CAPACITANCE TYPE

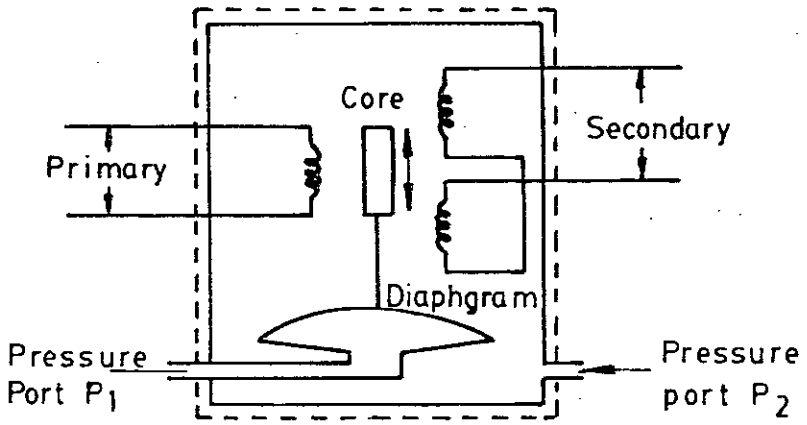

(c) INDUCTANCE TYPE

FIG· 4·11 SCHEMETIC OF PRESSURE TRANSDUCERS

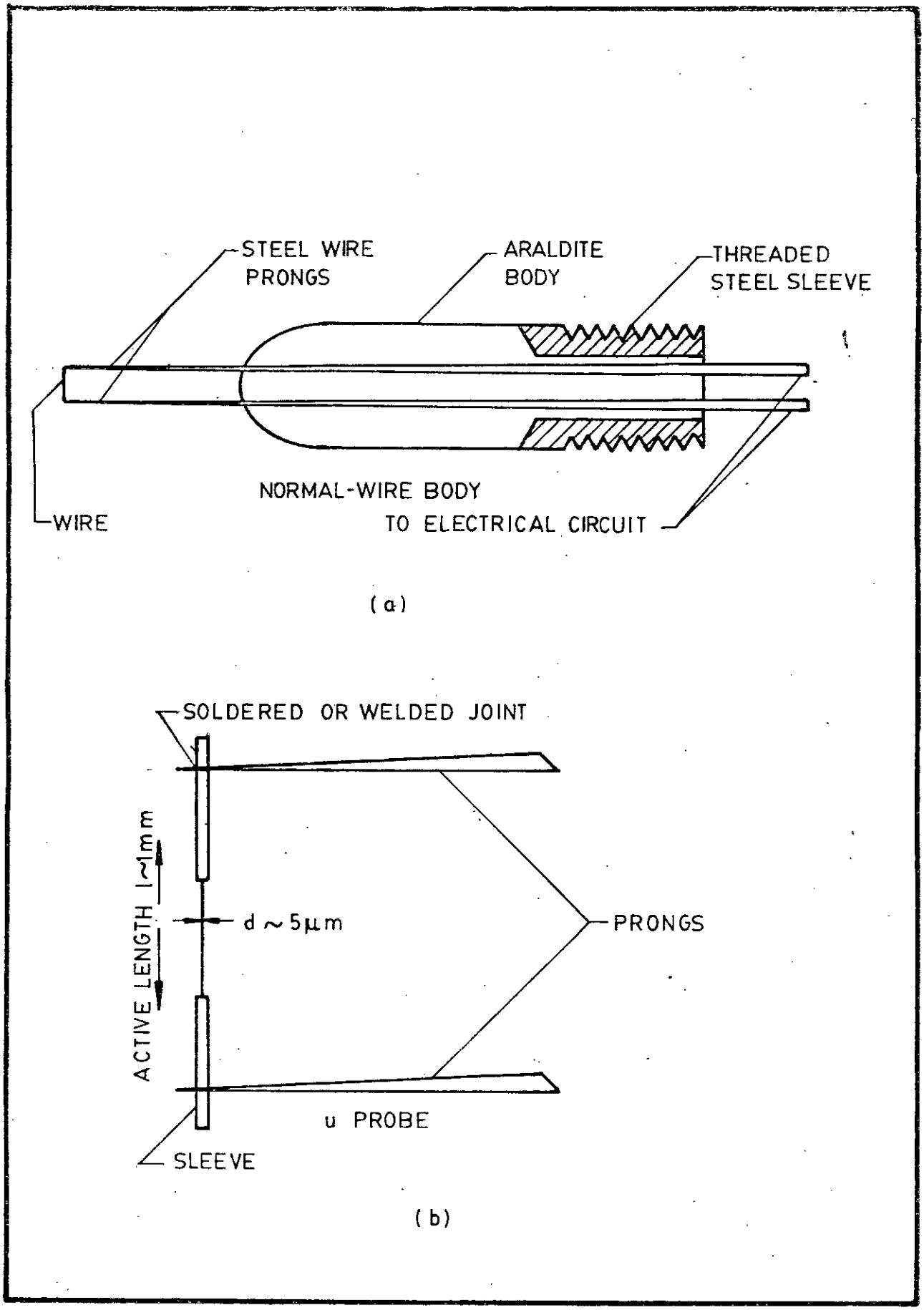

FIG. 4·12 a HOT WIRE PROBE CONNECTIONS

FIG. 4·12 b HOT WIRE PROBE

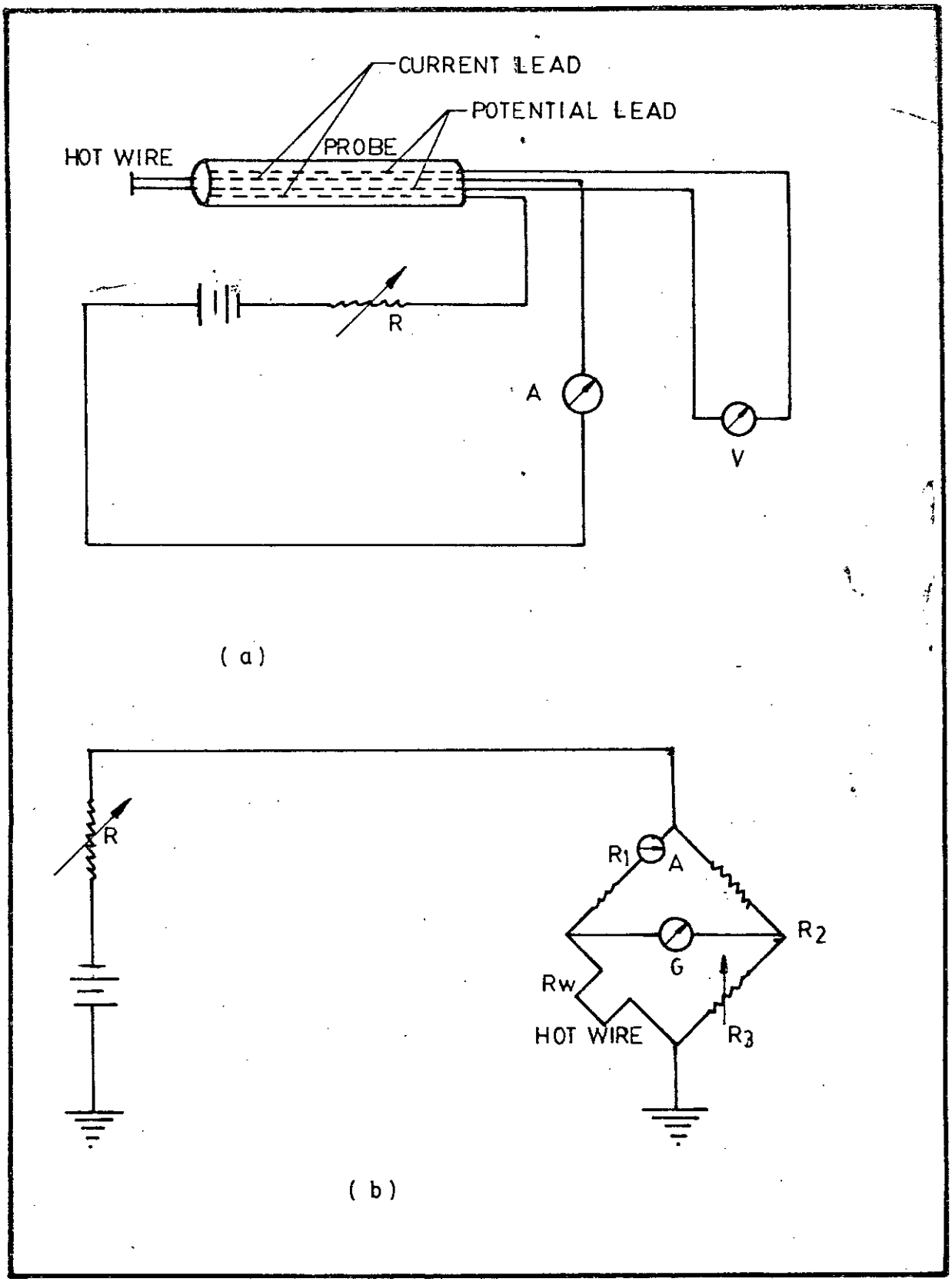

FIG. 4·13 a BASIC HOT WIRE CIRCUIT

FIG. 4·13 b BASIC HOT WIRE BRIDGE CIRCUIT

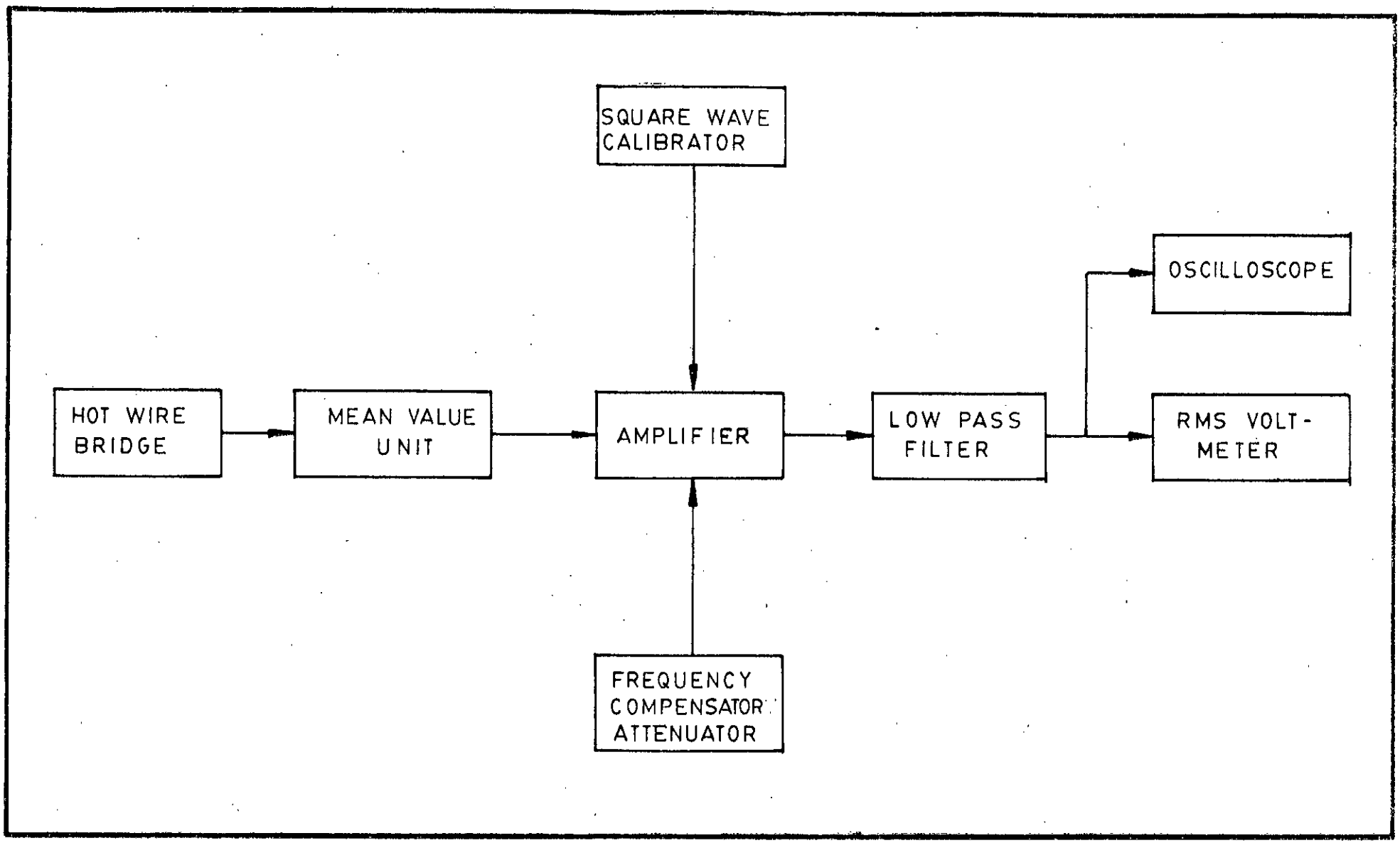

FIG. 4·14 HOT WIRE INSTRUMENTATION CHART

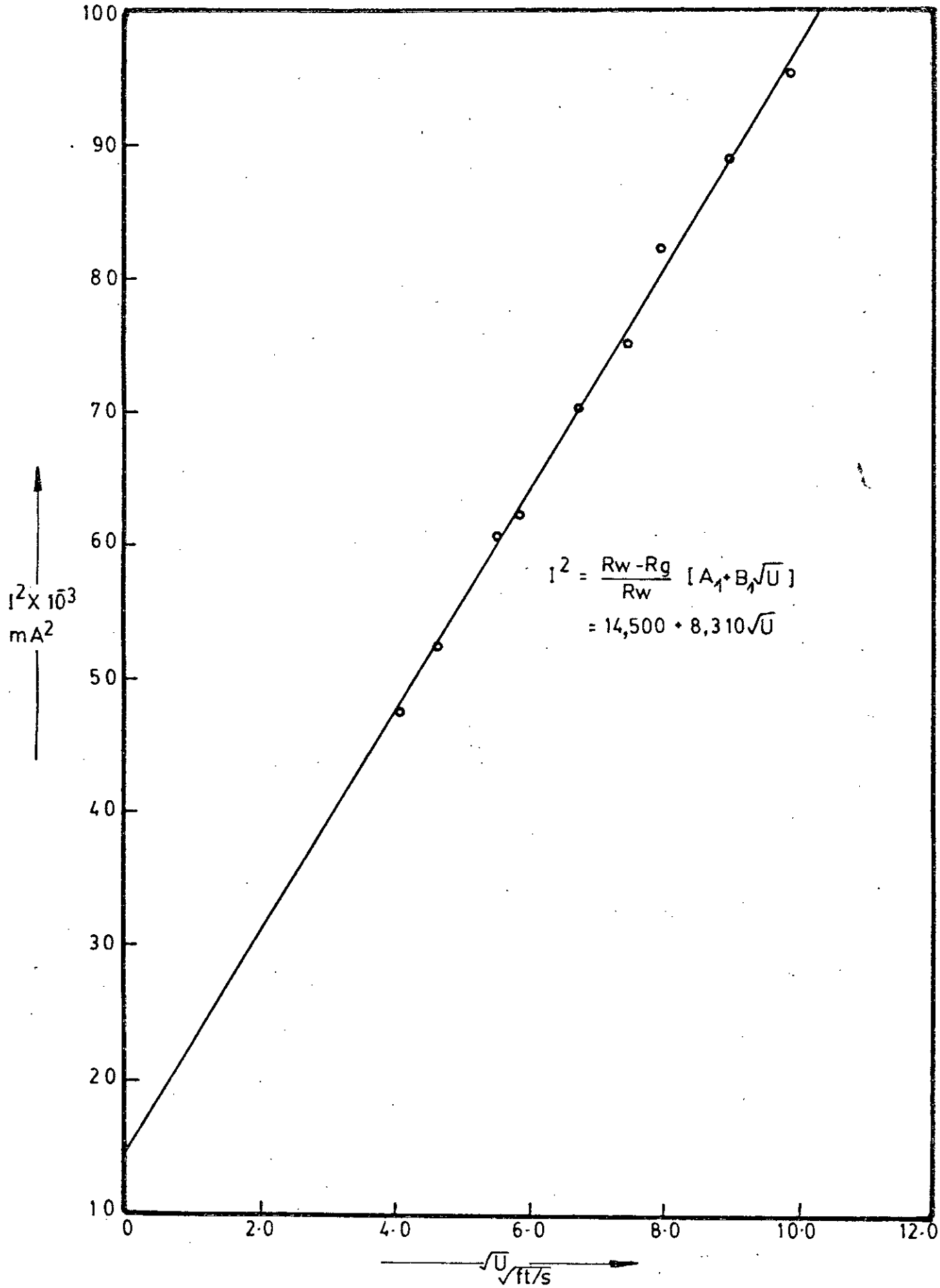

FIG·4.15 CALIBRATION CURVE FOR THE HOT WIRE

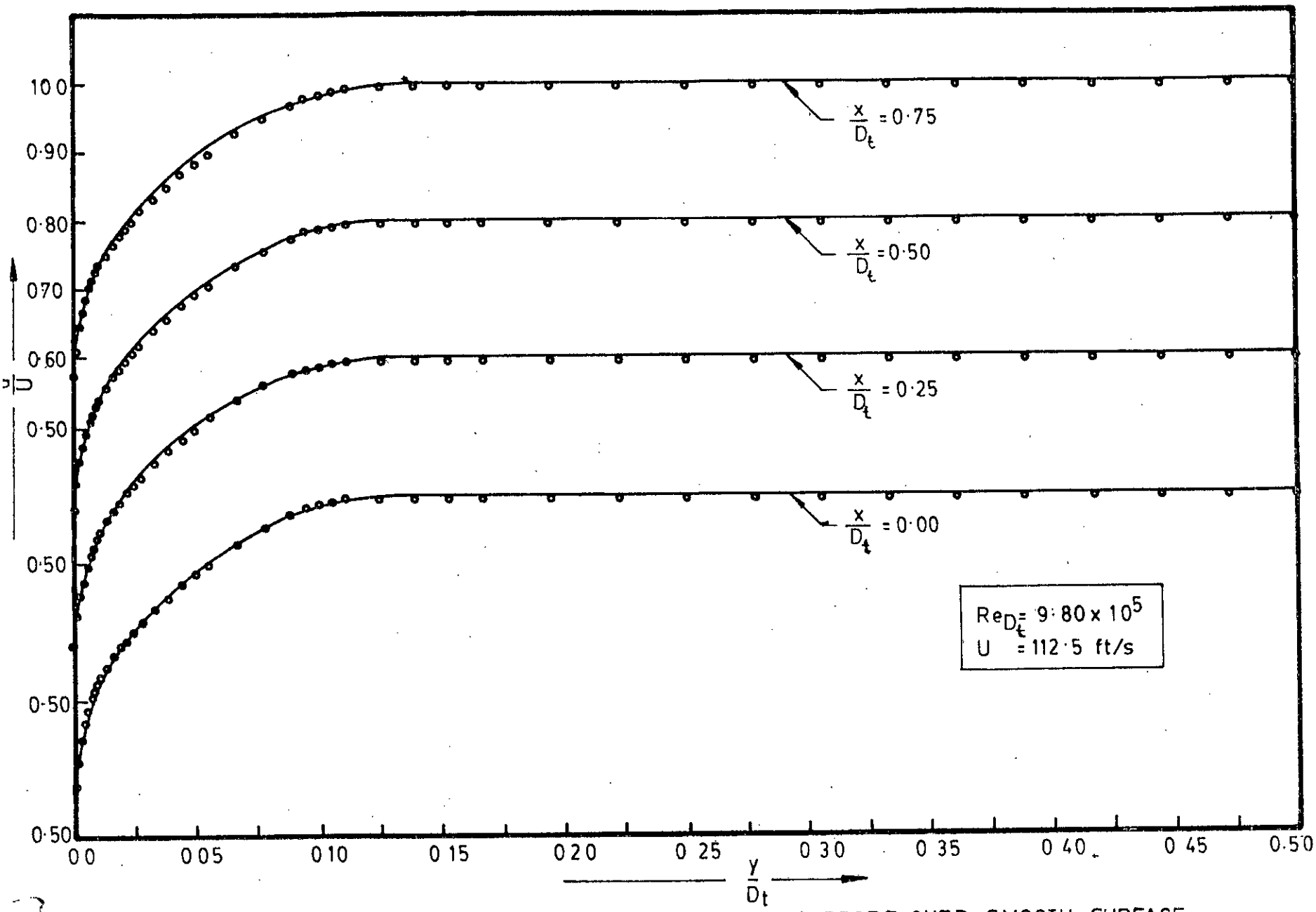

FIG·5·1 a MEAN VELOCITY PROFILE MEASURED BY PITOT STATIC PROBE OVER SMOOTH SURFACE

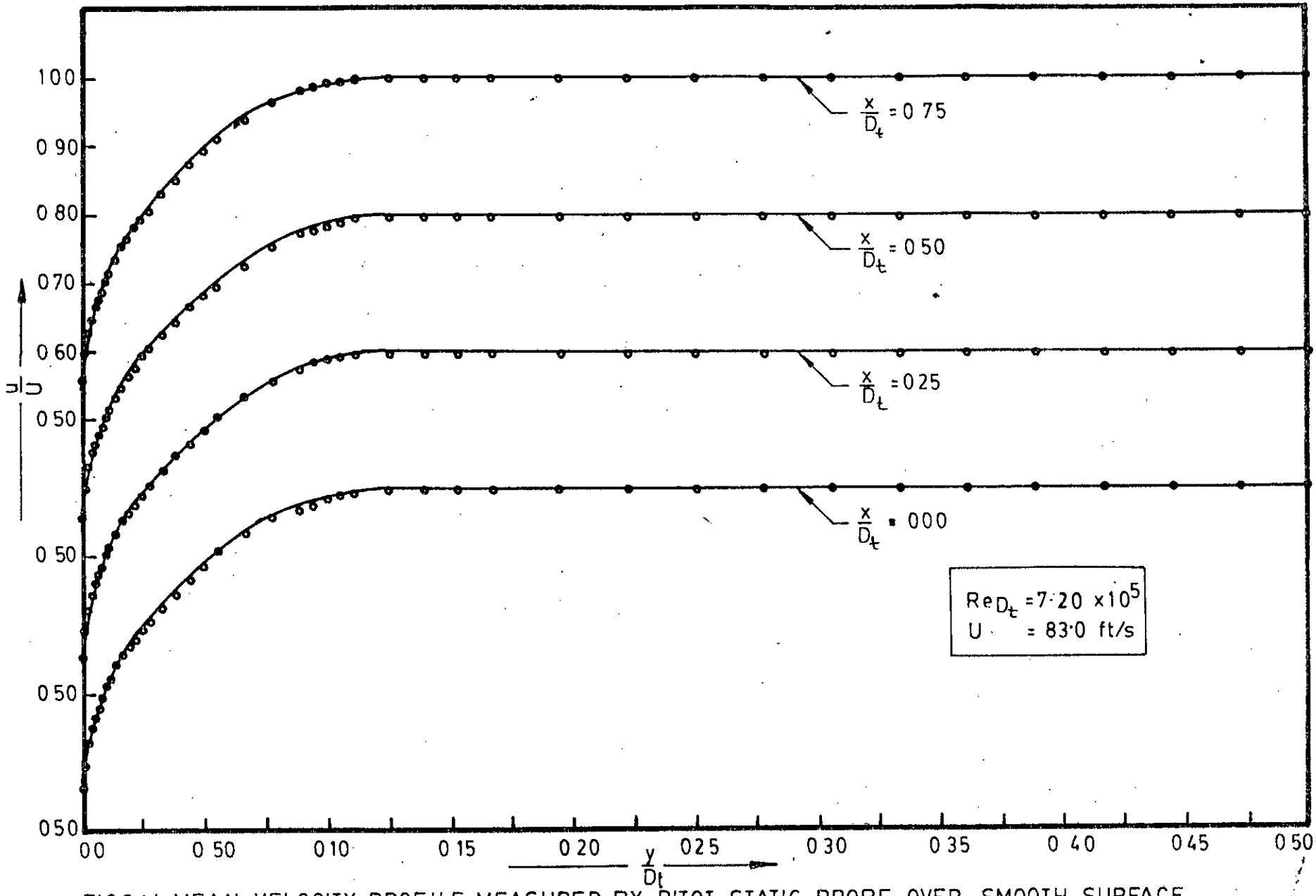

FIG·5·1 b MEAN VELOCITY PROFILE MEASURED BY PITOT STATIC PROBE OVER SMOOTH SURFACE

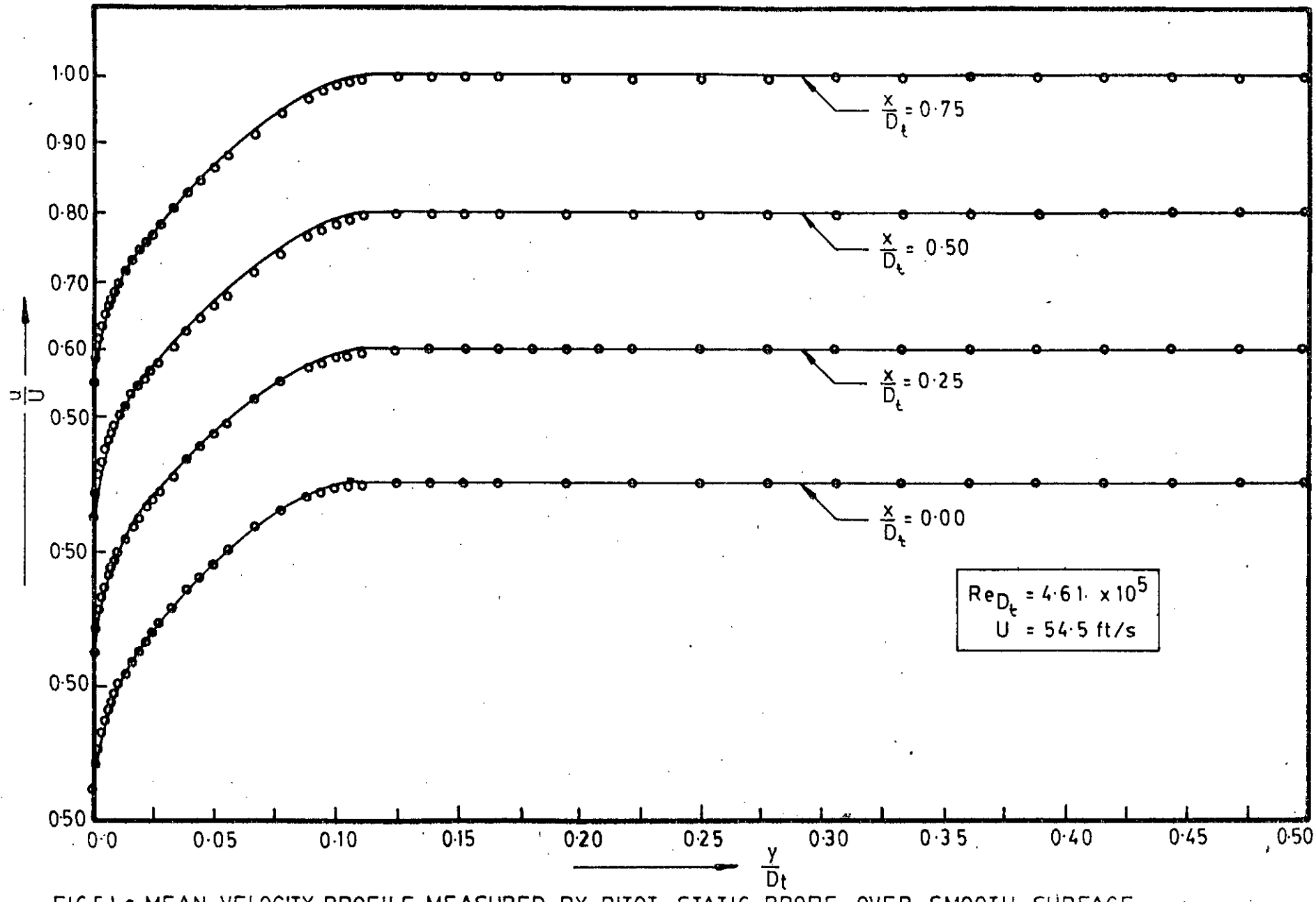

FIG 5·1 c MEAN VELOCITY PROFILE MEASURED BY PITOT STATIC PROBE OVER SMOOTH SURFACE

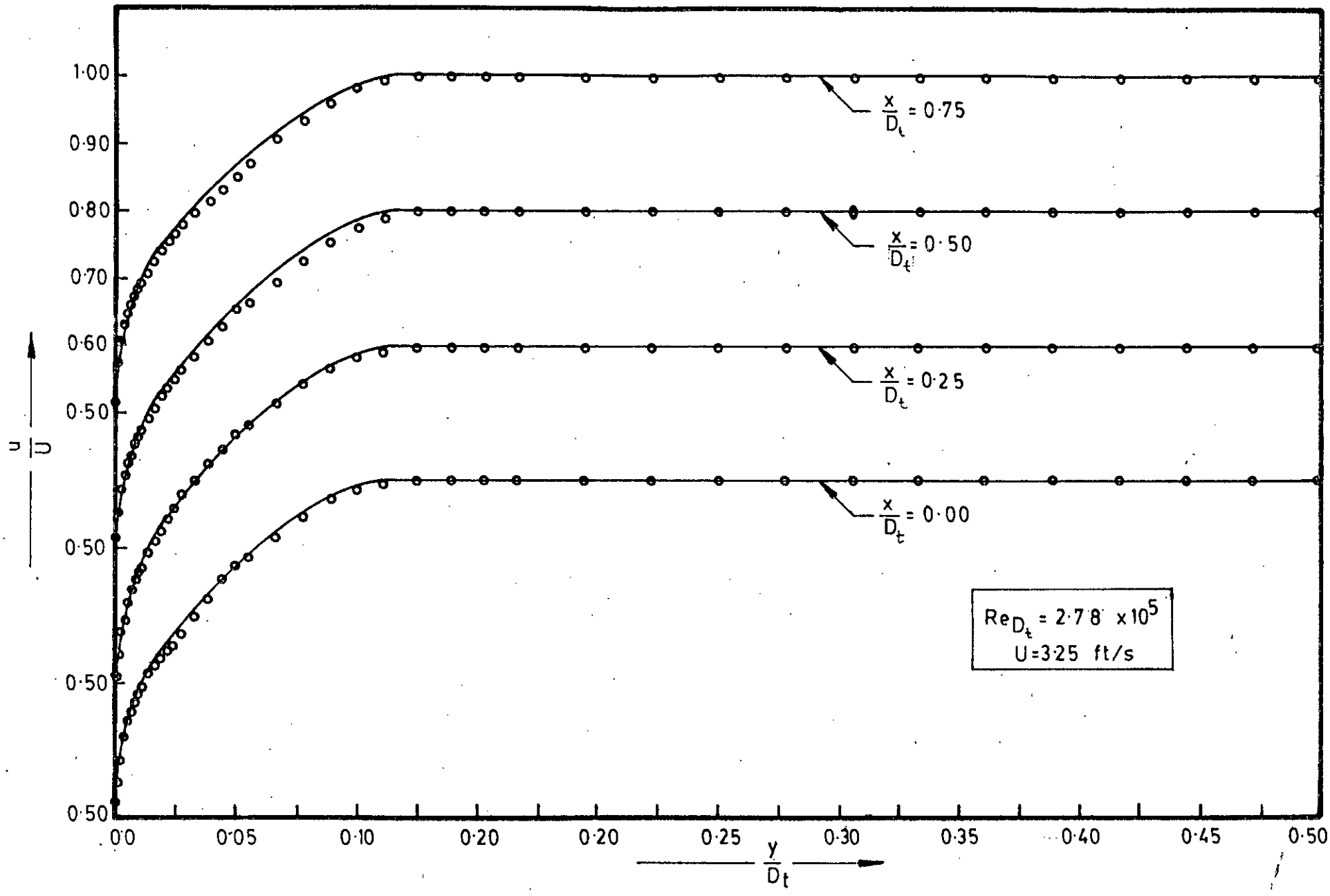

FIG.5·1 d MEAN VELOCITY PROFILE MEASURED BY PITOT STATIC PROBE OVER SMOOTH SURFACE

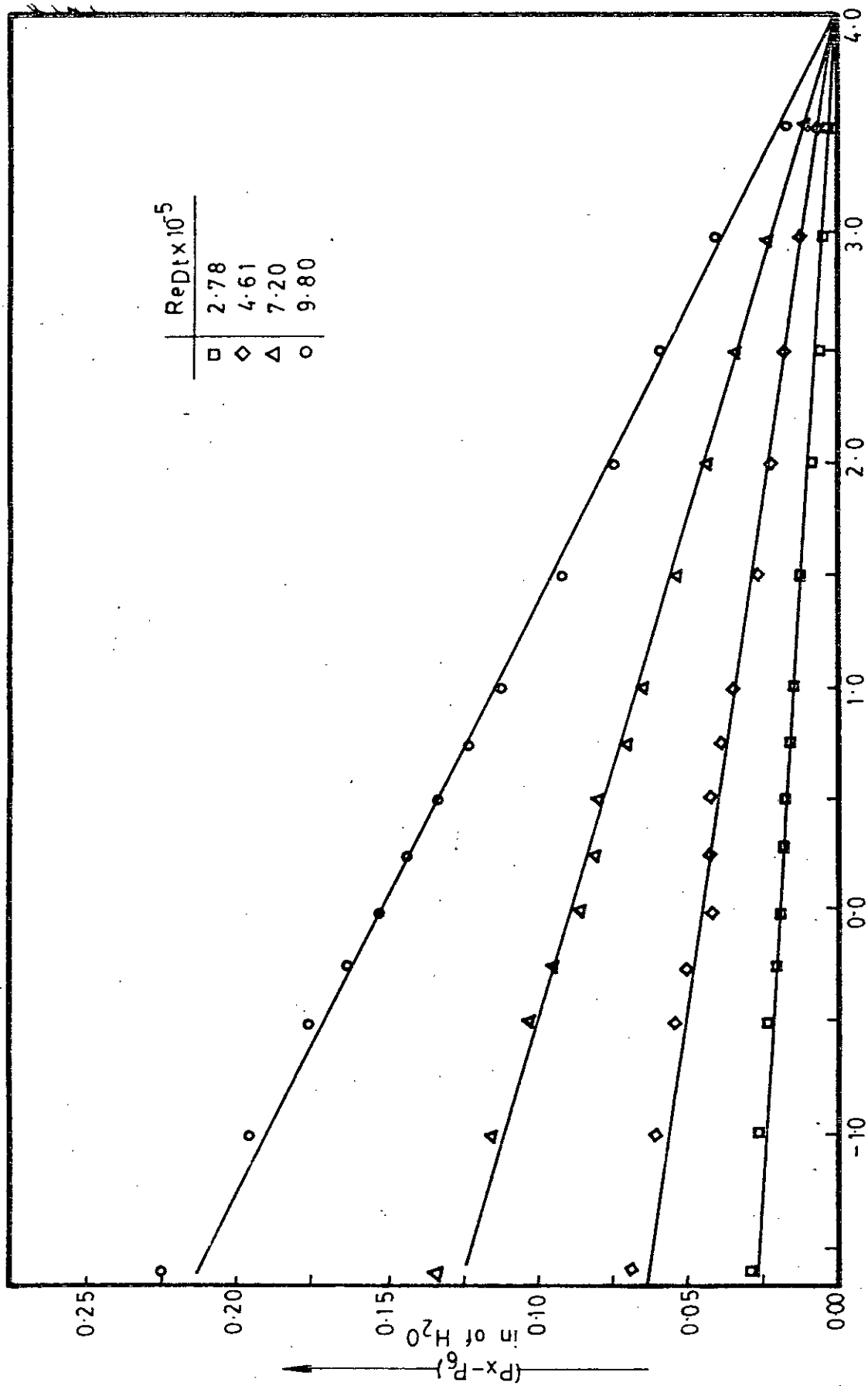

FIG·5.2 AXIAL PRESSURE GRAIDENT FOR SMOOTH DUCT

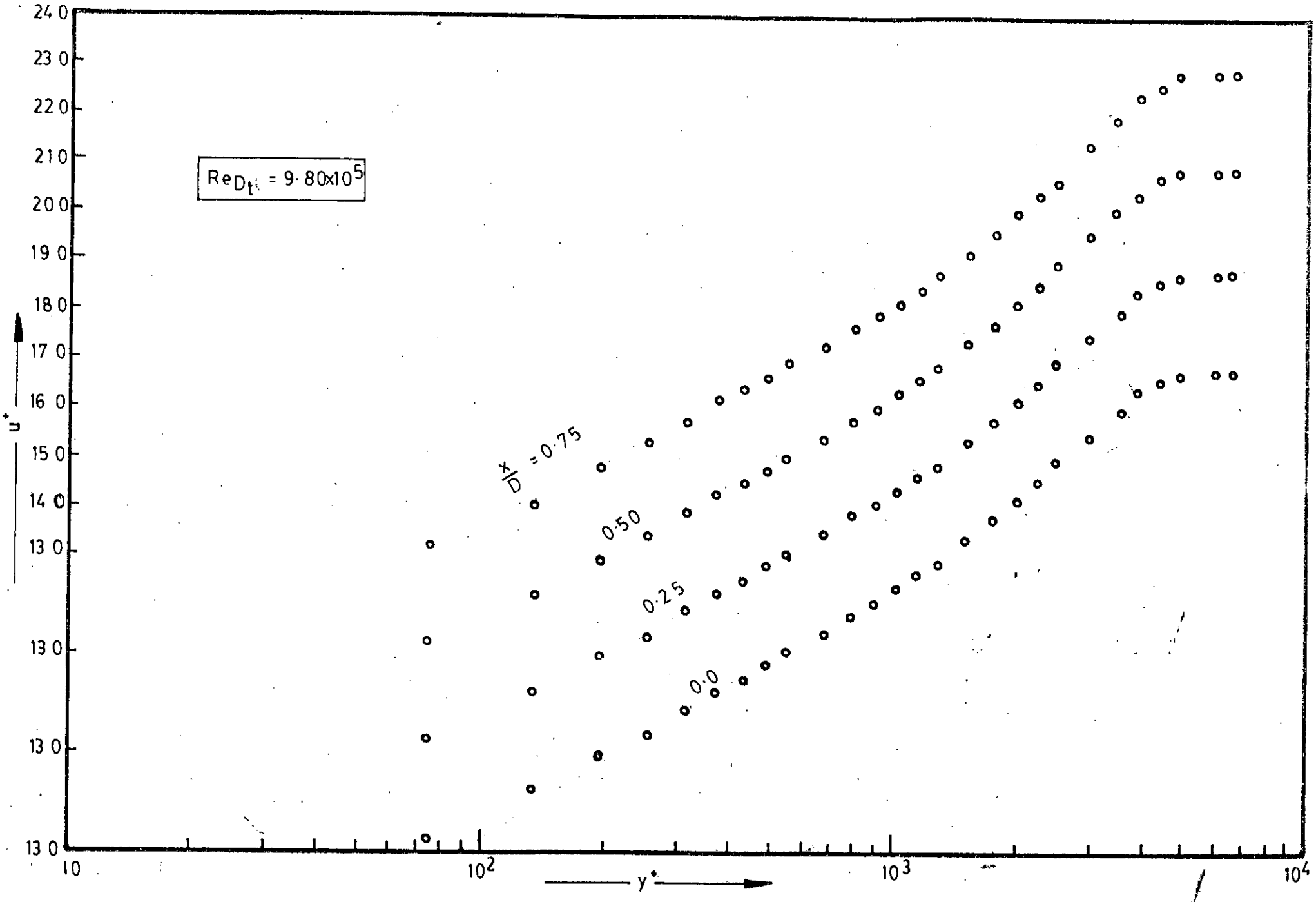

FIG. 5·3 (a) LOGARITHMIC VELOCIT PROFILE NEAR THE SMOOTH SURFACE

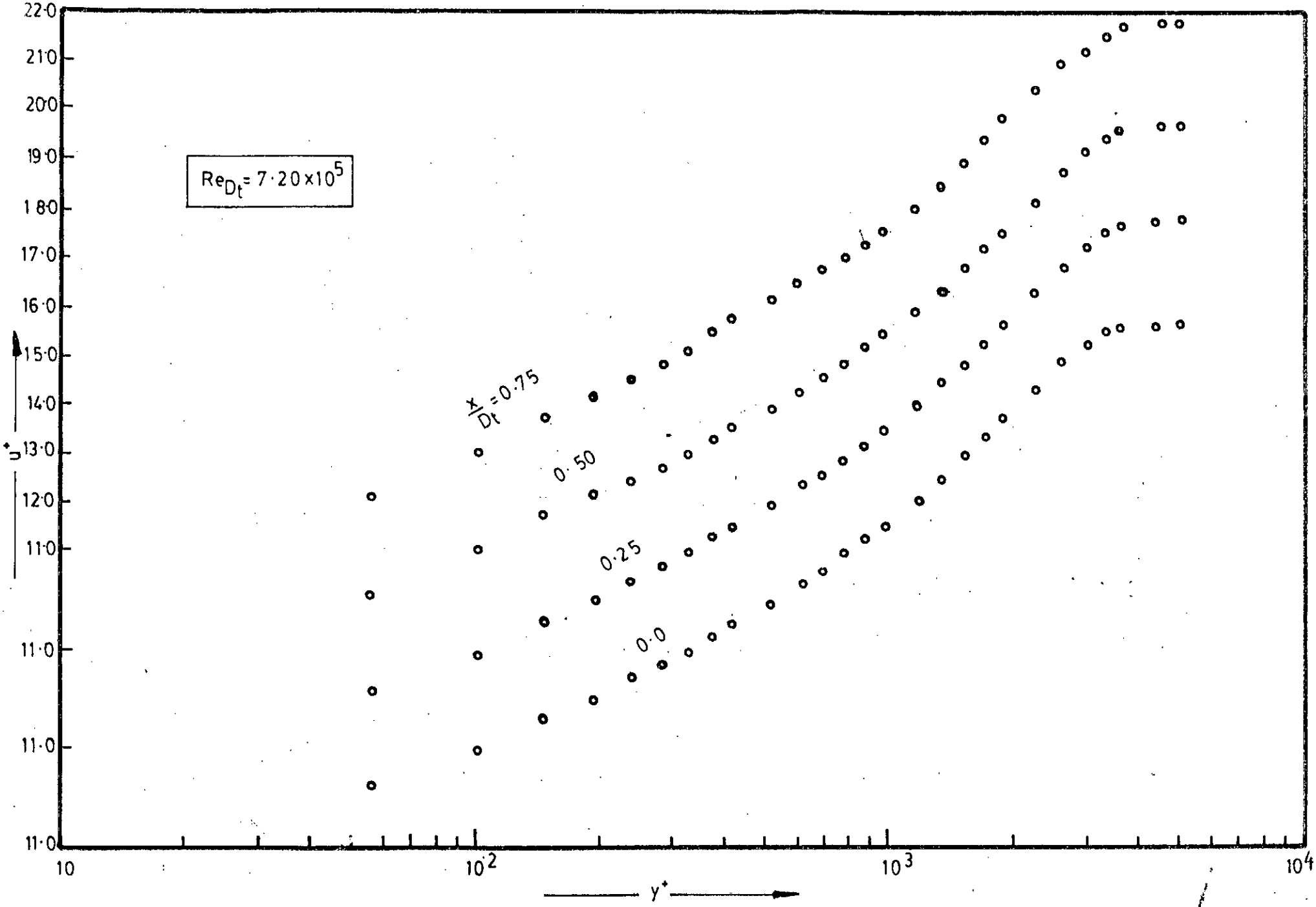

FIG·5·3 (b) LOGARITHMIC VELOCITY PROFILE NEAR THE SMOOTH SURFACE

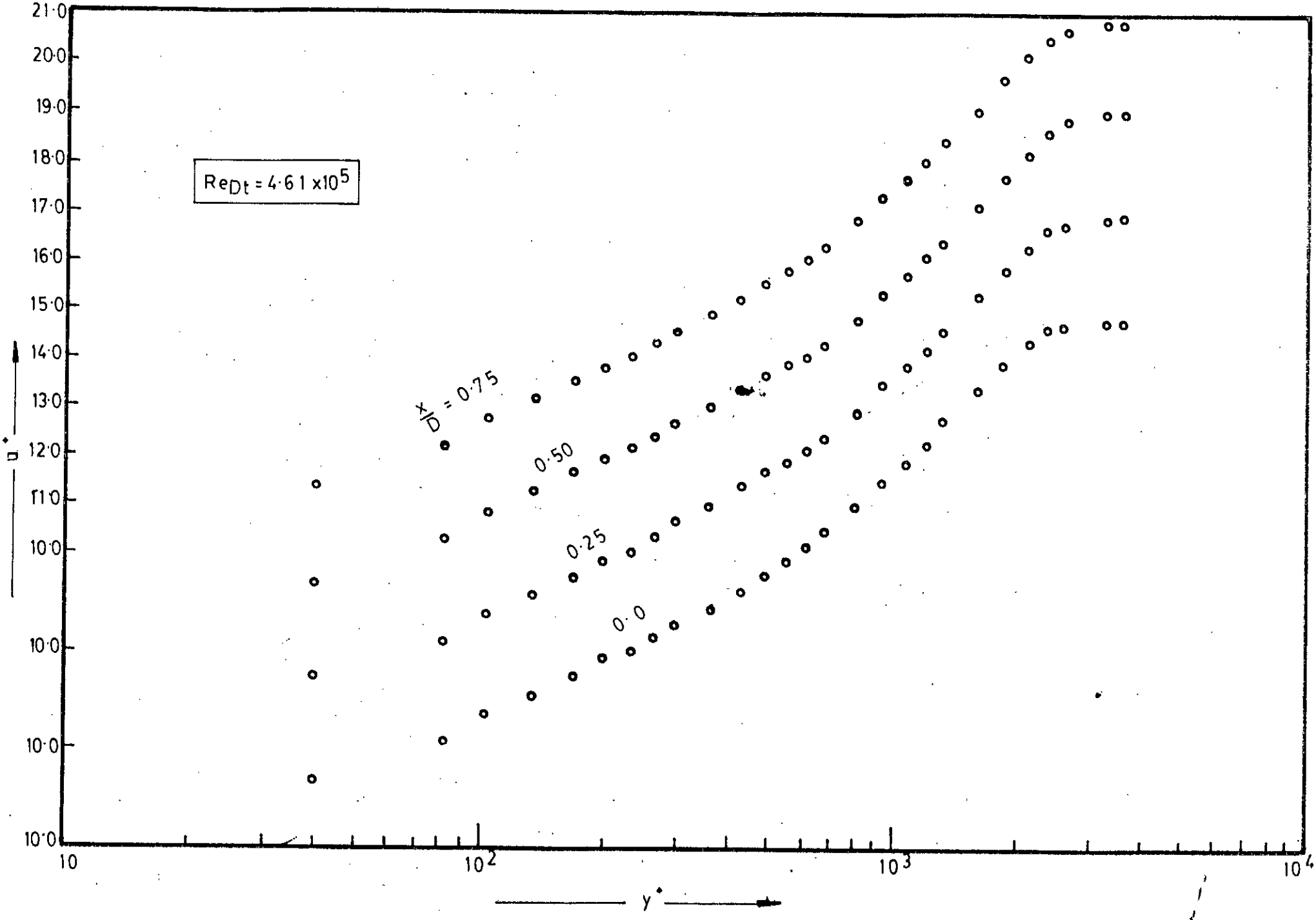

FIG·5·3 (c) LOGARITHMIC VELOCITY PROFILE NEAR THE SMOOTH SURFACE

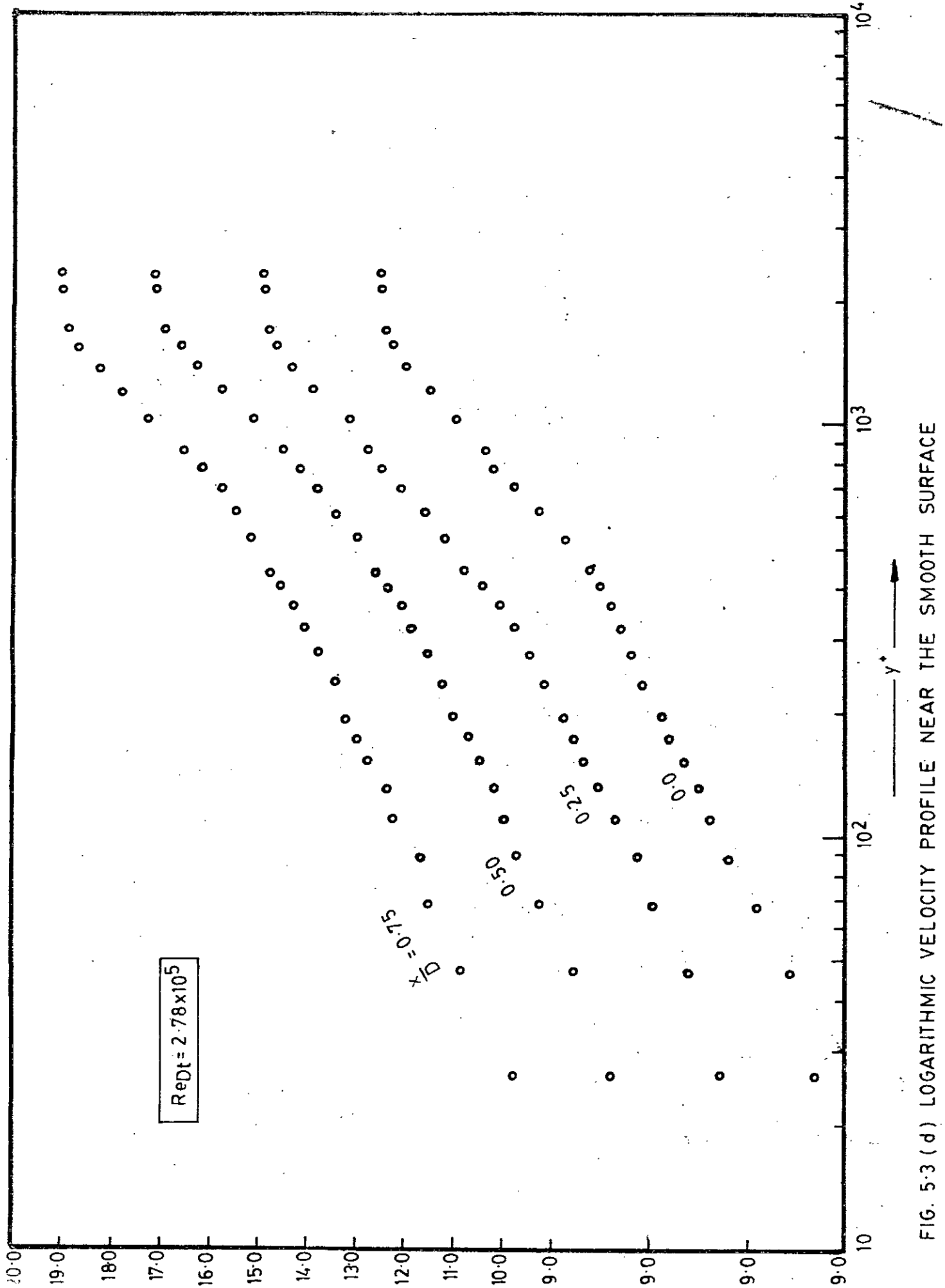

FIG. 5·3 (d) LOGARITHMIC VELOCITY PROFILE NEAR THE SMOOTH SURFACE

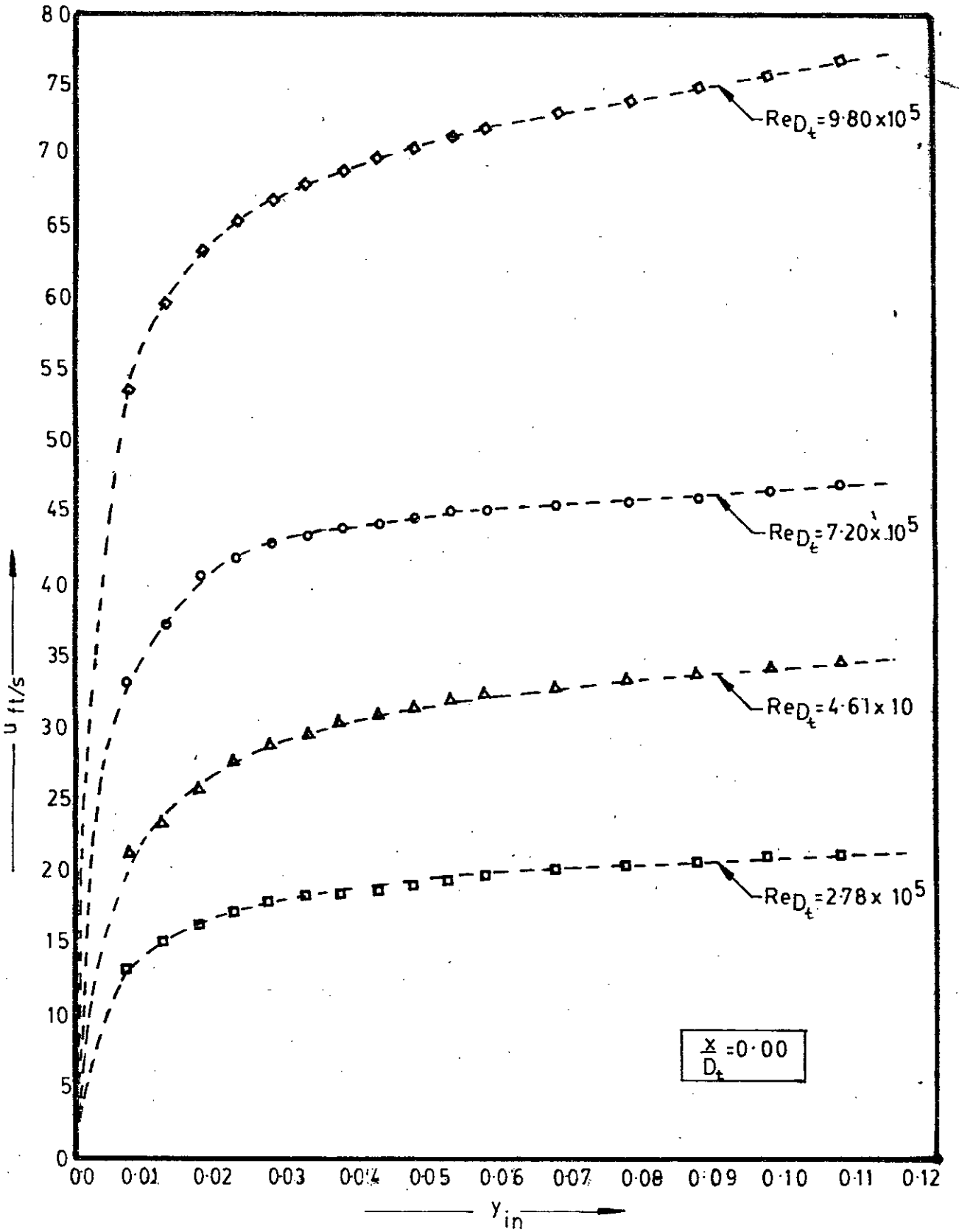

FIG. 5·4 MEAN VELOCITY PROFLE MEASURED BY BOUNDARY LAYER PROBE CLOSE TO THE SMOOTH SURFACE

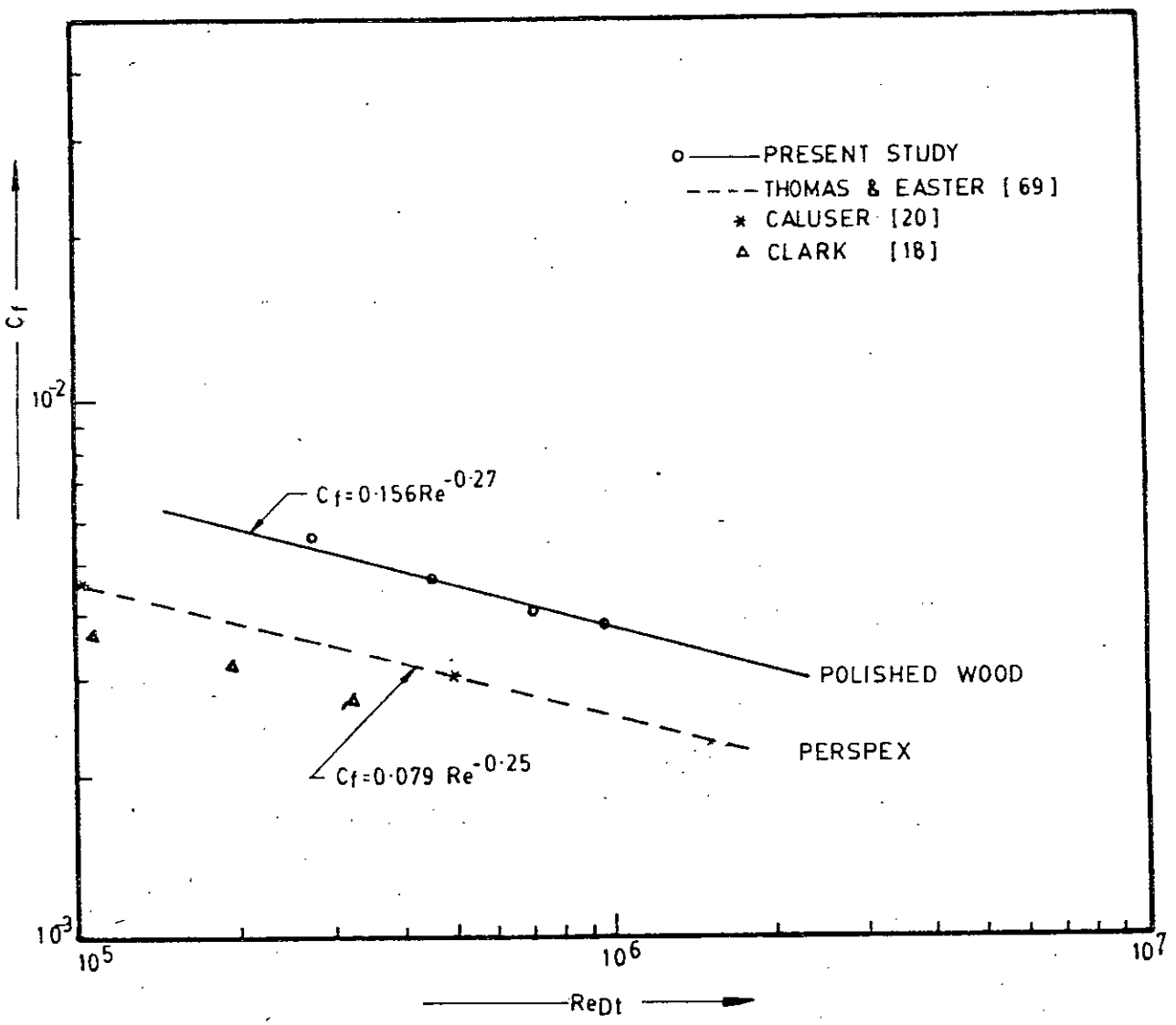

FIG·5·5 FRICTION FACTOR VERSUS REYNOLDS NUMBER FOR SMOOTH SURFACE

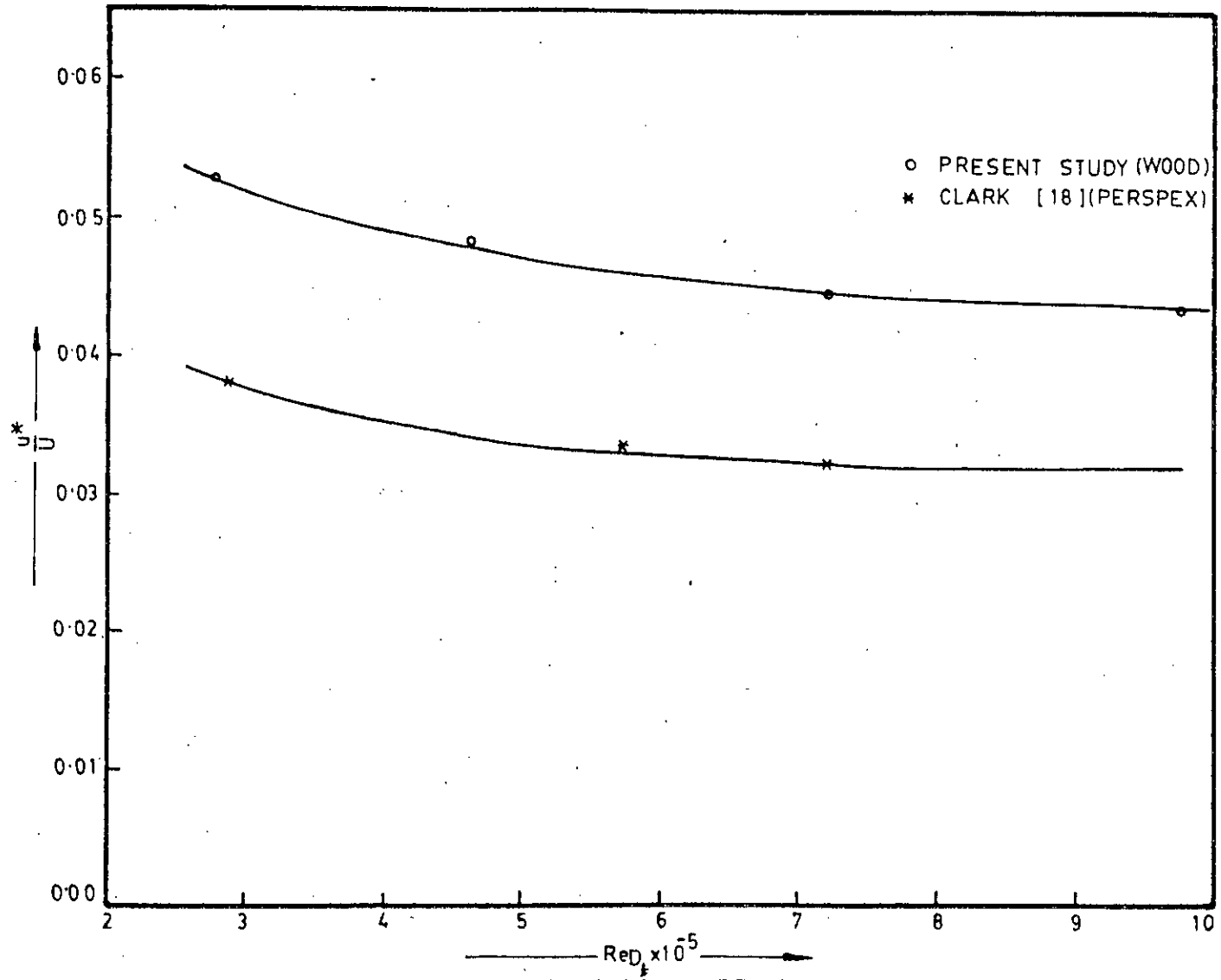

FIG· 5·6 FRICTION VELOCITY VERSUS REYNOLDS NUMBER FOR SMOOTH SURFACE

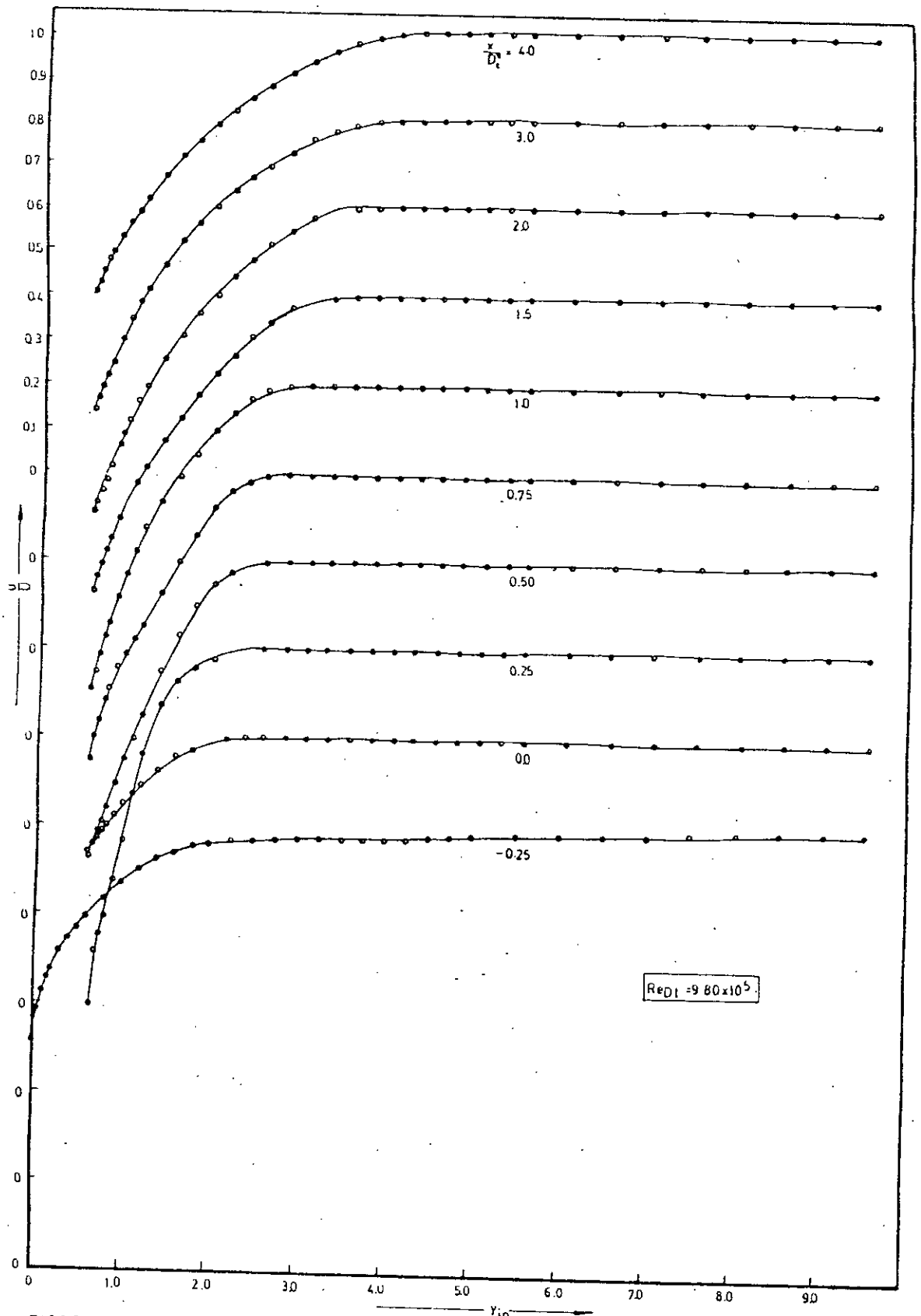

FIG·5·7 a MEAN VELOCITY PROFILES OVER ROUGH SURFACE

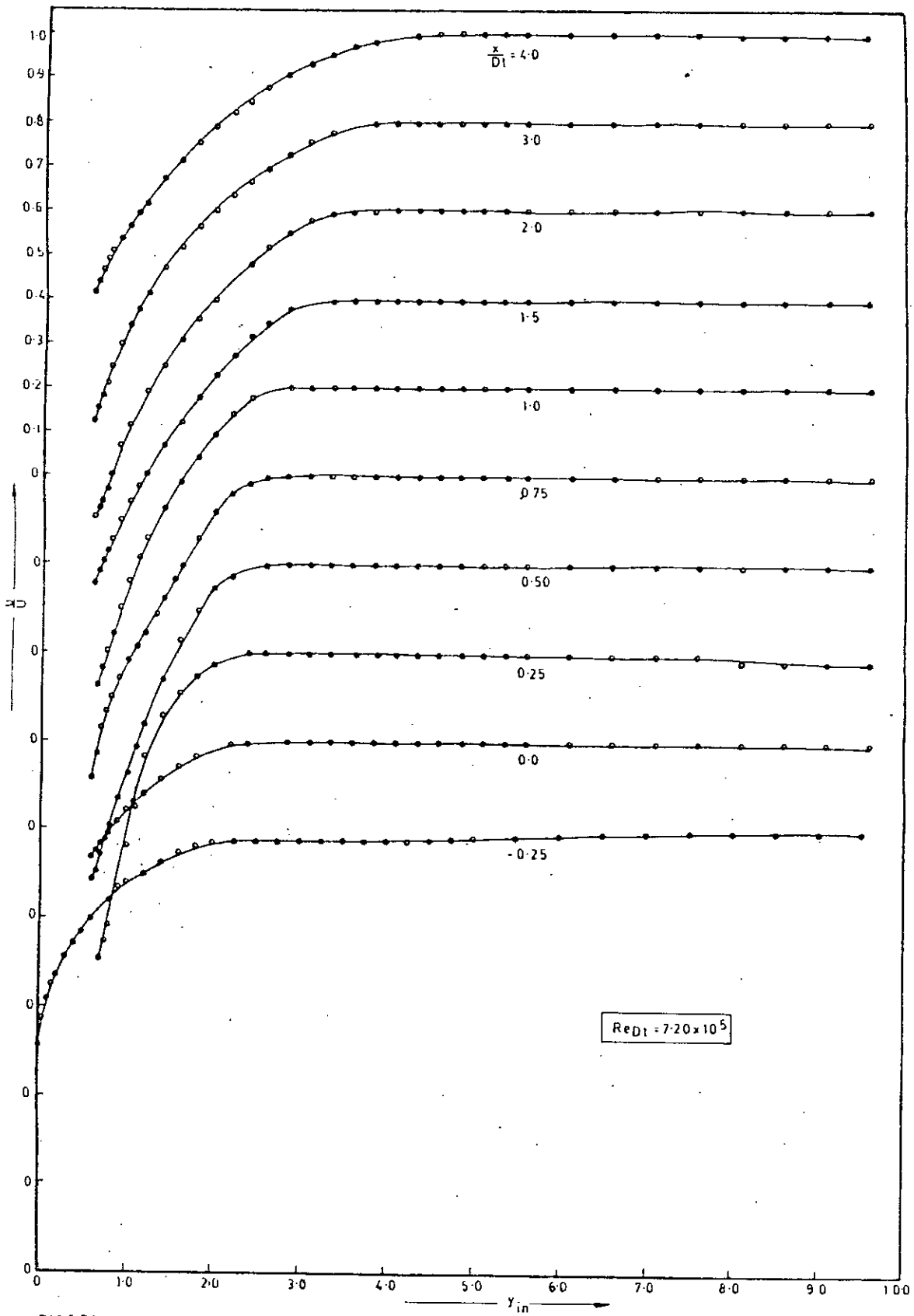

FIG.57 b MEAN VELOCITY PROFILES OVER ROUGH SURFACE

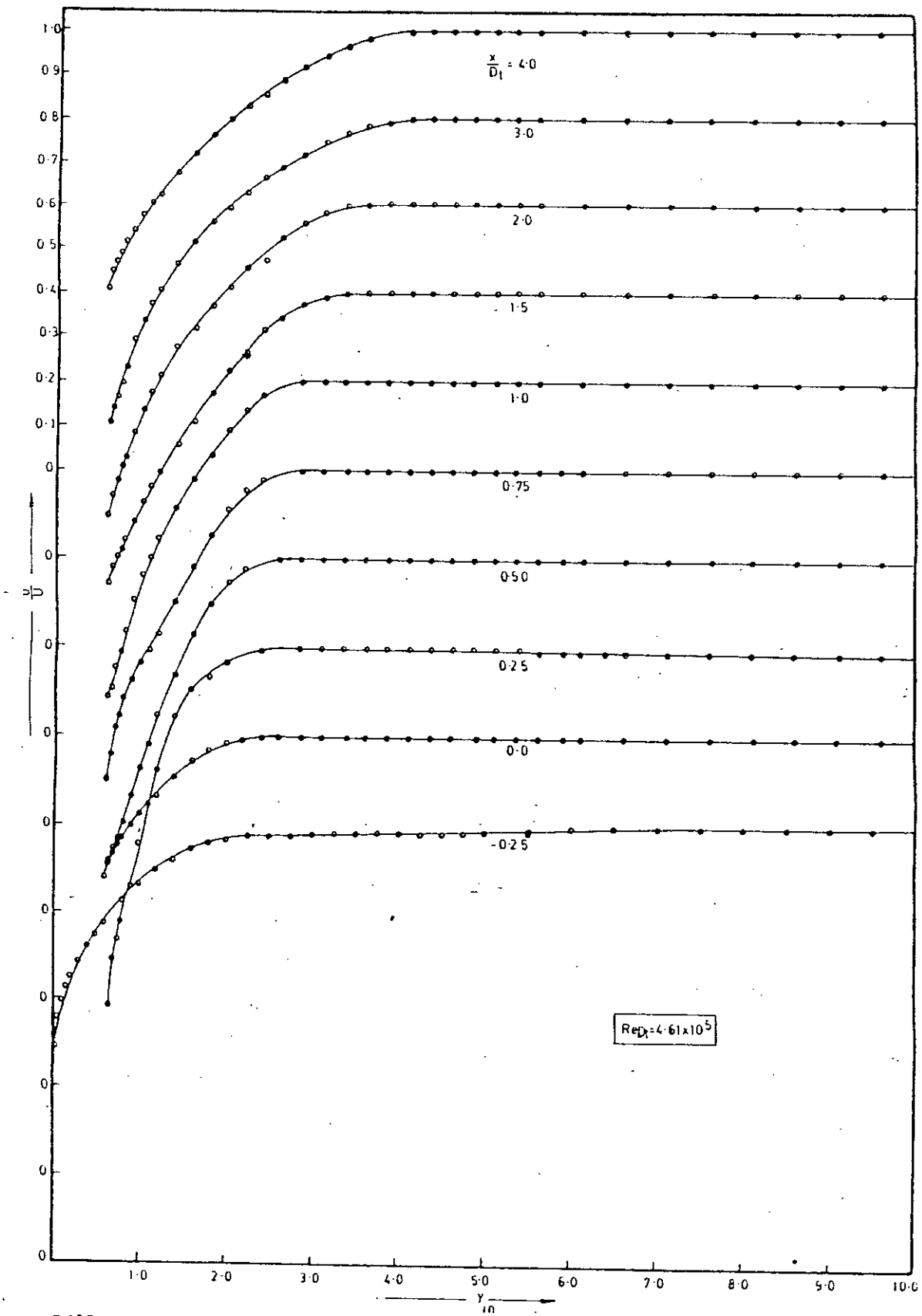

FIG5·7 c MEAN VELOCITY PROFILES OVER ROUGH SURFACE

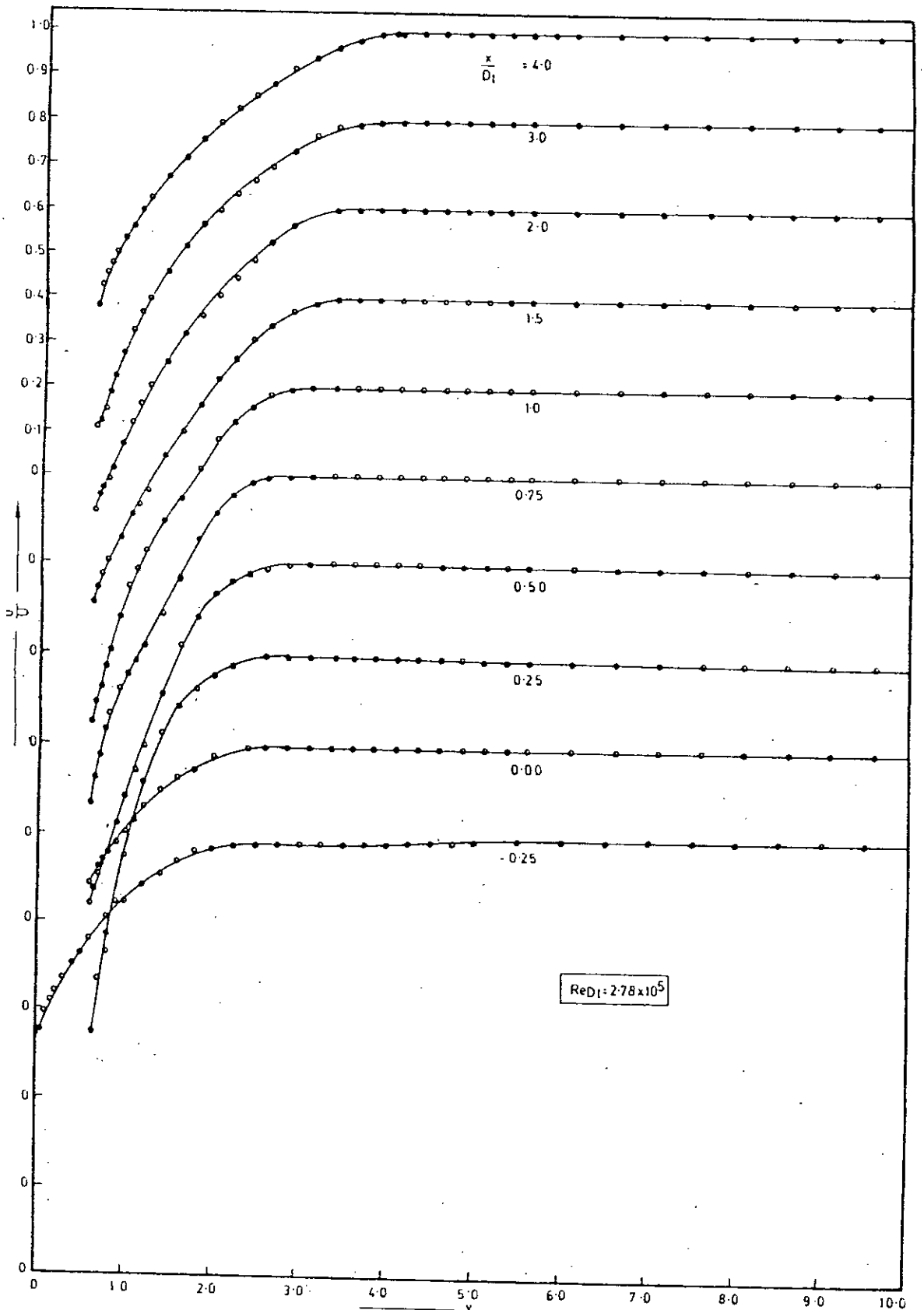

FIG·5·7d MEAN VELOCITY PROFILE OVER ROUGH SURFACE

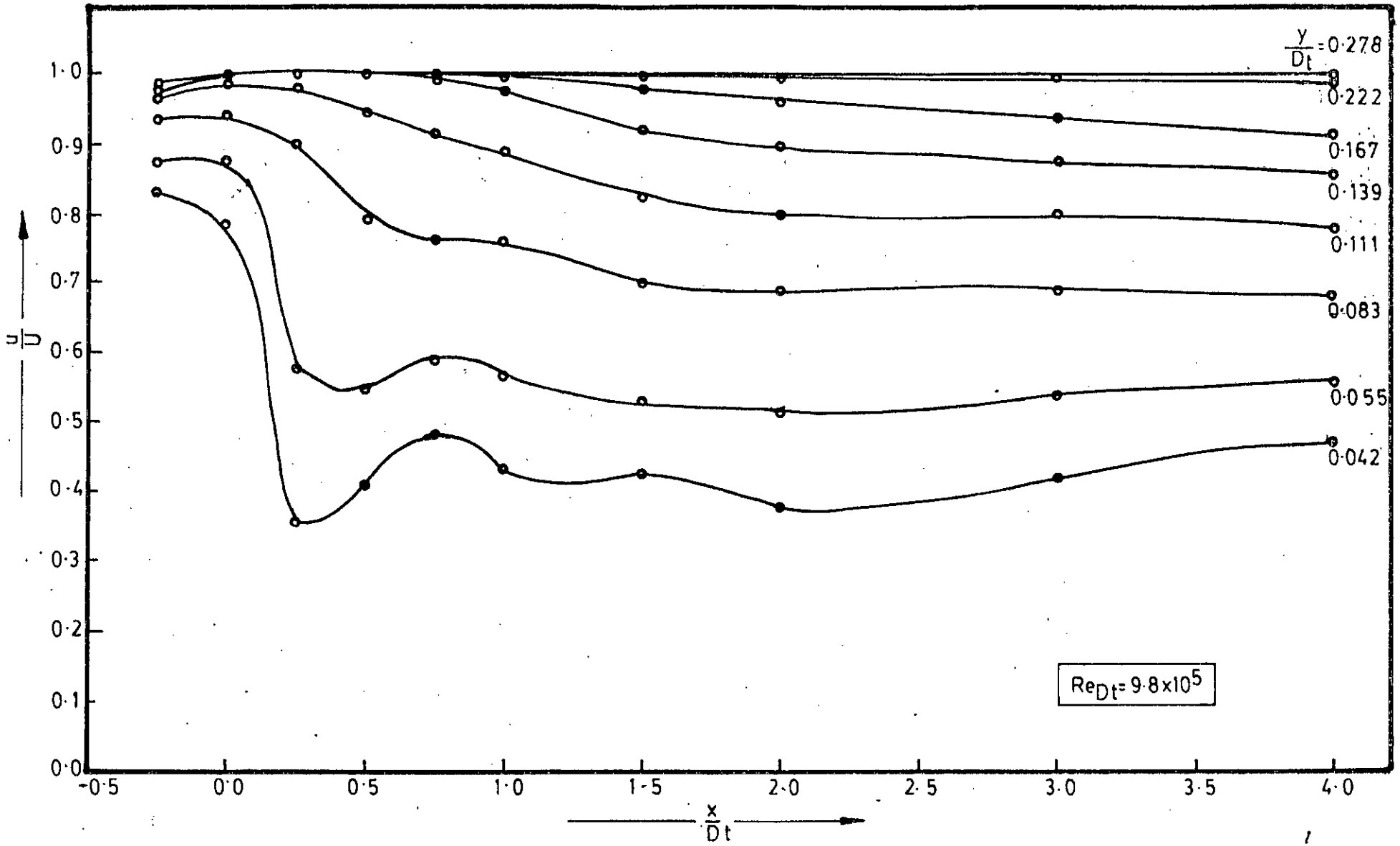

FIG·5·8 a AXIAL MEAN VELOCITY DISTRIBUTION IN TRANSITION FROM SMOOTH TO ROUGH SURFACE

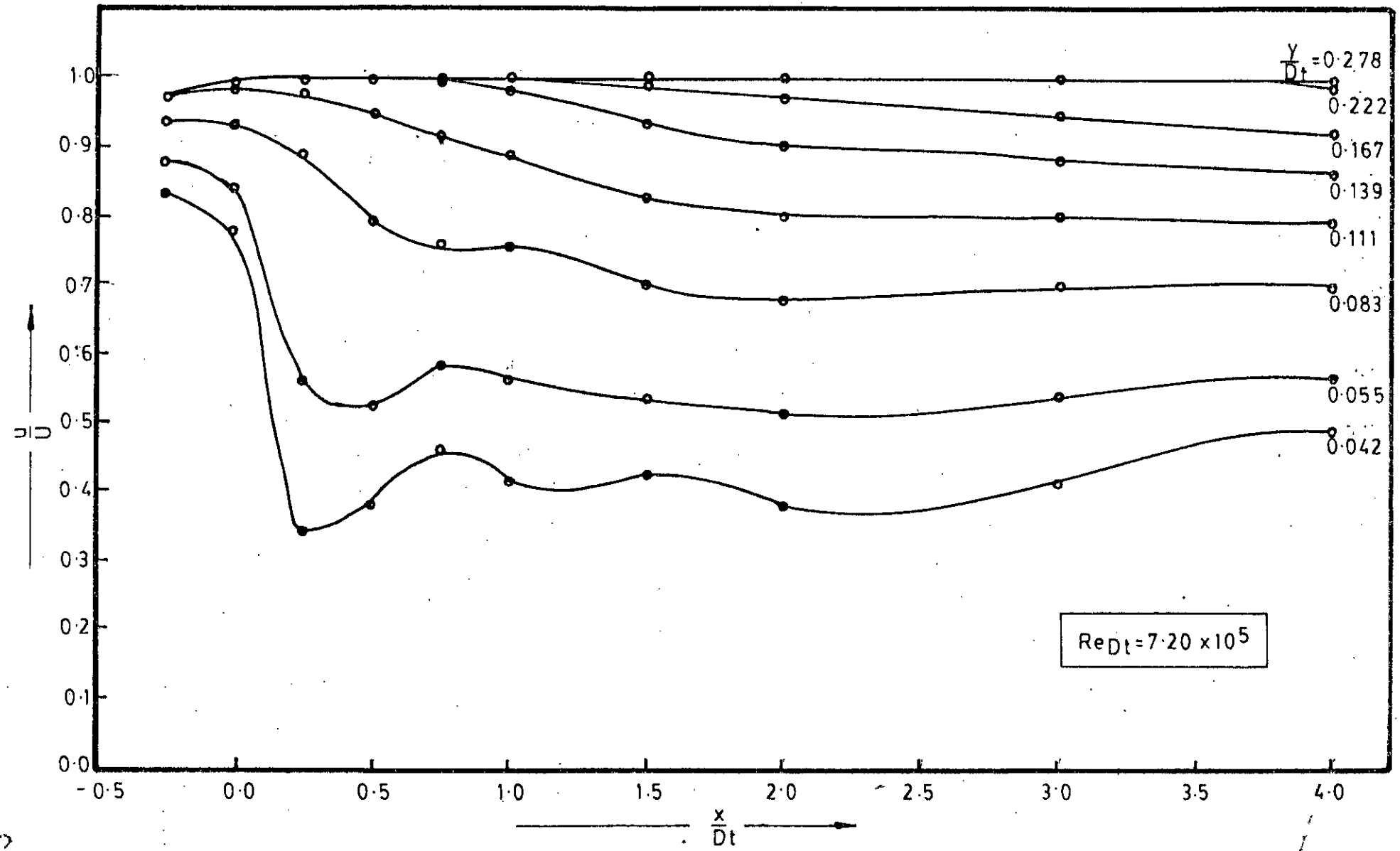

FIG. 5·8 b AXIAL MEAN VELOCITY DISTRIBUTION IN TRANSITION FROM SMOOTH TO ROUGH SURFACE

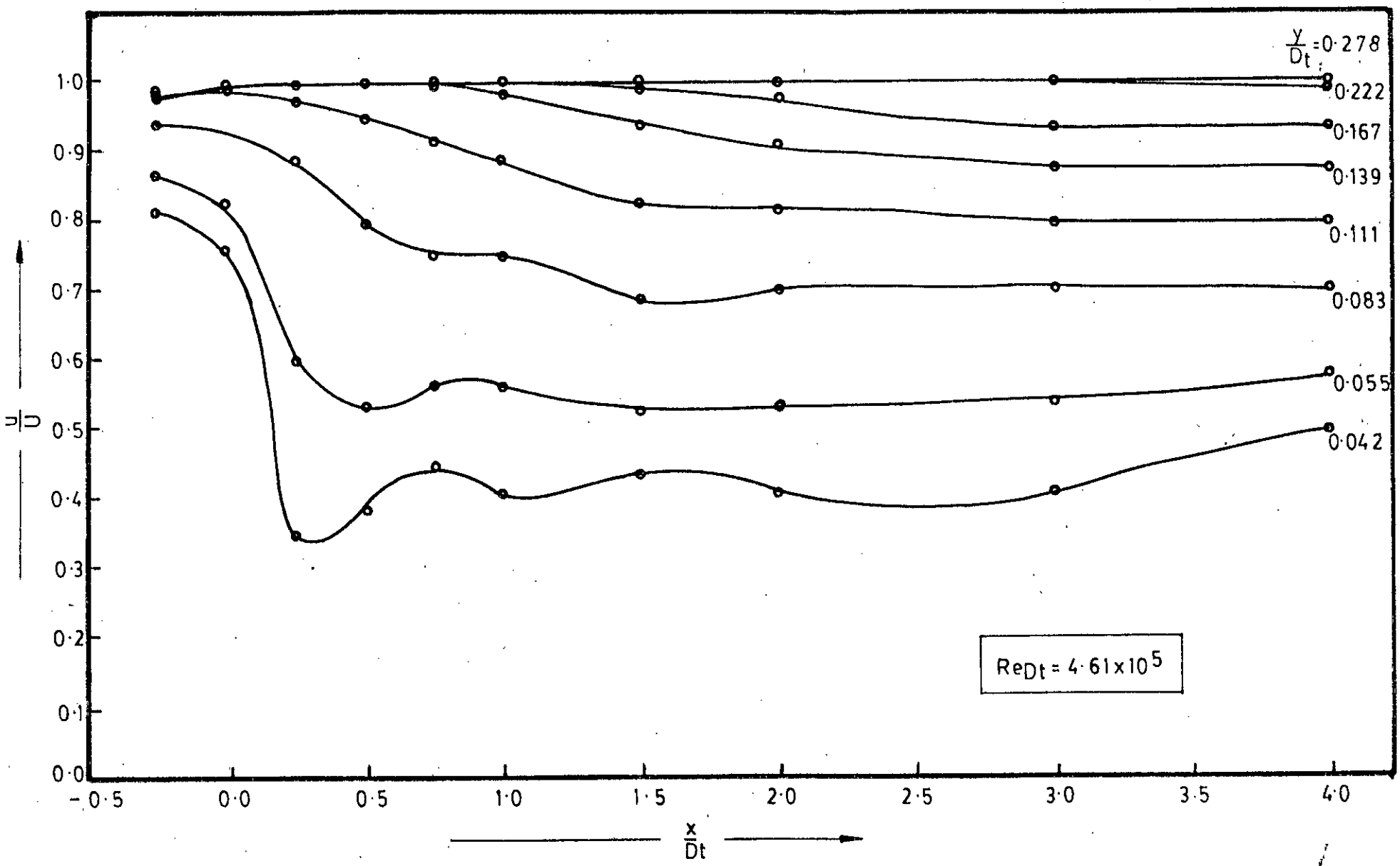

FIG·5·8t AXIAL MEAN VELOCITY DISTRIBUTION IN TRANSITION FROM SMOOTH TO ROUGH SURFACE

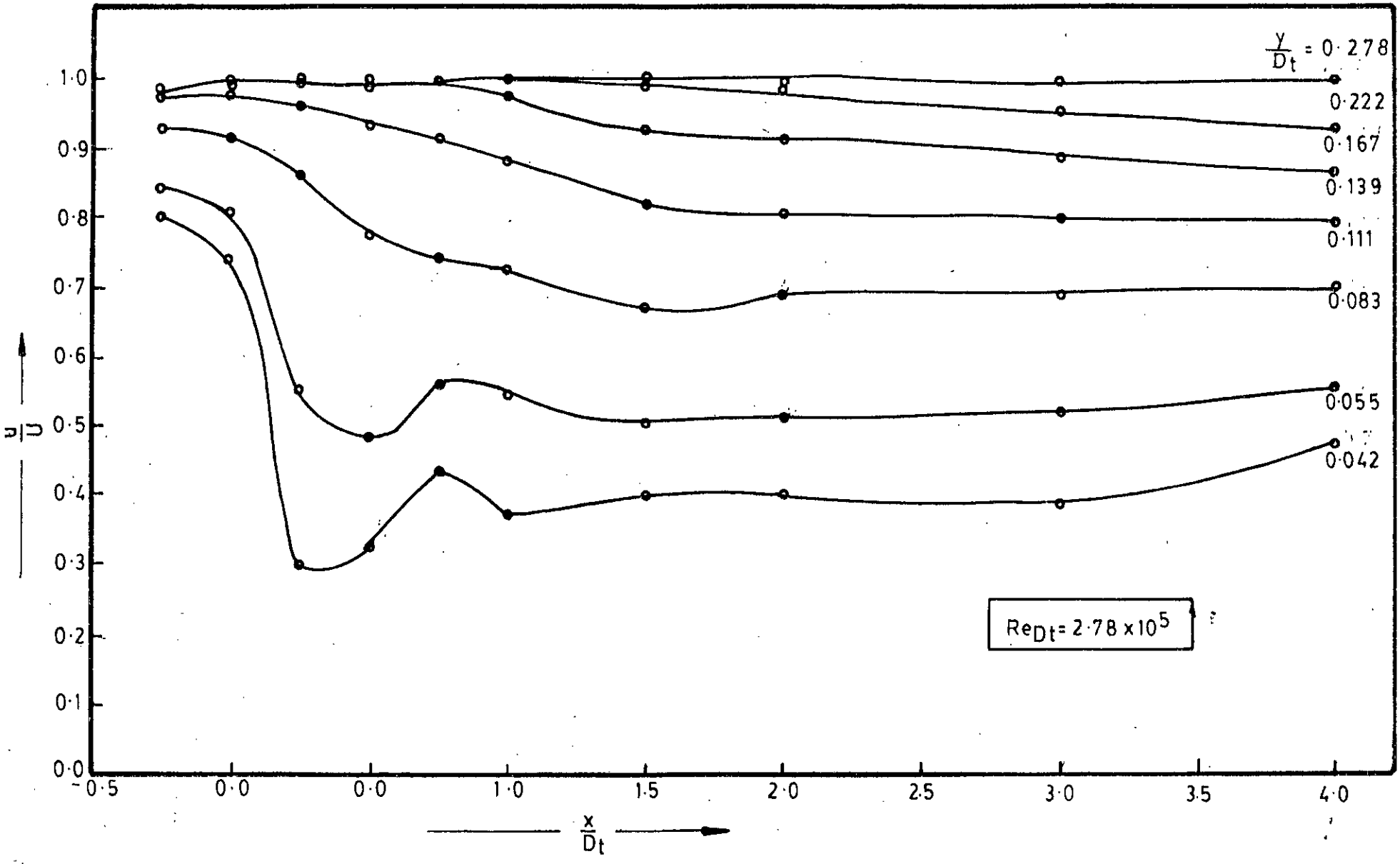

FIG·5·8 d AXIAL MEAN VELOCITY DISTRIBUTION IN TRANSITION FROM SMOOTH TO ROUGH SURFACE

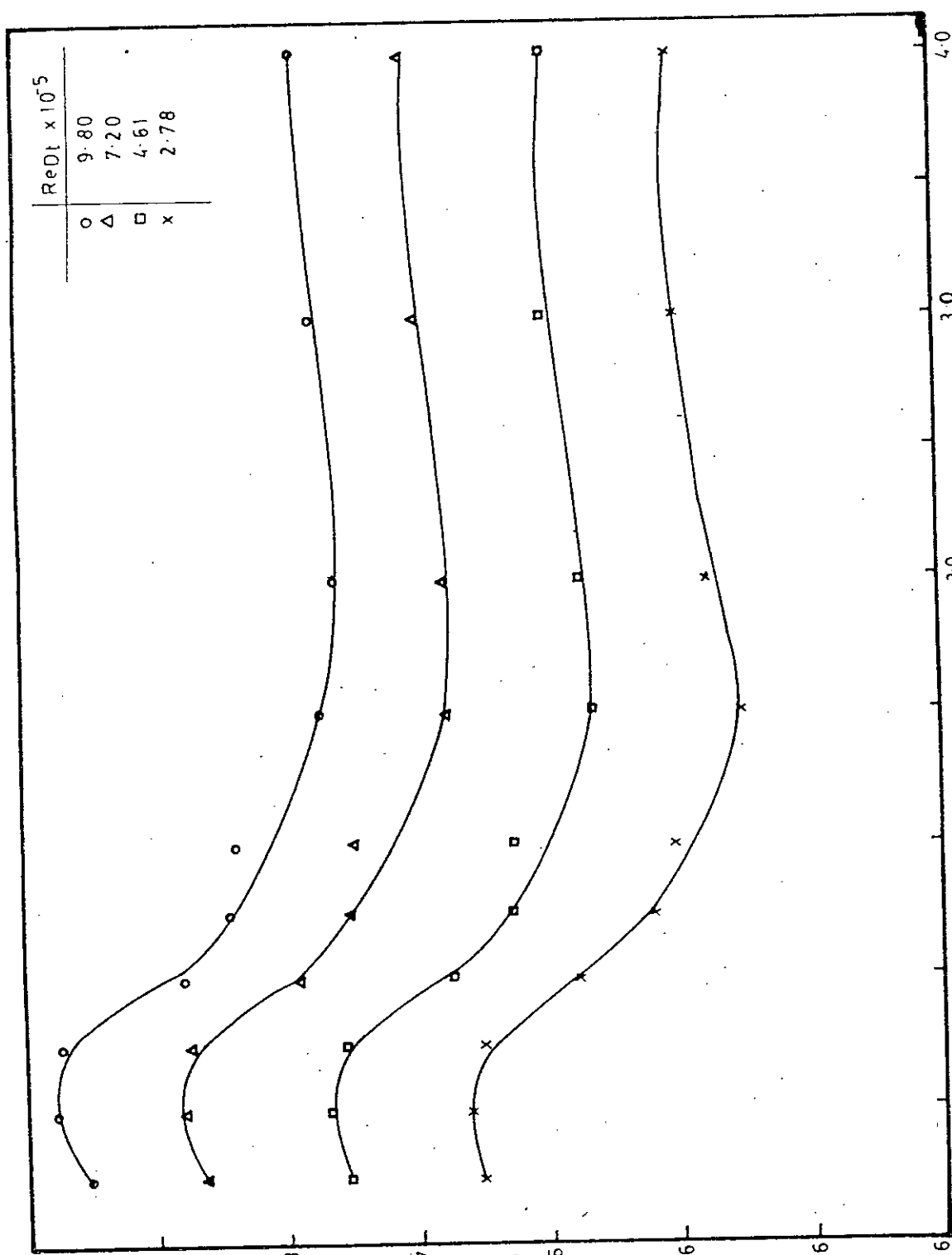

FIG. 5.8 e MEAN AXIAL VELOCITY DISTRIBUTION AT $y = 1{\cdot}6$ in

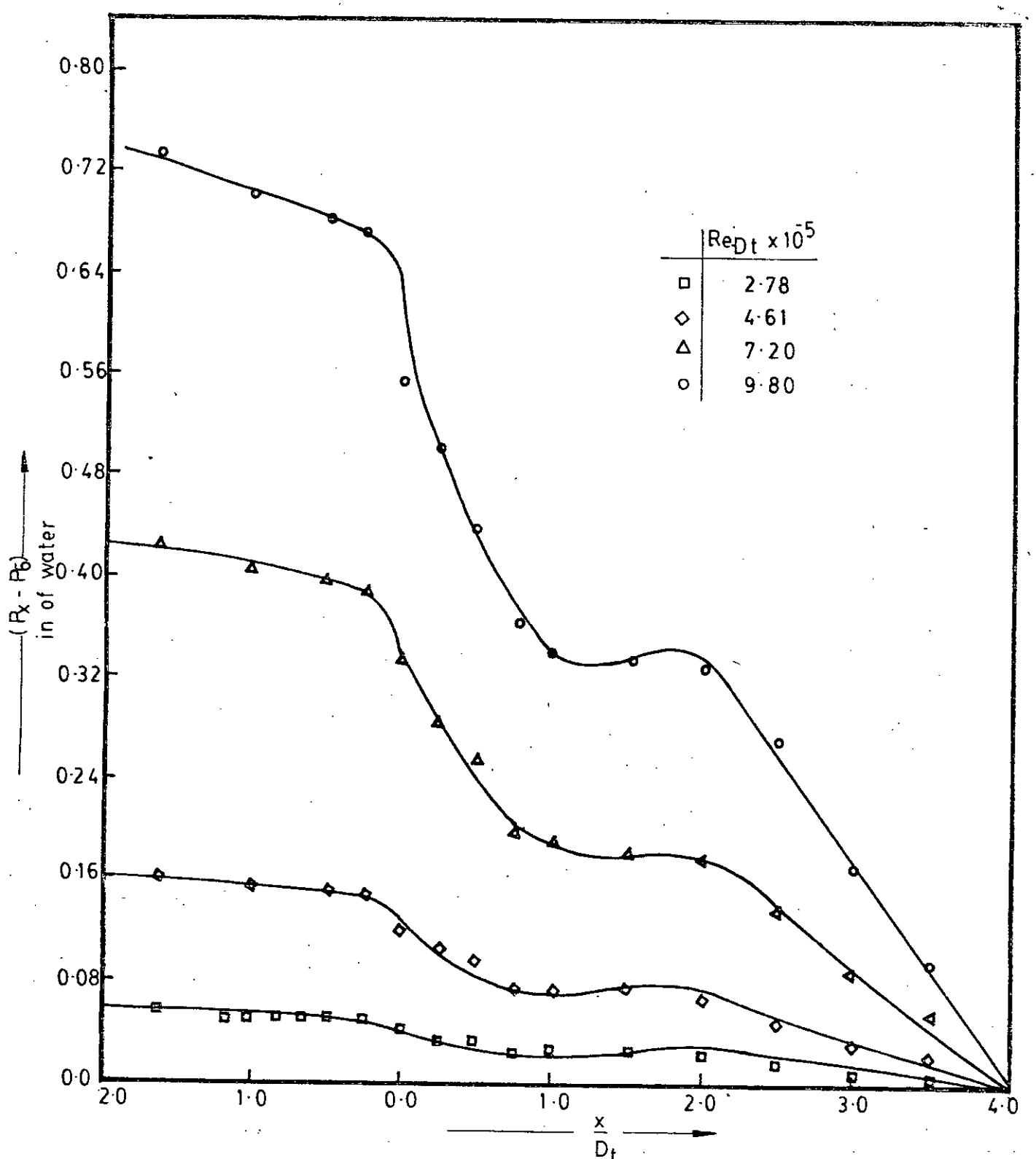

FIG. 5·9 PRESSURE GRADIENT ALONG THE FLOW DIRECTION WITH ROUGH SURFACE

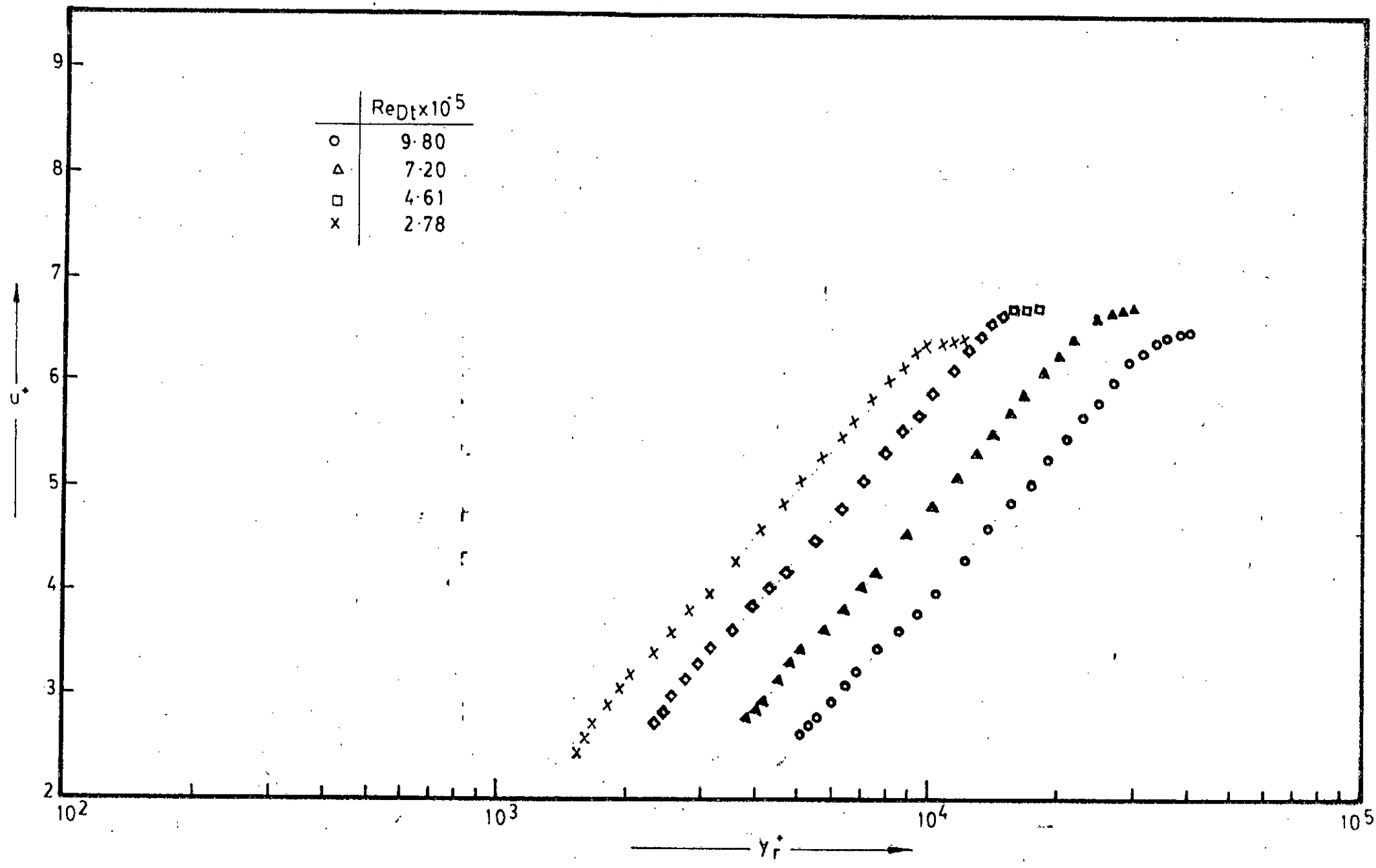

- FIG.5-10 LOG-LAW PLOTS FOR ROUGH SURFACE AT x/Dt = 4·0

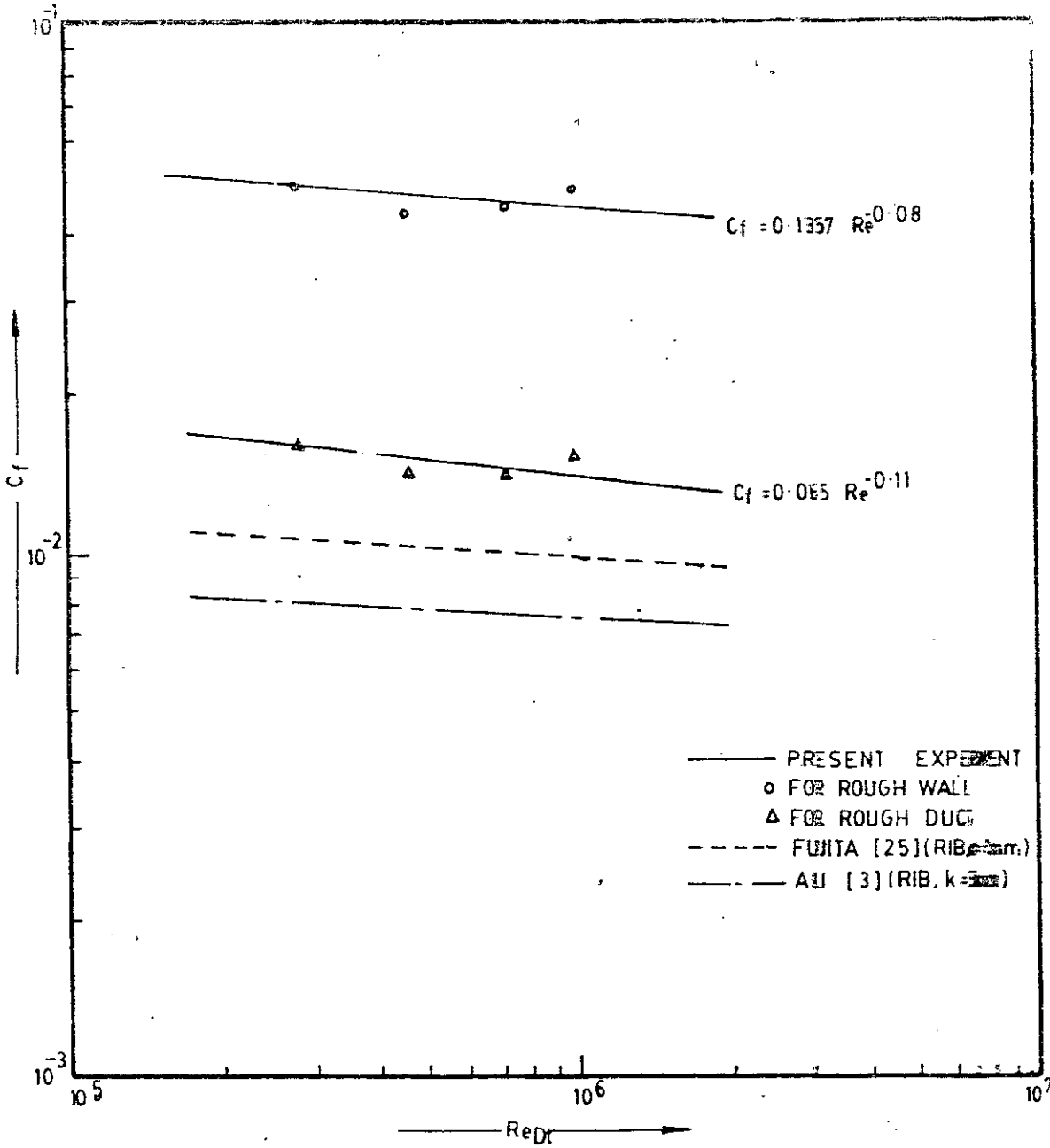

FIG.5.11 FRICTION FACTOR VERSUS REYNOLDS NUMBER FOR ROUGH SURFACE

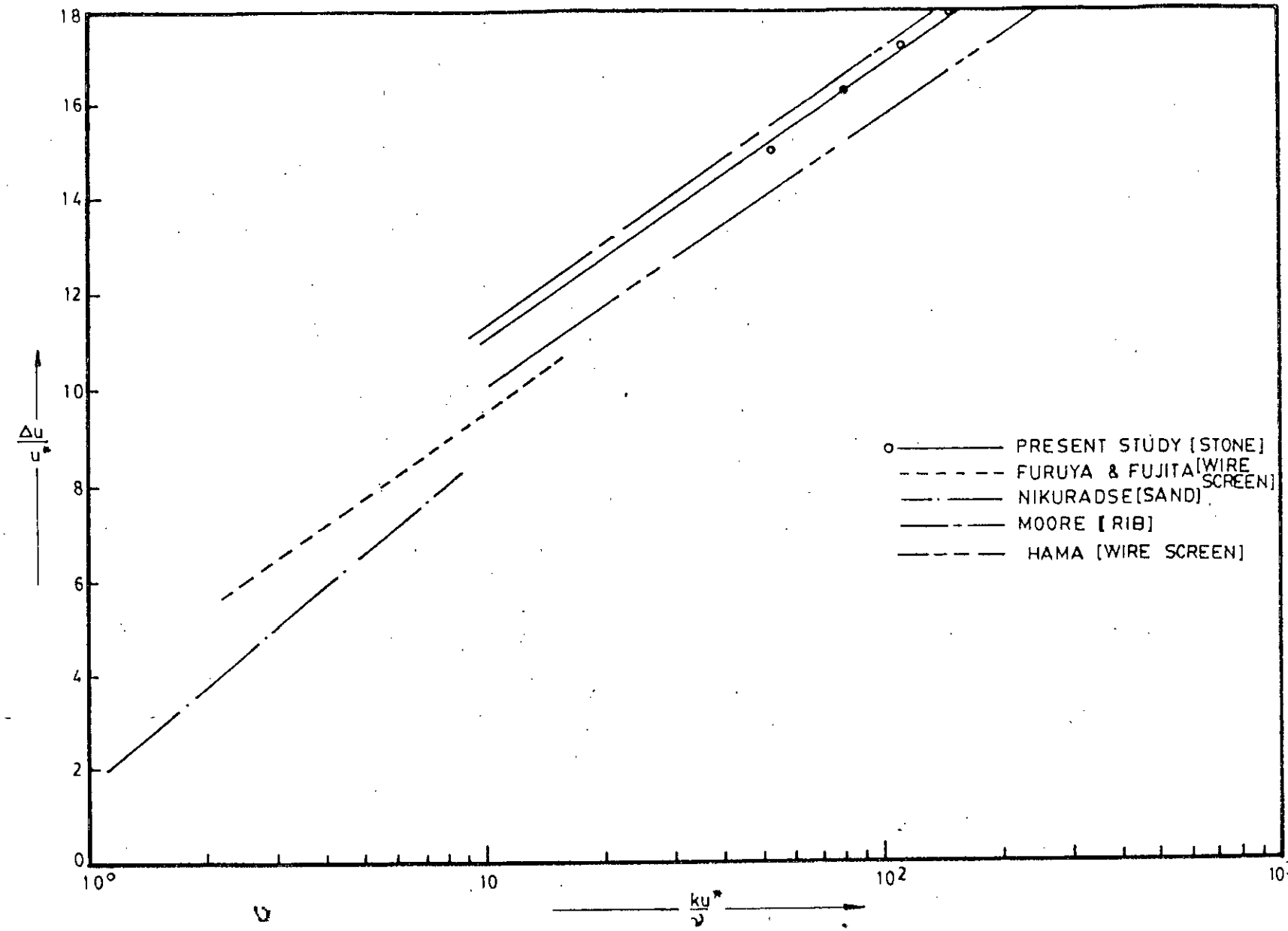

FIG. 5.12 RELATION BETWEEN WALL FUNCTION AND ROUGHNESS REYNOLDS NUMBER

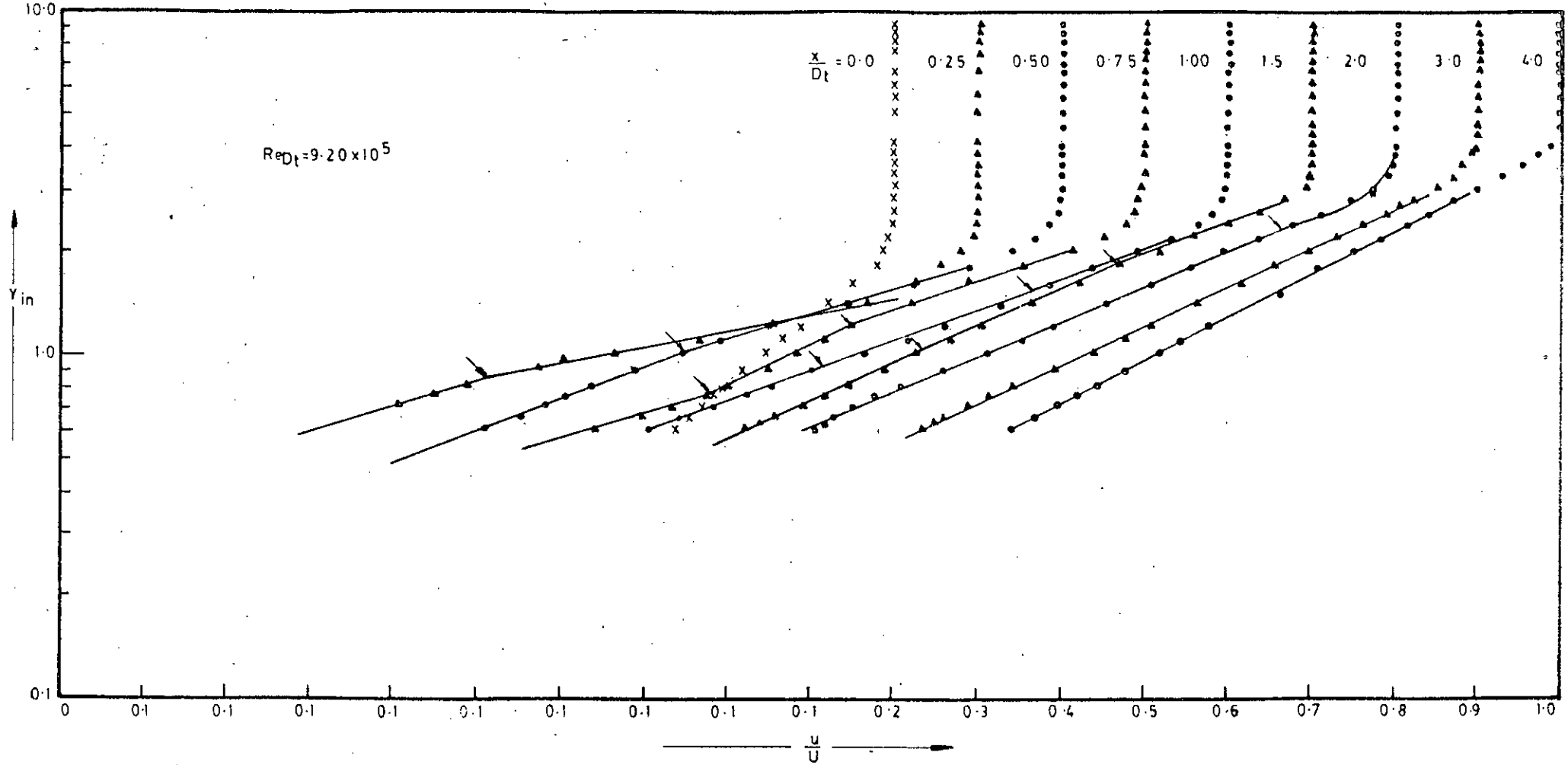

FIG 5·13a LOGARITHMIC VELOCITY PROFILES OVER ROUGH SURFACE

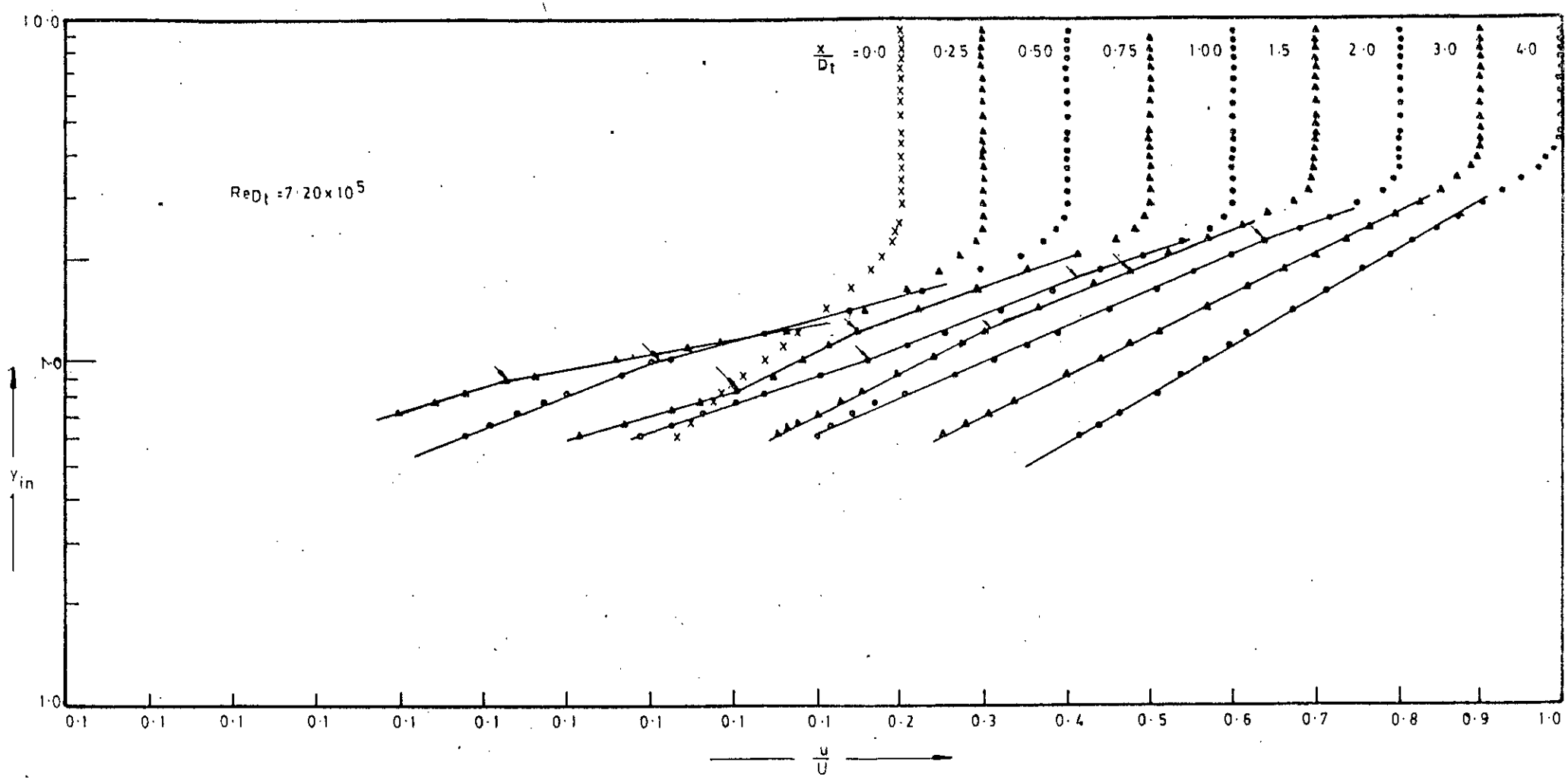

FIG·5·13 b LOGARITHMIC VELOCITY PROFILES OVER SURFACE

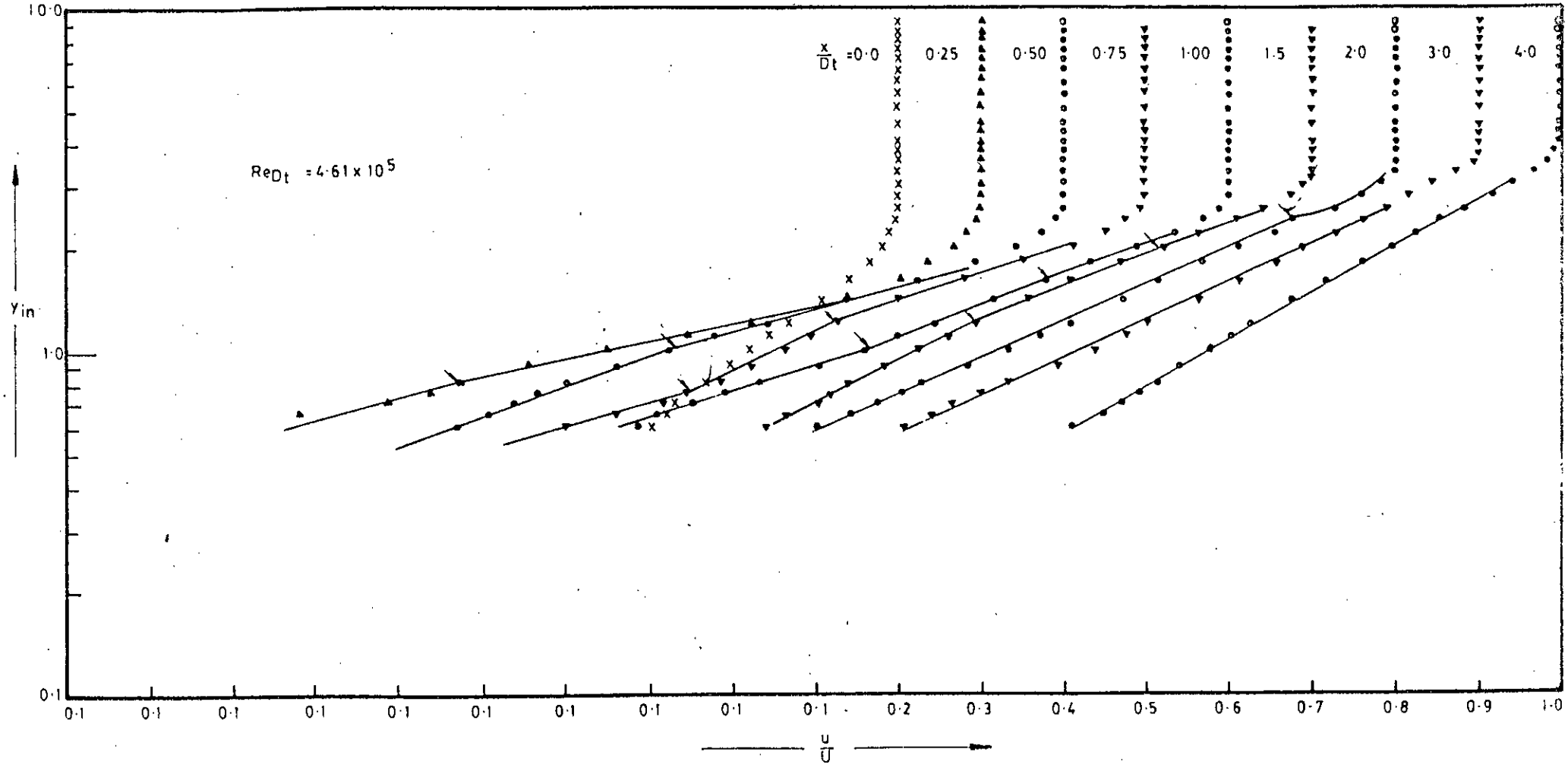

FIG·5·13 c LOGARITHMIC VELOCITY PROFILES OVER ROUGH SURFACE

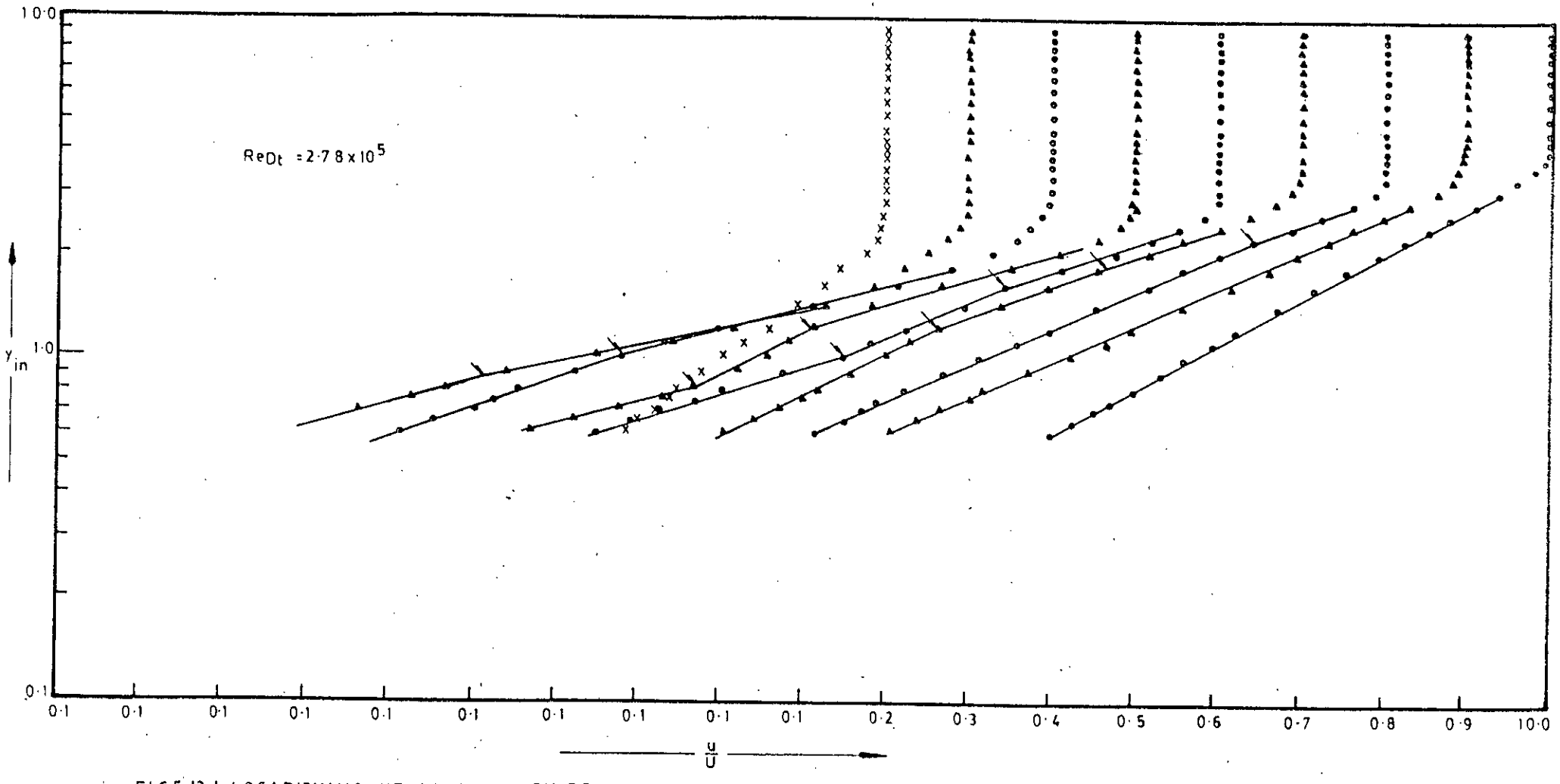

FIG 5·13 d LOGARITHMIC VELOCITY PROFILES OVER ROUGH SURFACE

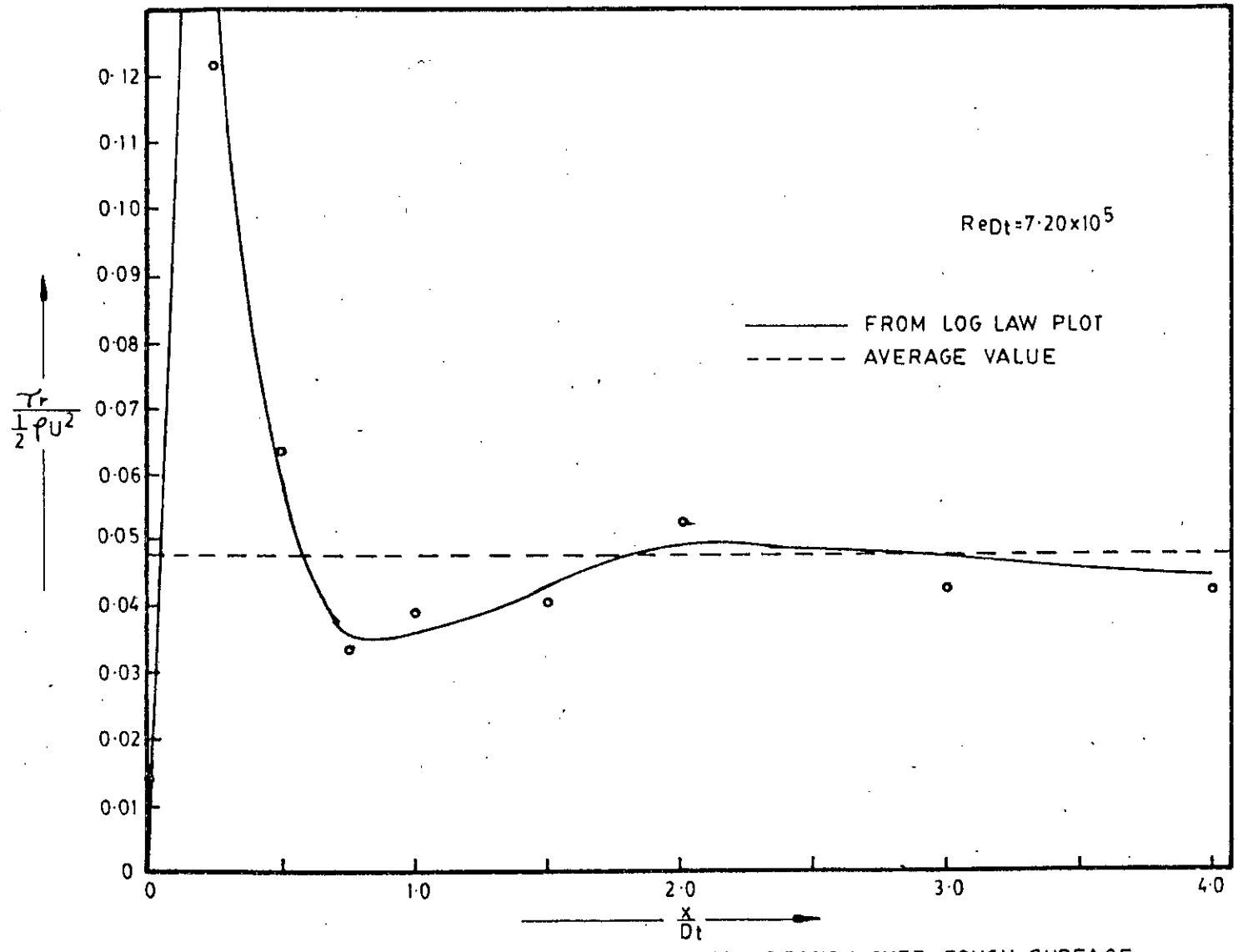

FIG 5·14 SHEAR STRESS VARIATION IN THE AXIAL DIRECTION OVER ROUGH SURFACE

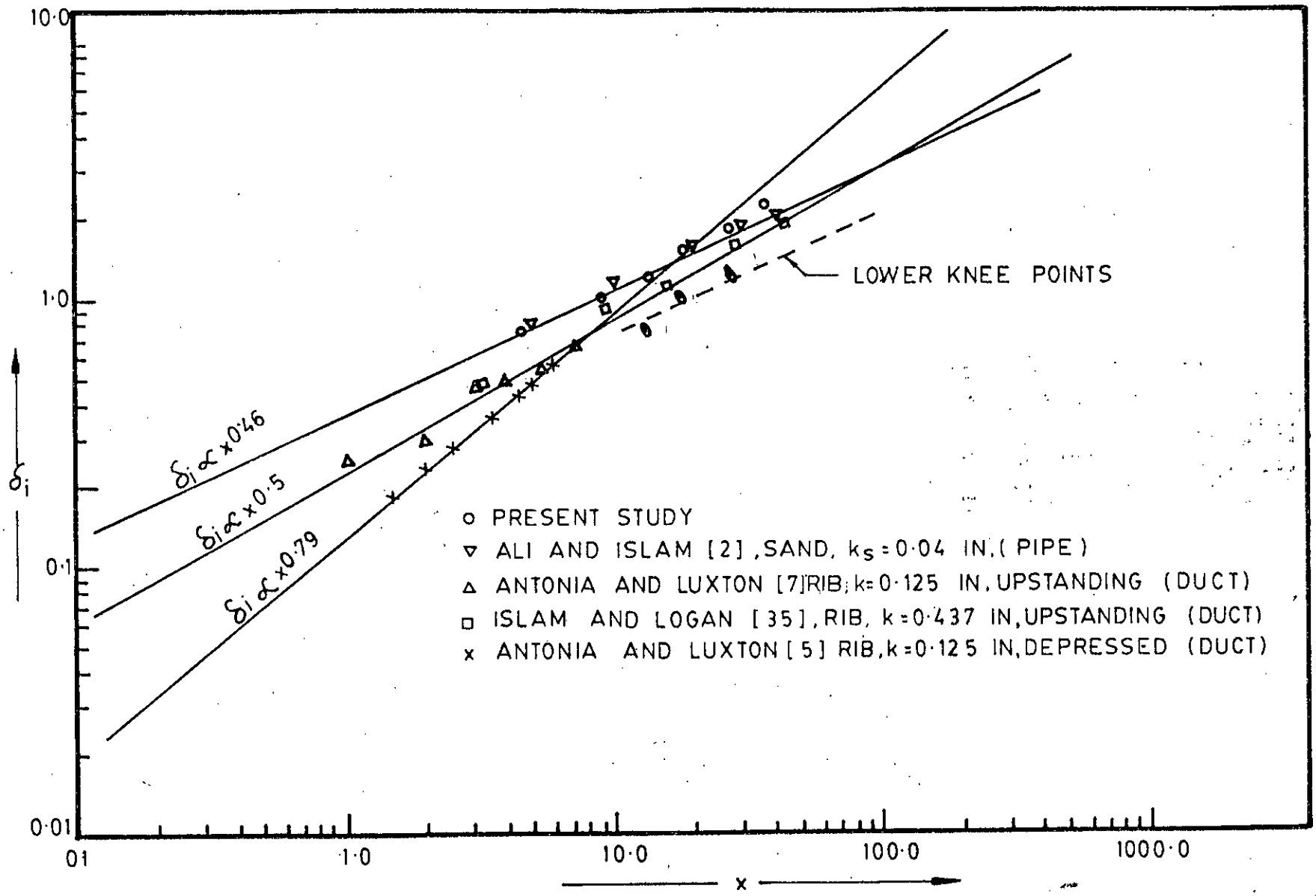

FIG·5·15 GROWTH RATES OF INTERNAL BOUNDARY LAYERS

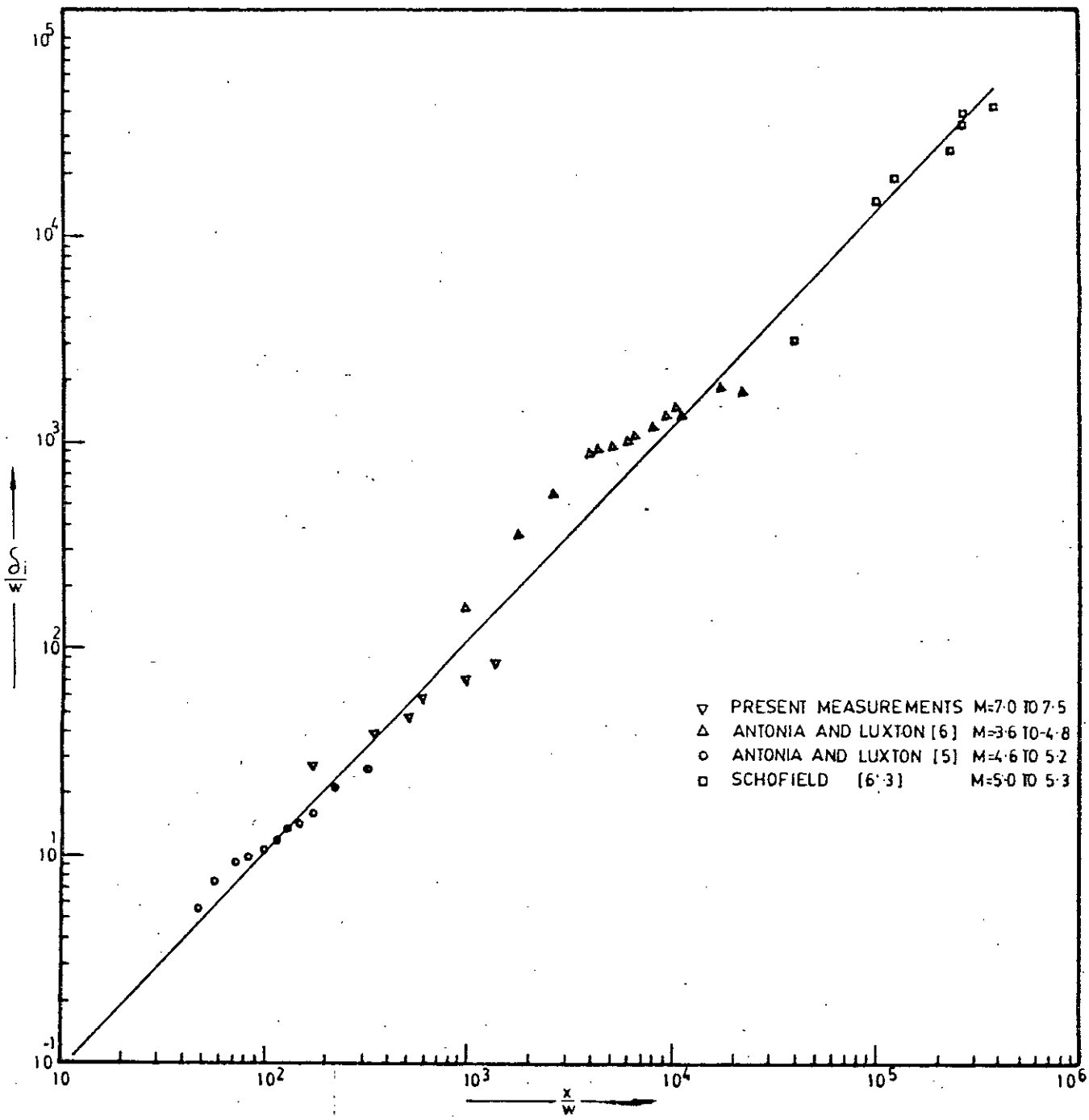

FIG. 5.16 CORRELATION OF INNER LAYER GROWTH RATE

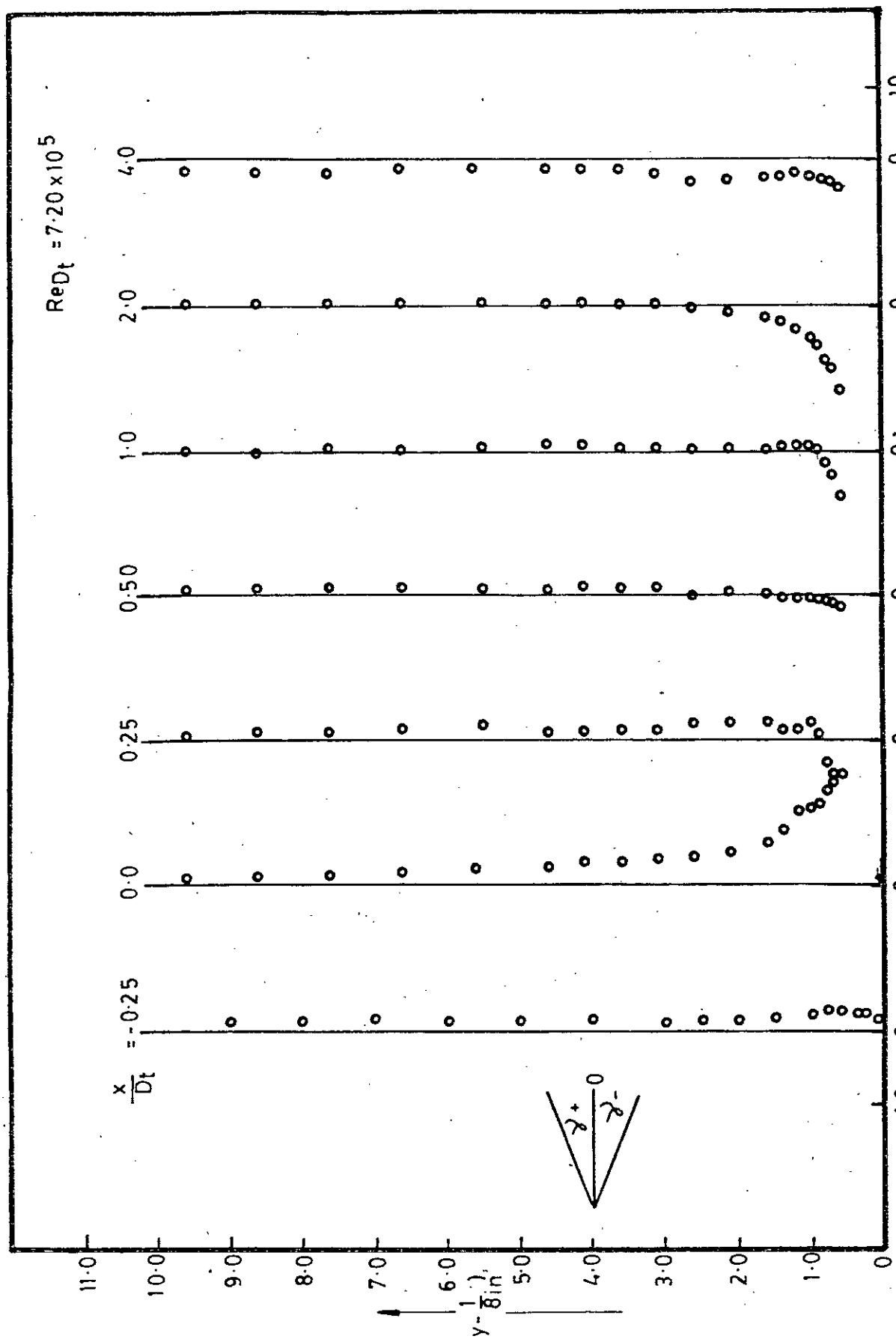

FIG.5:17a ANGLES OF ACTUAL MAIN FLOW DIRECTION IN MID-LONGITUDINAL SECTION

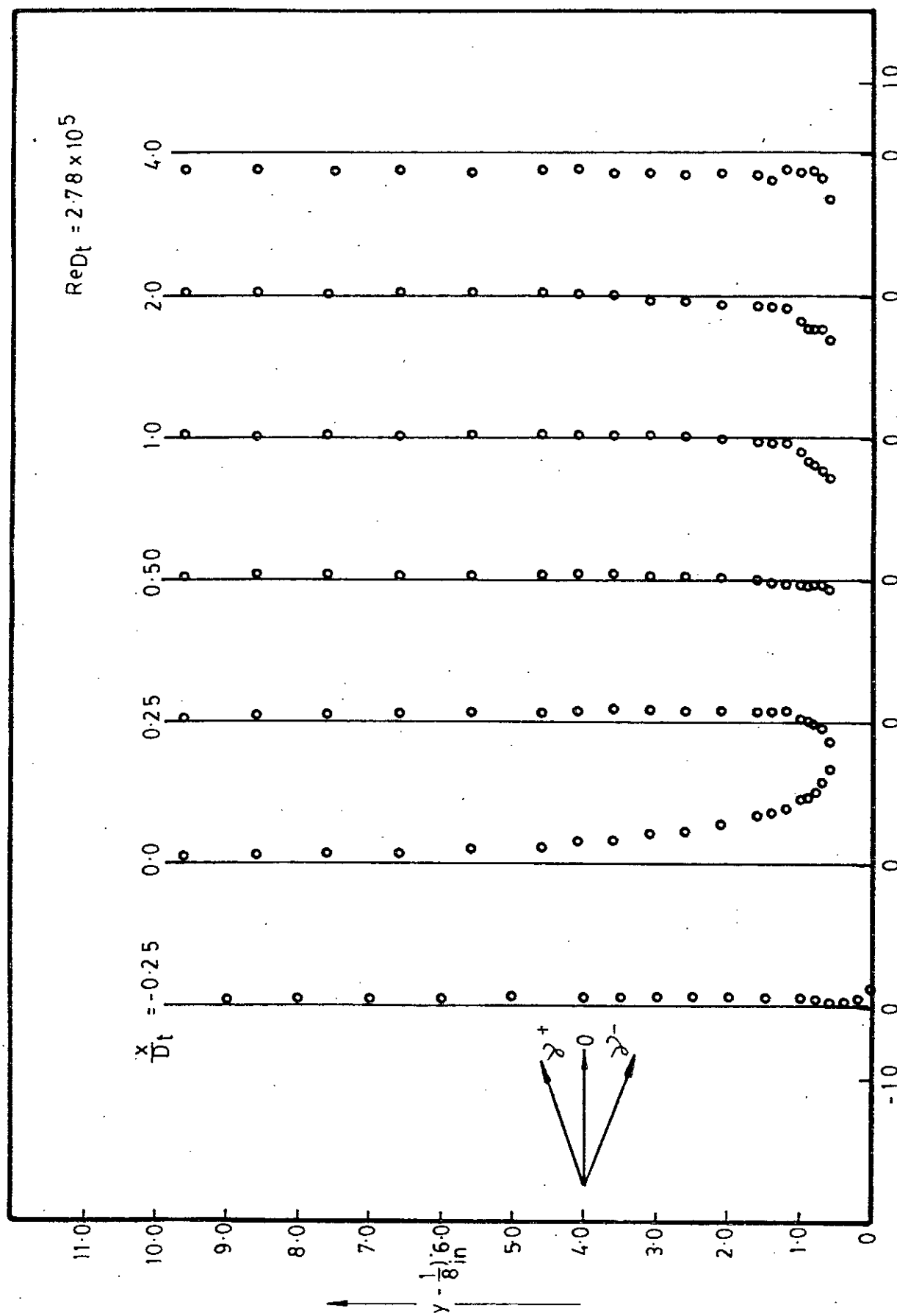

FIG·5·17 b ANGLES OF ACTUAL MAIN FLOW DIRECTION MID-LONGITUDINAL SECTION

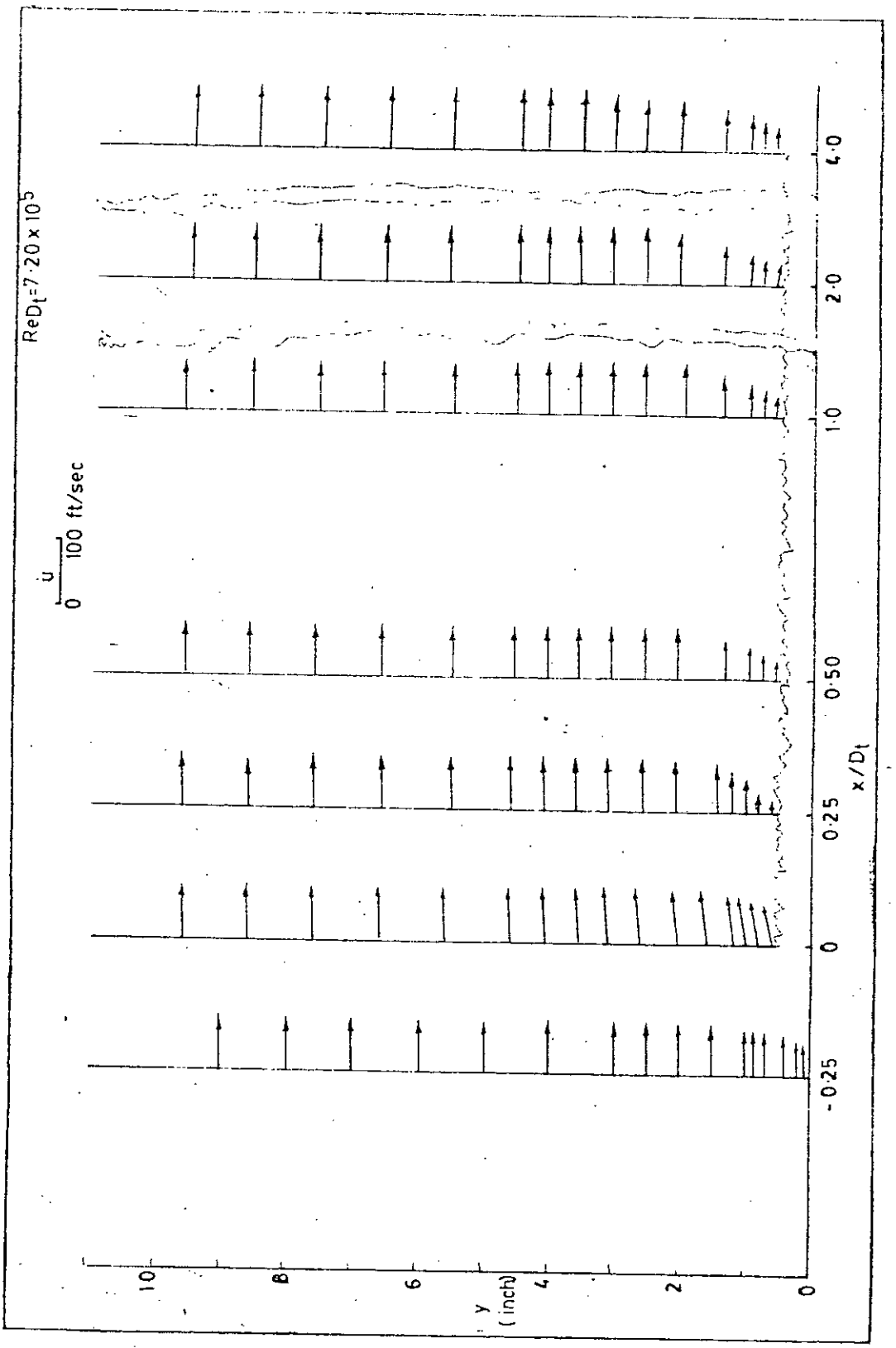

FIG·5·18 MEAN VELOCITY VECTORS OF MAIN STREAM FROM SMOOTH TO ROUGH WALL

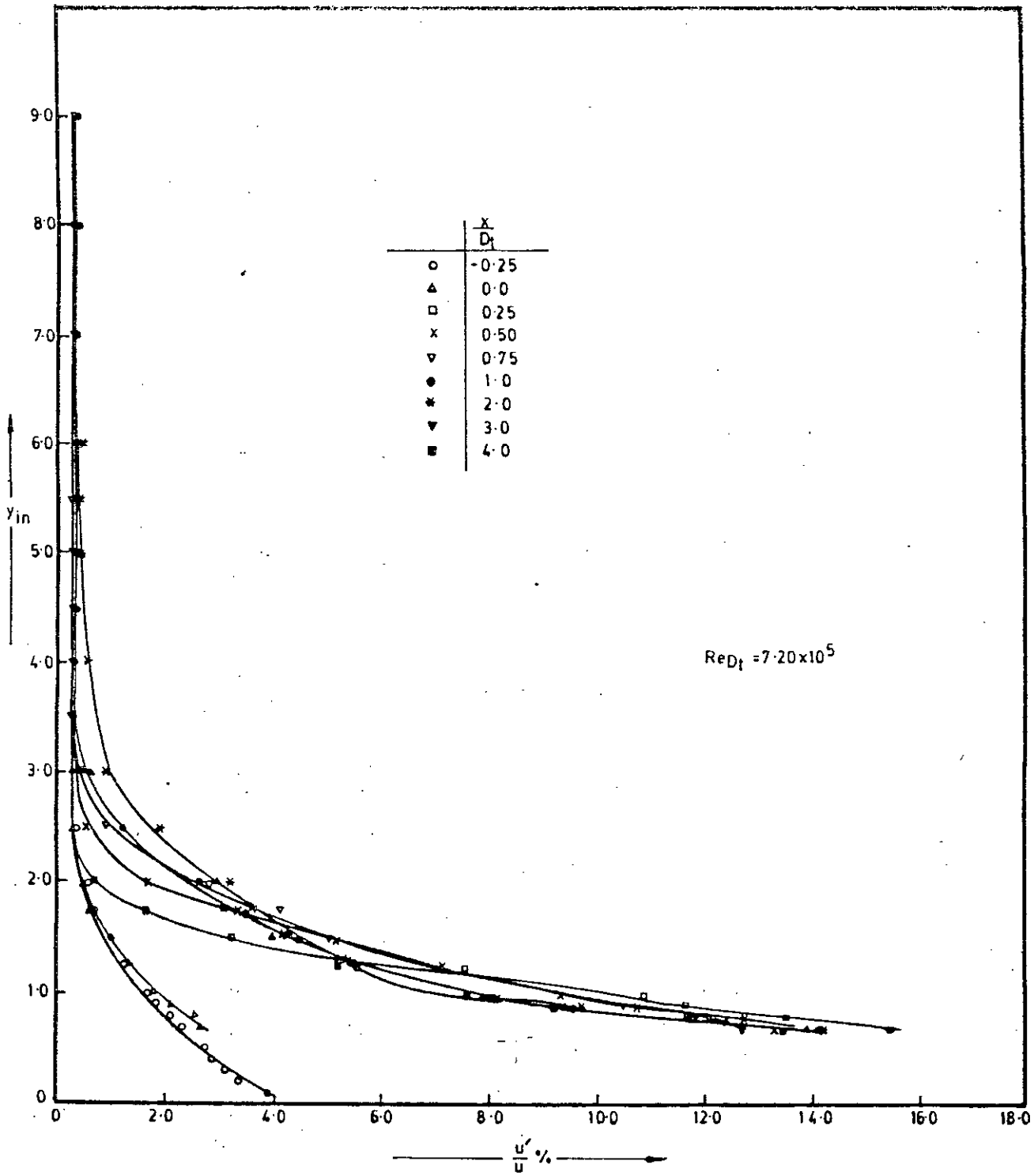

FIG 5·19 TURBULANCE INTENSITY PROFILES OVER ROUGH SURFACE

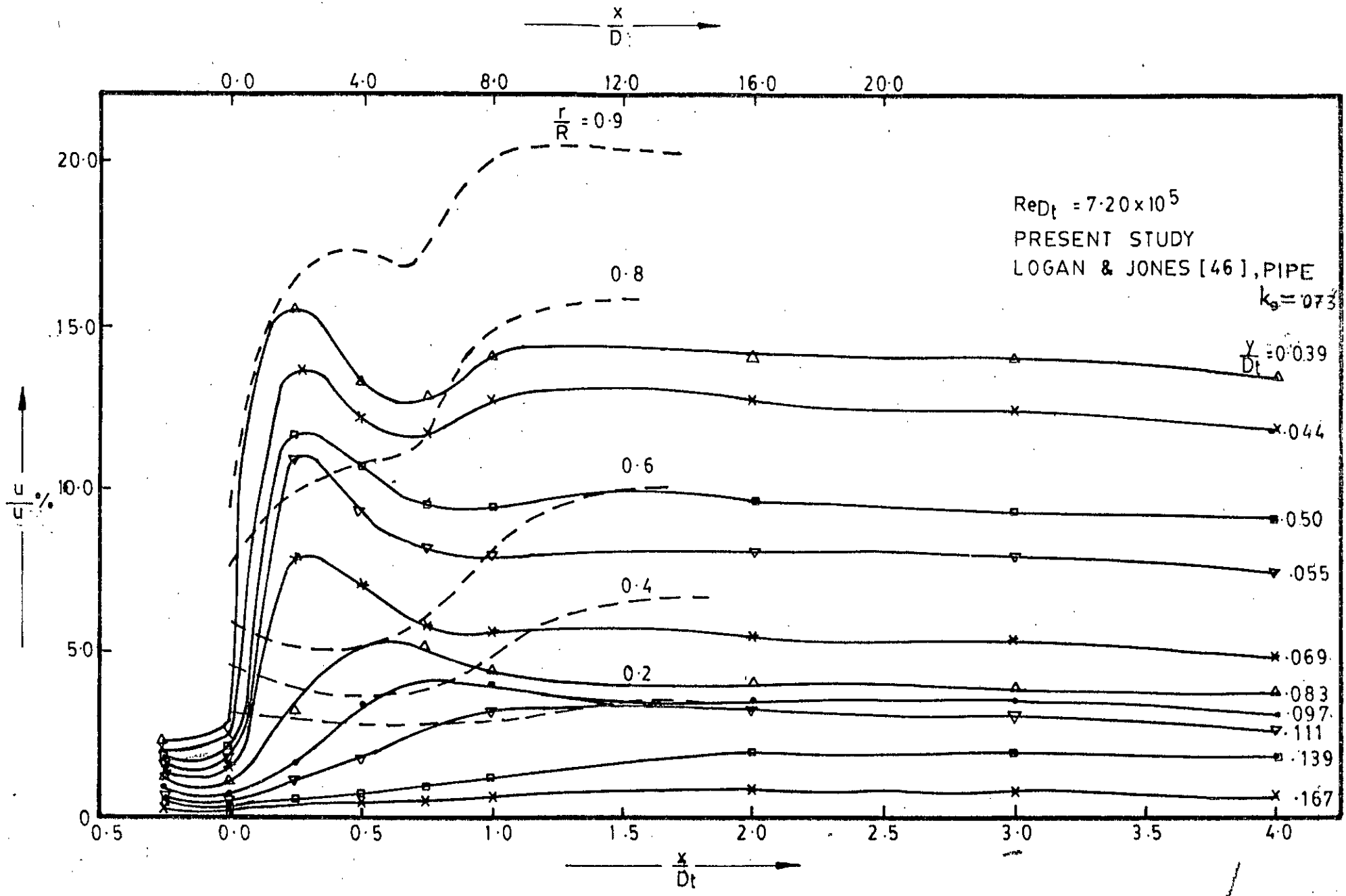

FIG.5·20 AXIAL DISTRIBUTION OF LONGITUDINAL TURBULANCE INTENSITY

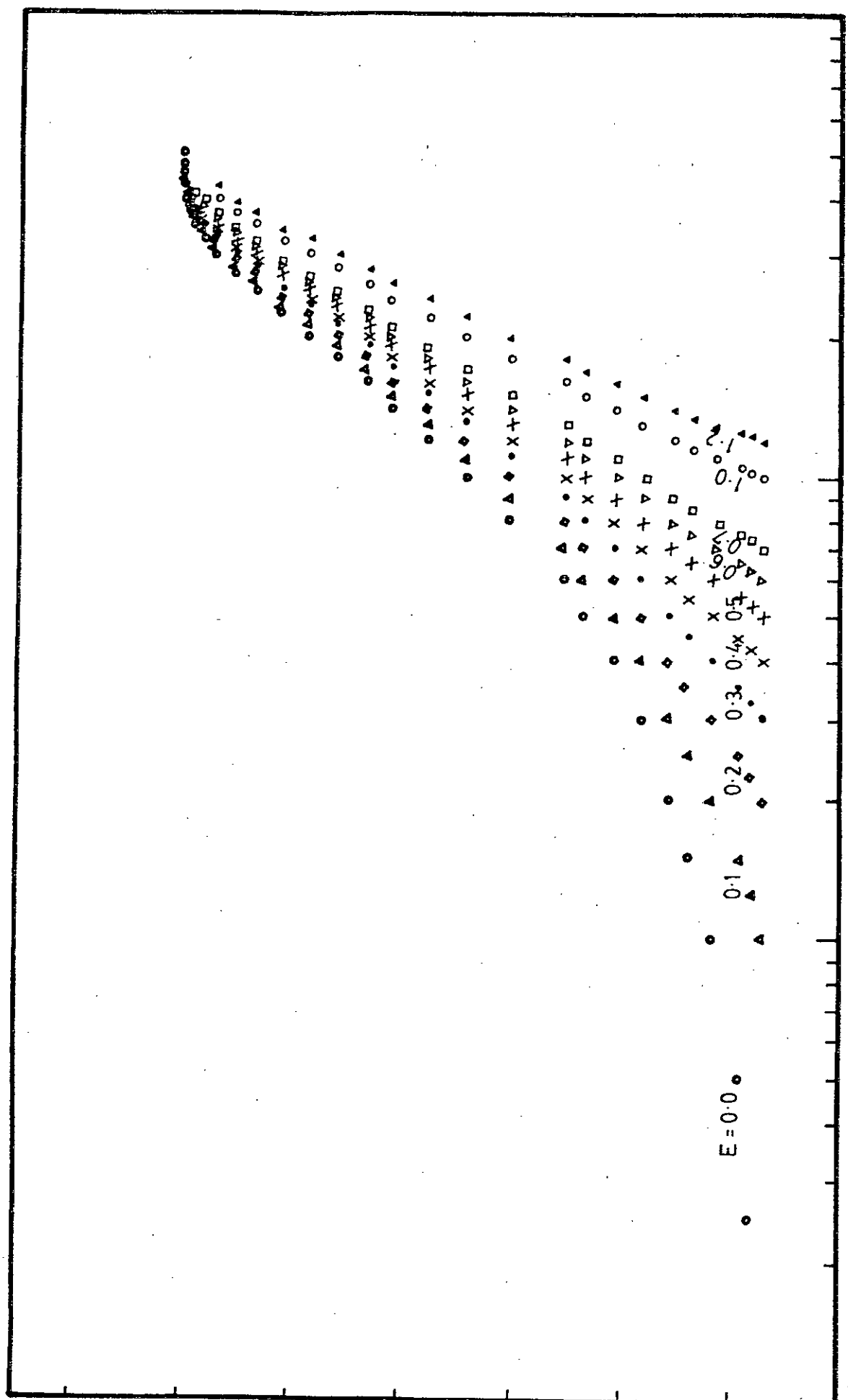

FIG·5·21 EFFECT OF POSITION OF ORIGIN ON ROUGH WALL LOG-LAW PROFILE

LIST OF PLATES

PLATE 4·1 STONE ROUGHENED SURFACE

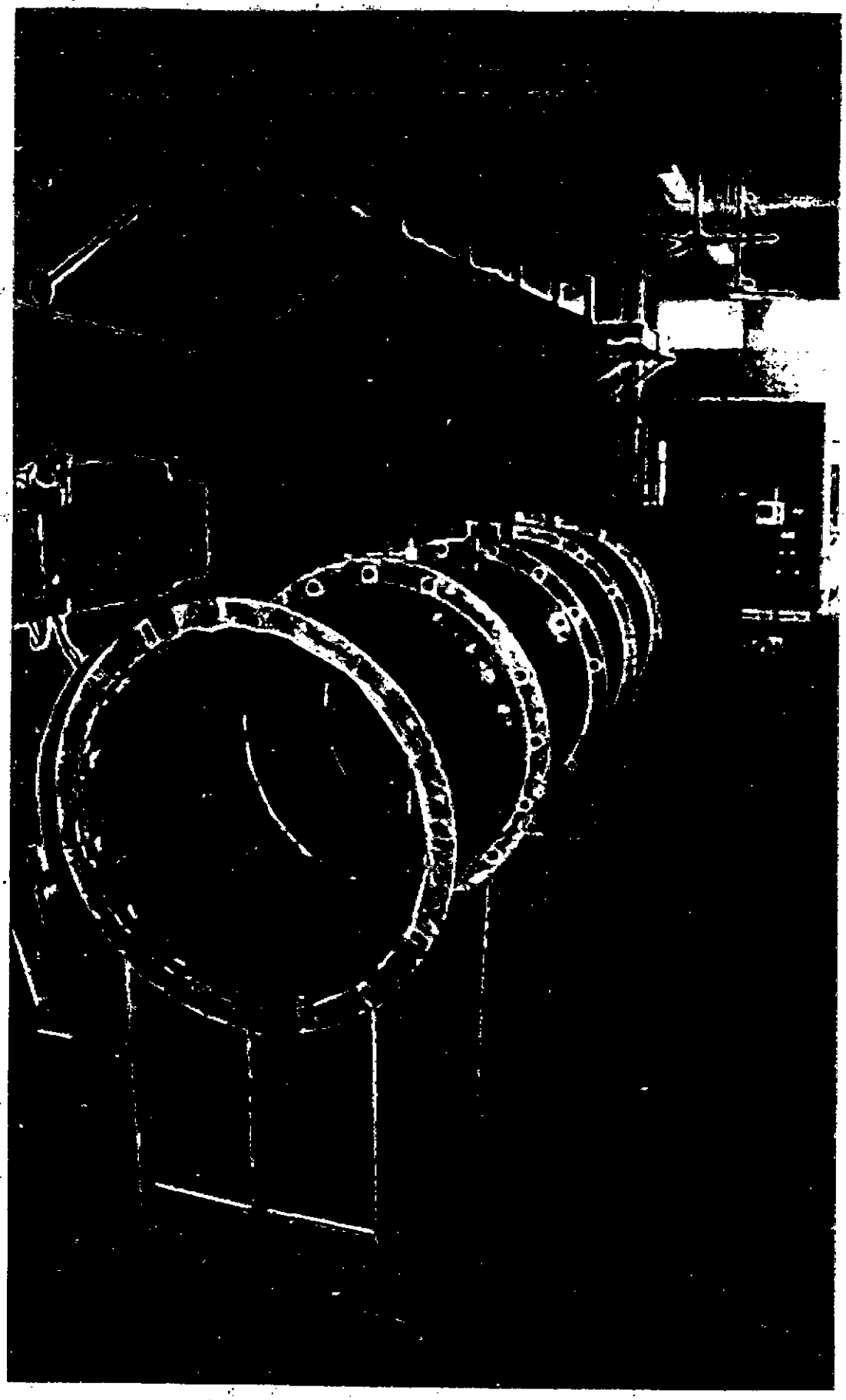

PLATE 4·2 WIND TUNNEL FRONT VIEW

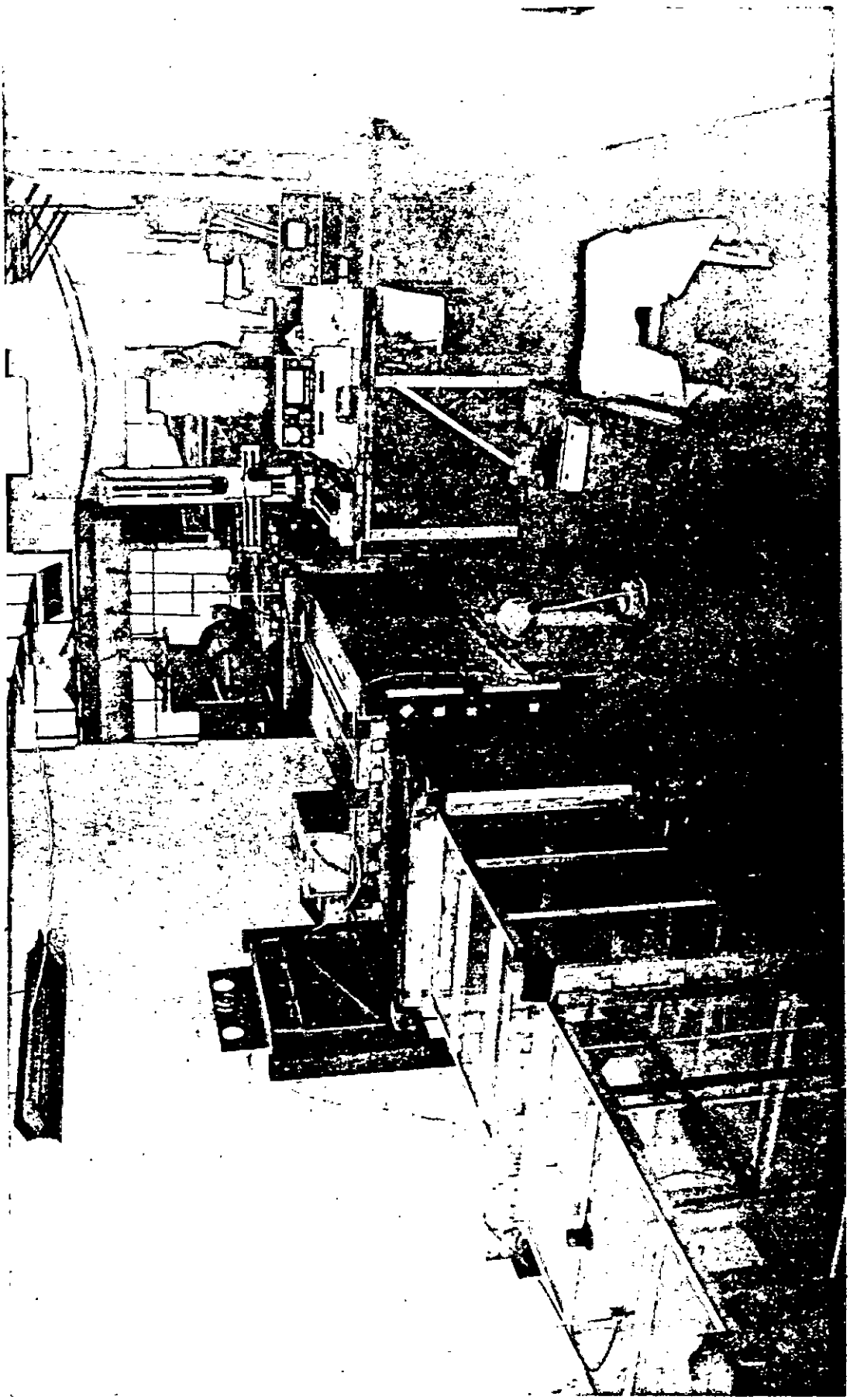

PLATE 4·3 WIND TUNNEL REAR VIEW

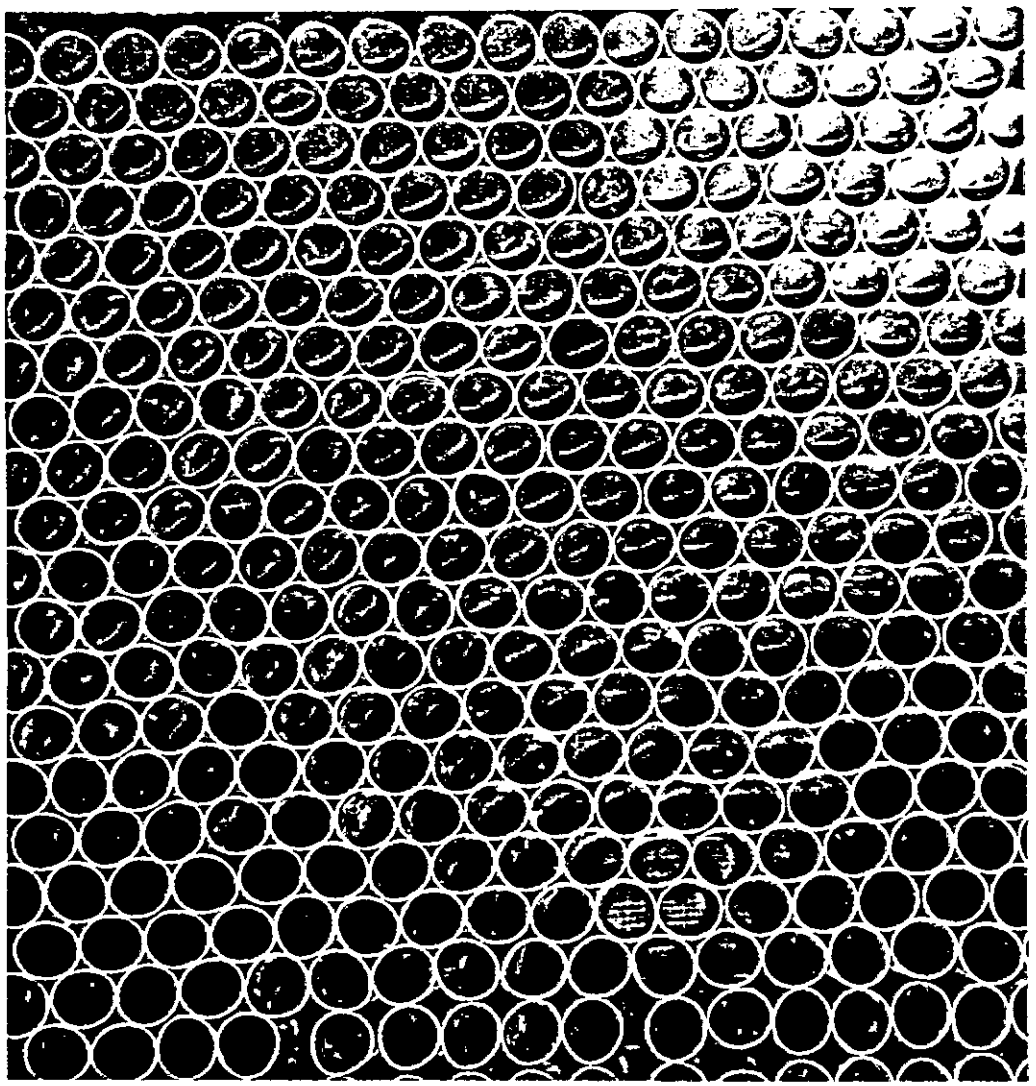

PLATE 4·4 HONEY COMB FLOW STRAIGHTENER

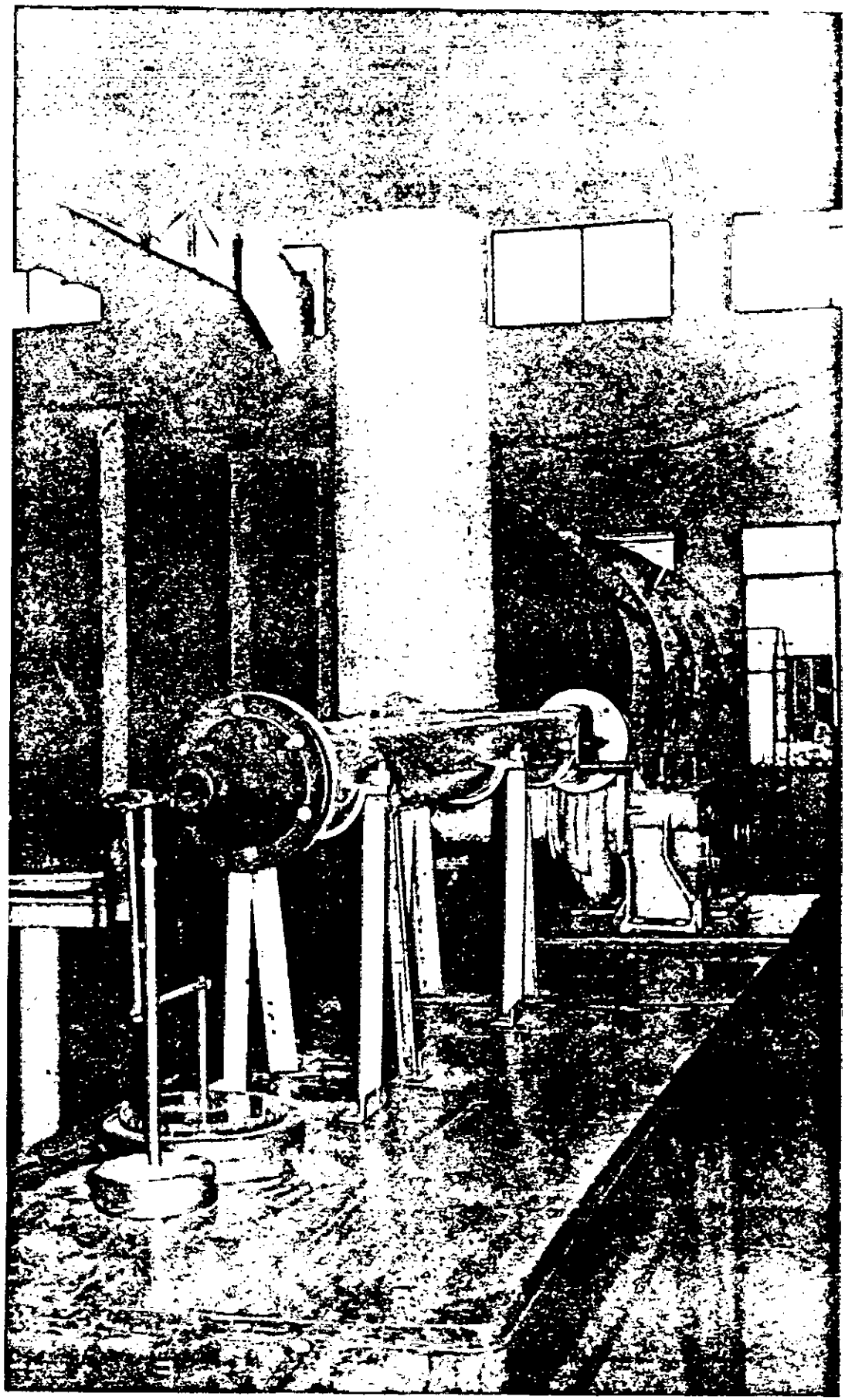

PLATE 4·5 CALIBRATION RIG

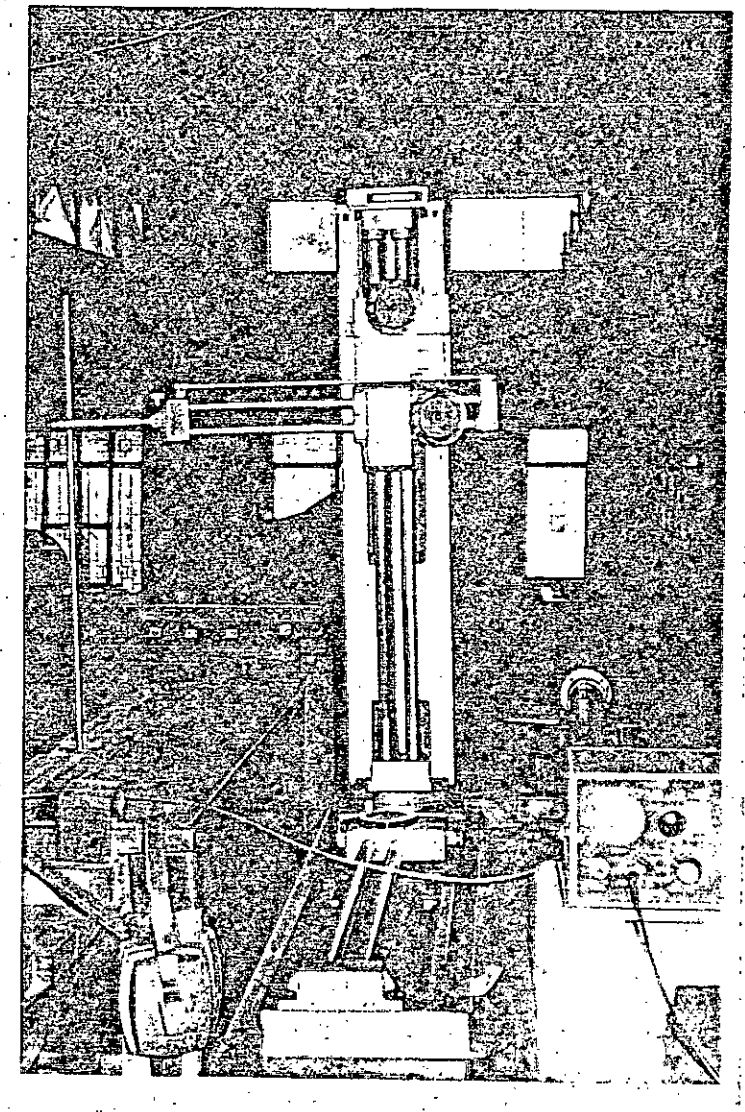

PLATE 4·6 VERTICAL TRAVERSING MECHANISM

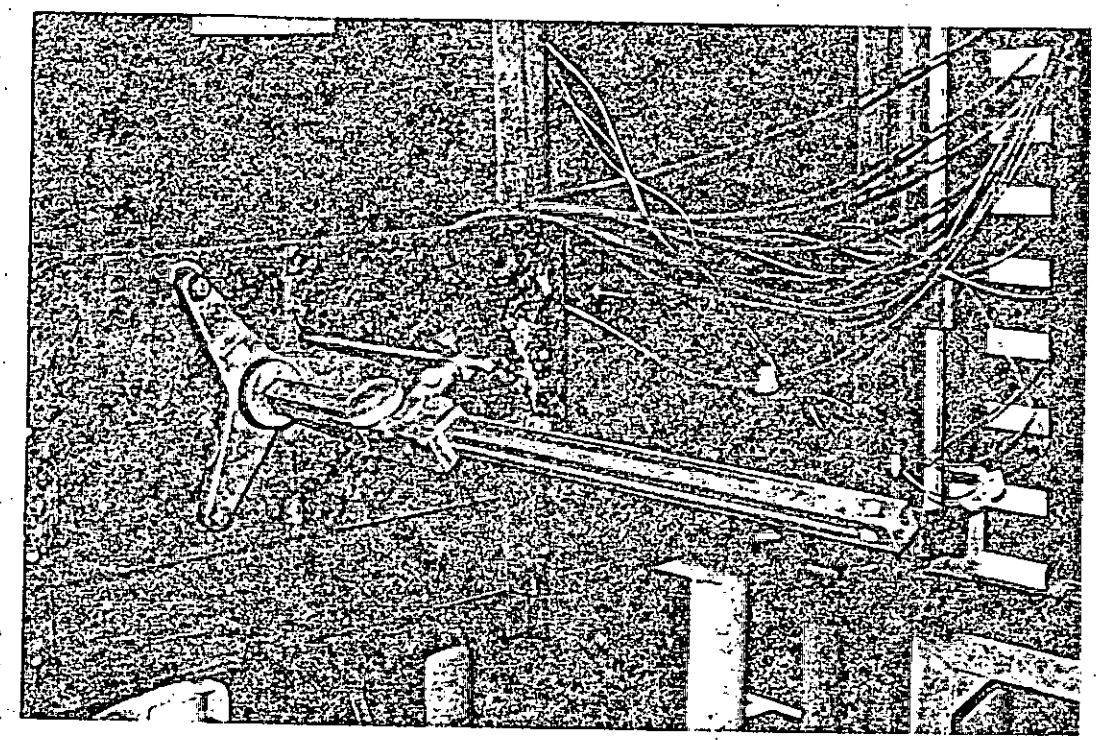

PLATE 4·7 HOIZONTAL TRAVERSING MECHANISM

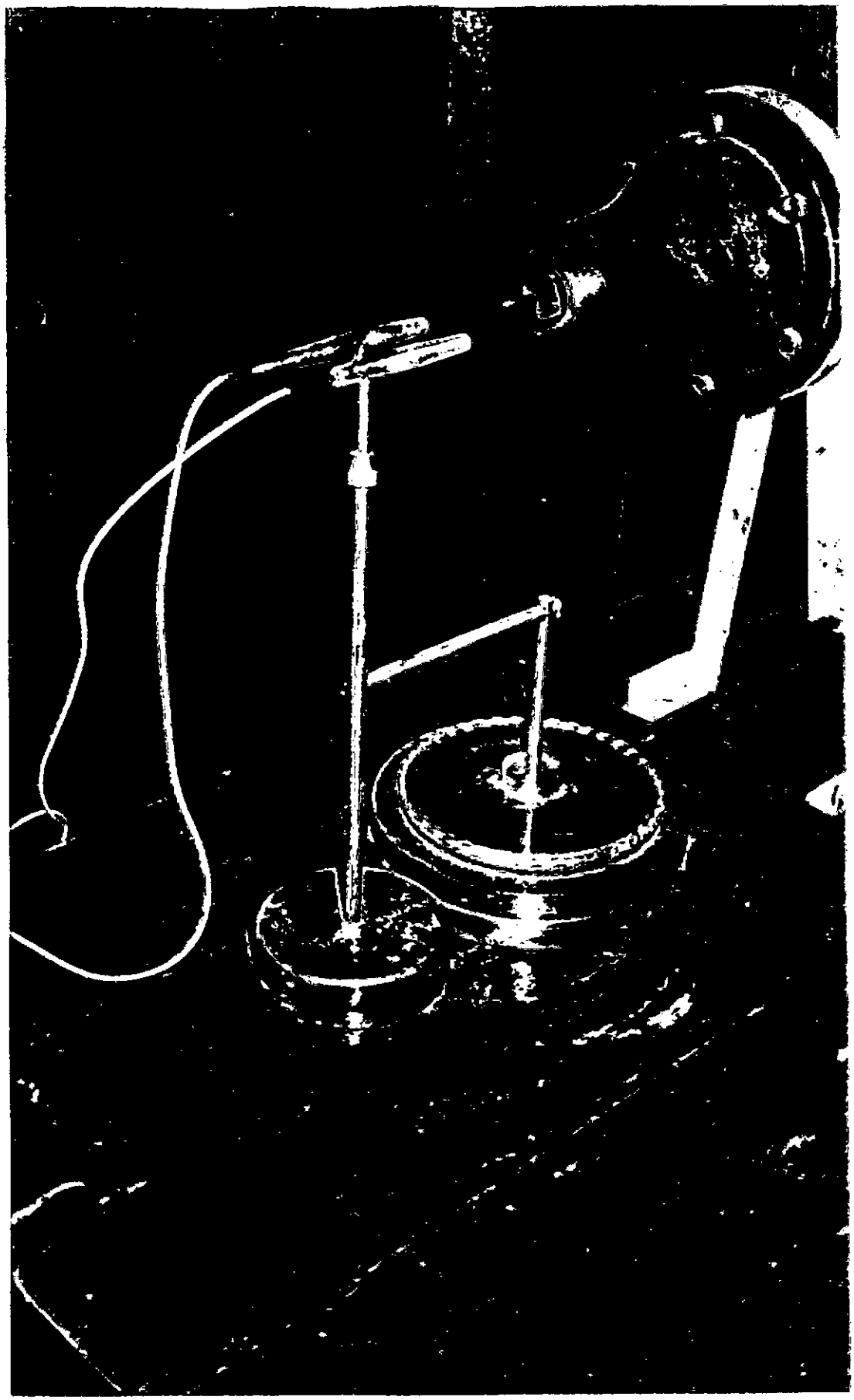

PLATE 4·8 PROBE HOLDERS FOR CALIBRATION

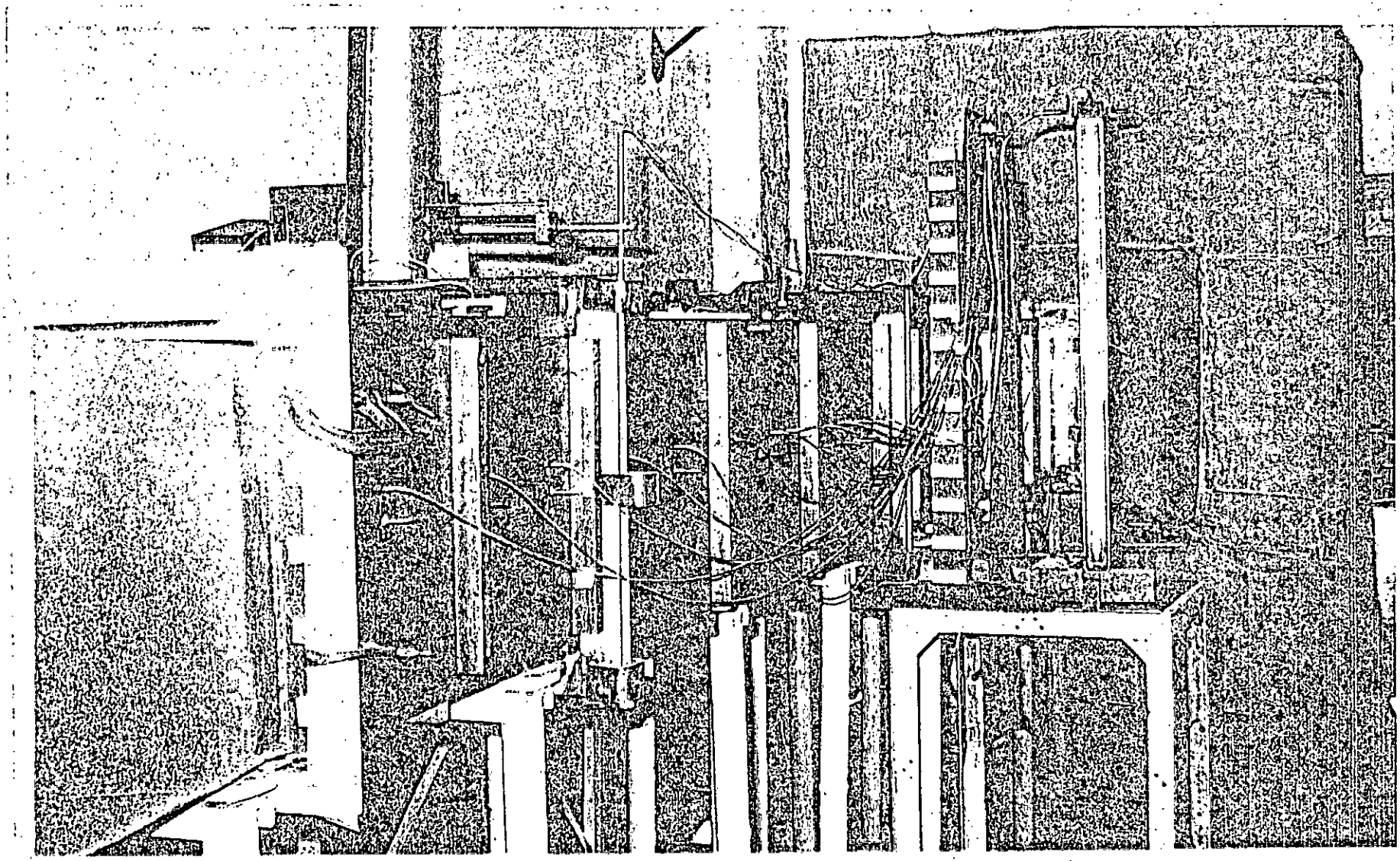

PLTE 4·9 WALL STATIC PRESSURE CONNECTIONS

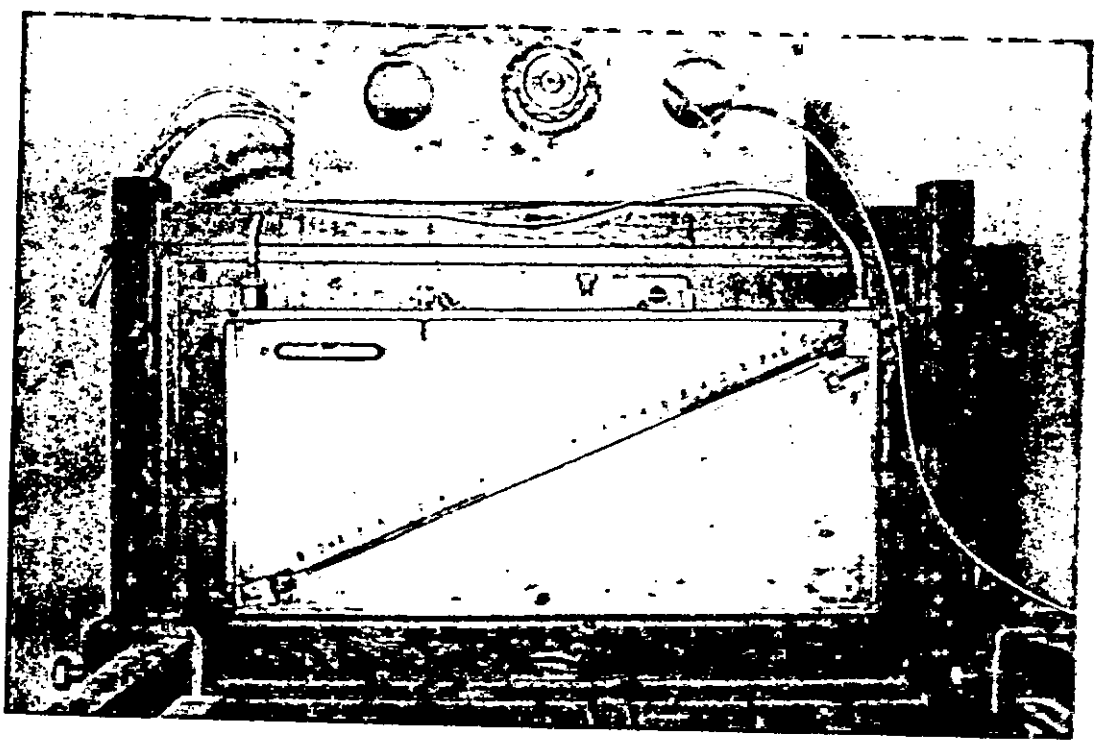

PLATE 4·10 MONITORING GAGE AND SELECTOR VALVE

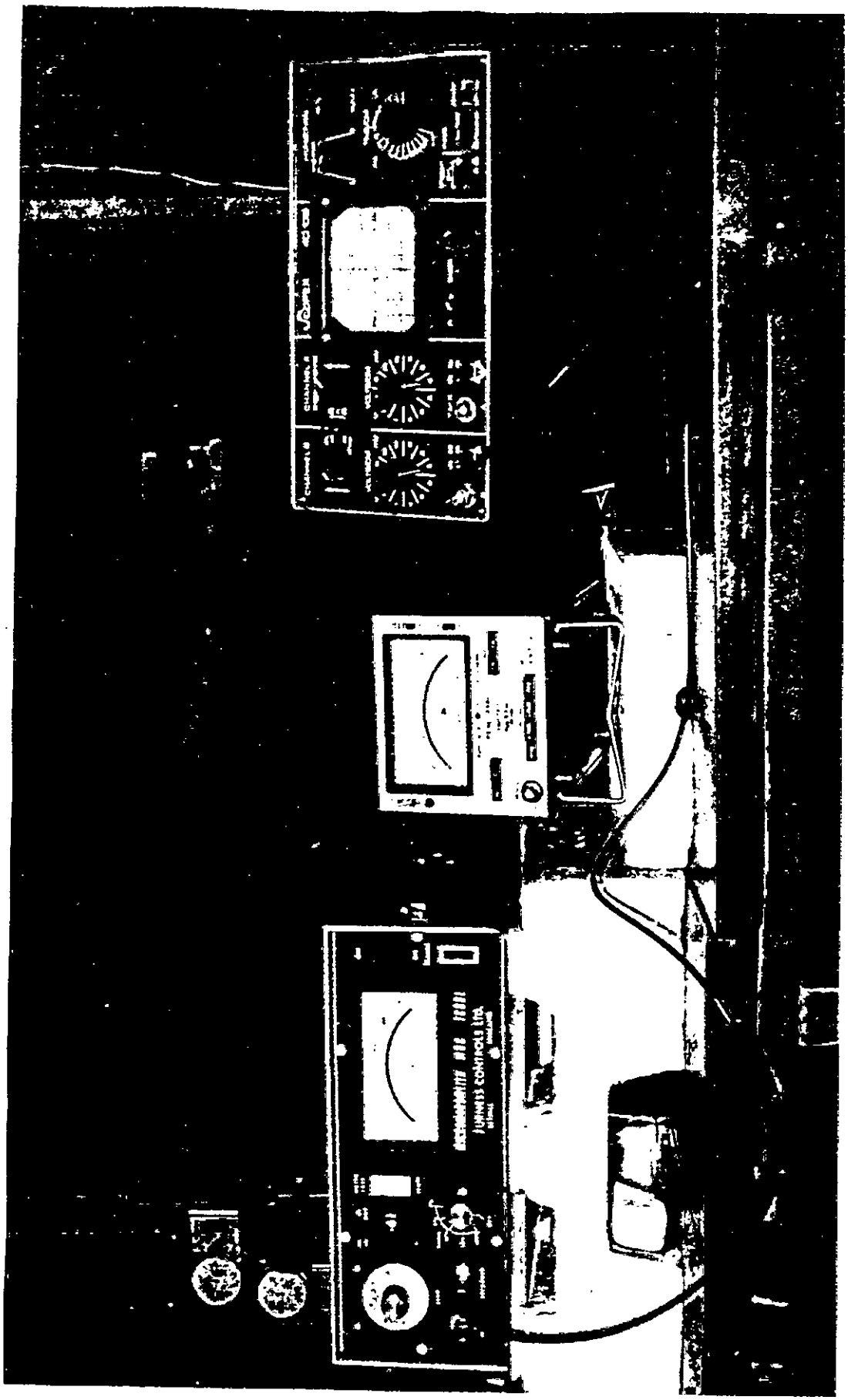

PLATE 4.11 INSTRUMENTATION FOR MEAN QUANTITY MEASUREMENTS

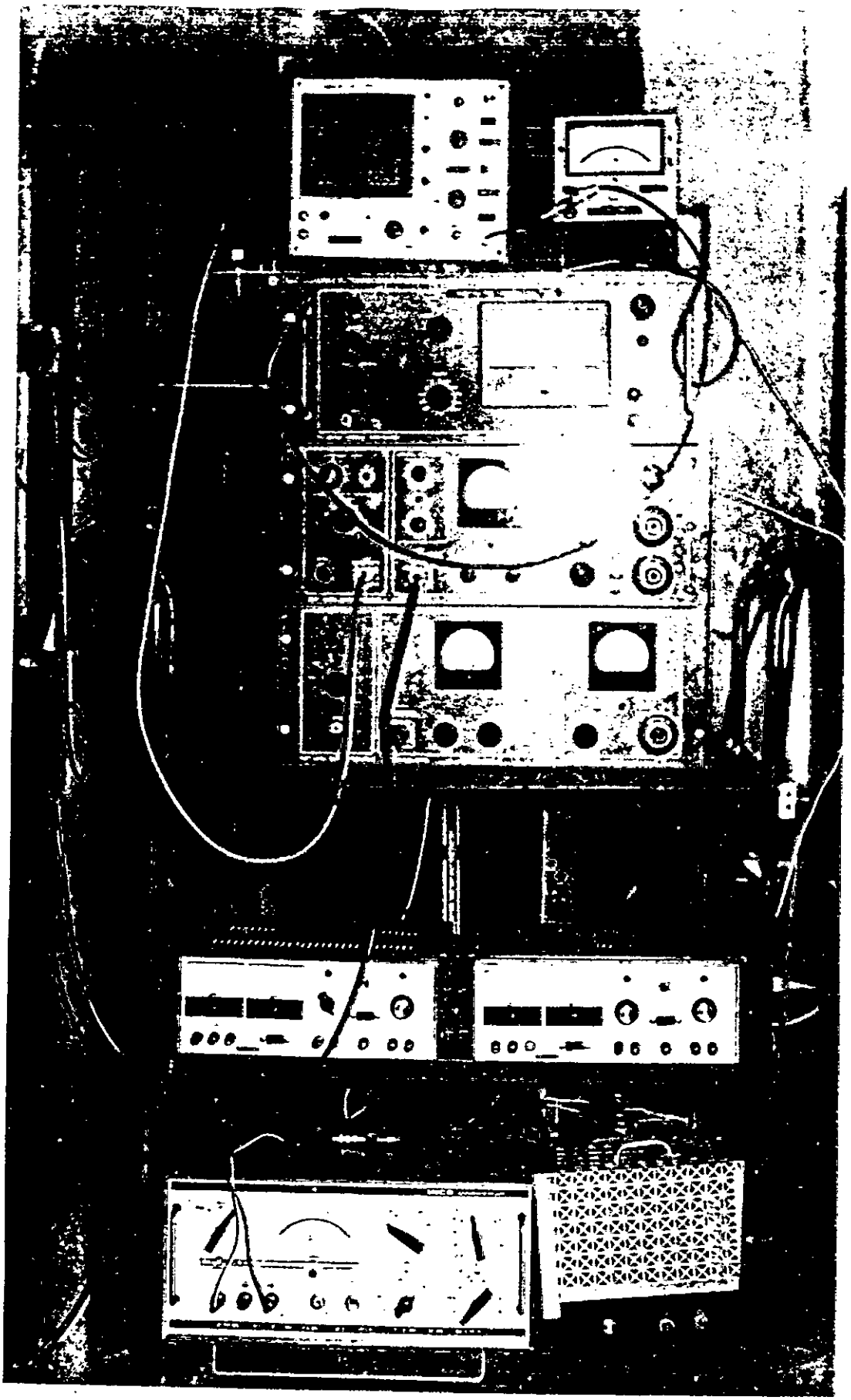

PLATE 4·12 INSTRUMENTATION FOR TURBULENT QUANTITY MEASUREMENTS

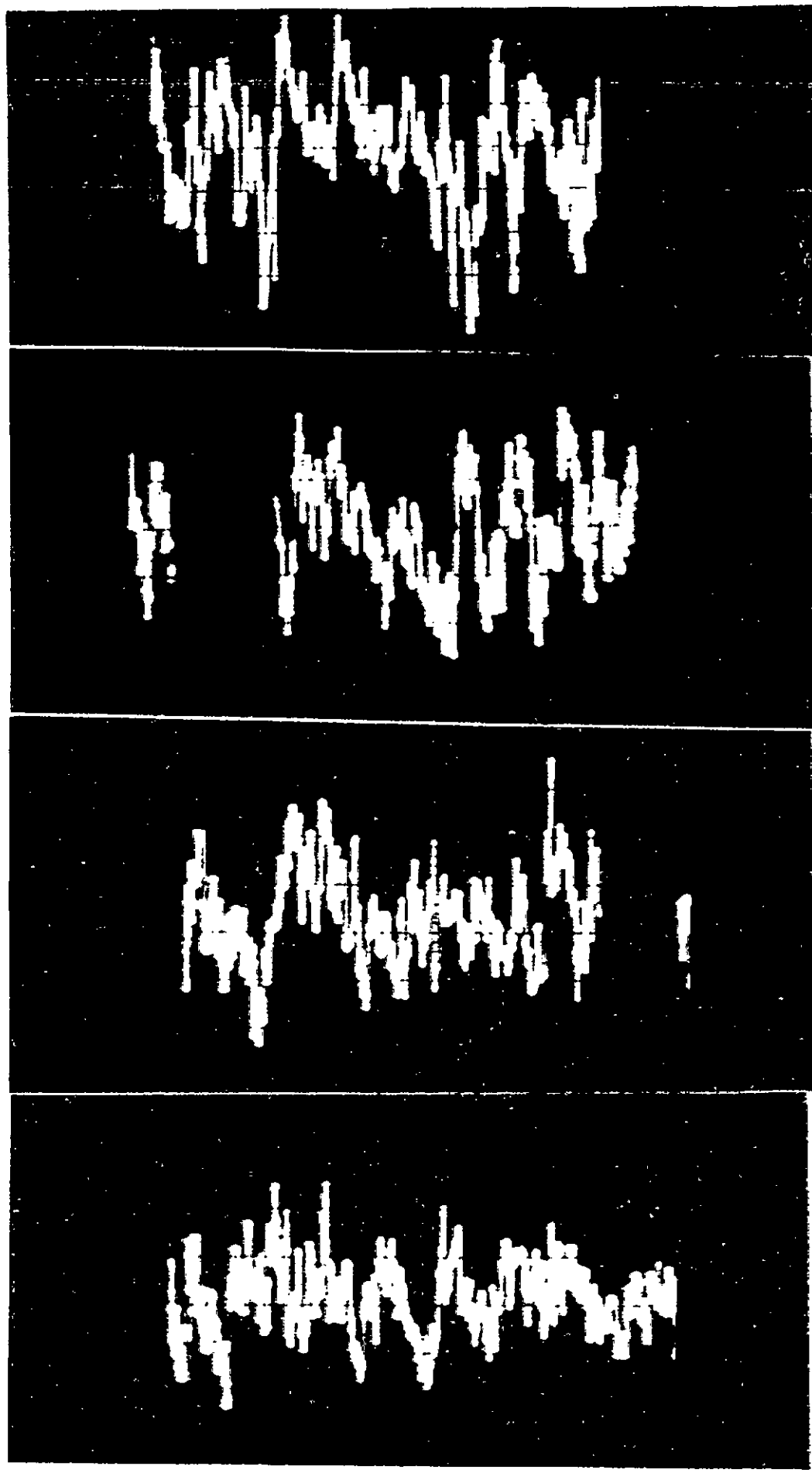

PLATE 5·1 OSCILLOGRAMS OF TURBULENCE INTENSITY

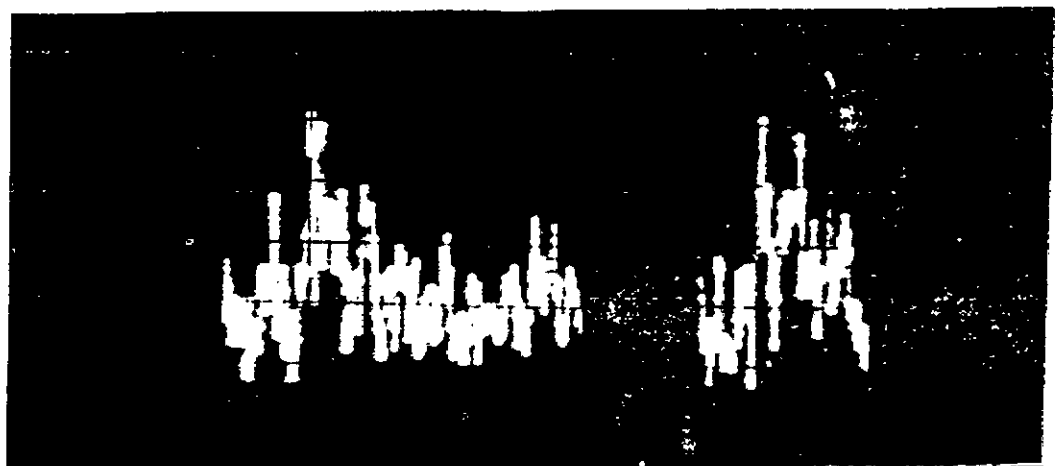

y -0·625=0·7 in

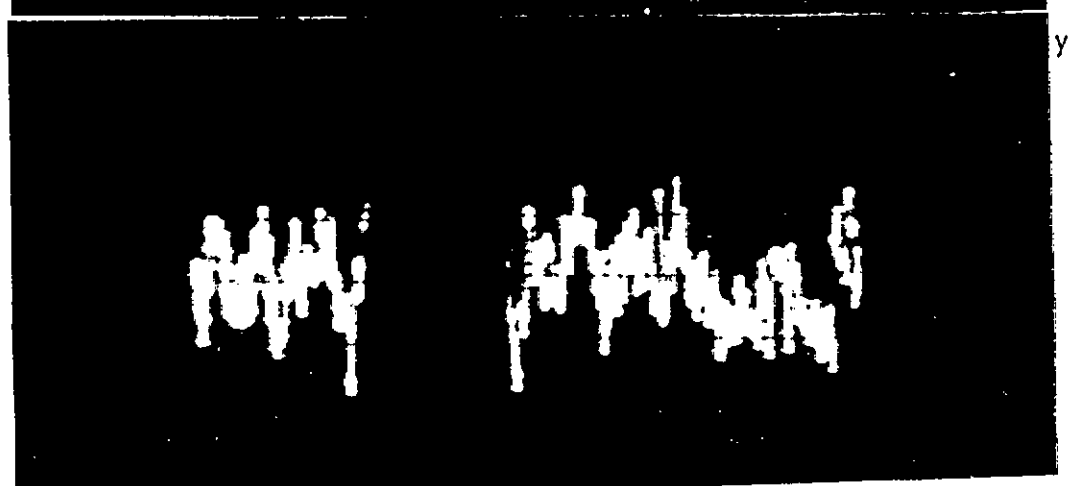

y -0·625=0·5 in

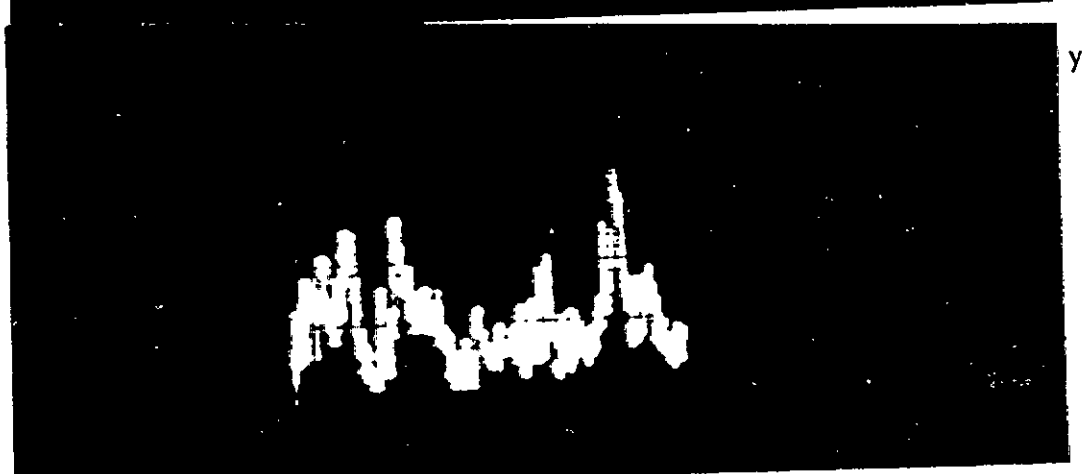

y -0·625=0·75 in

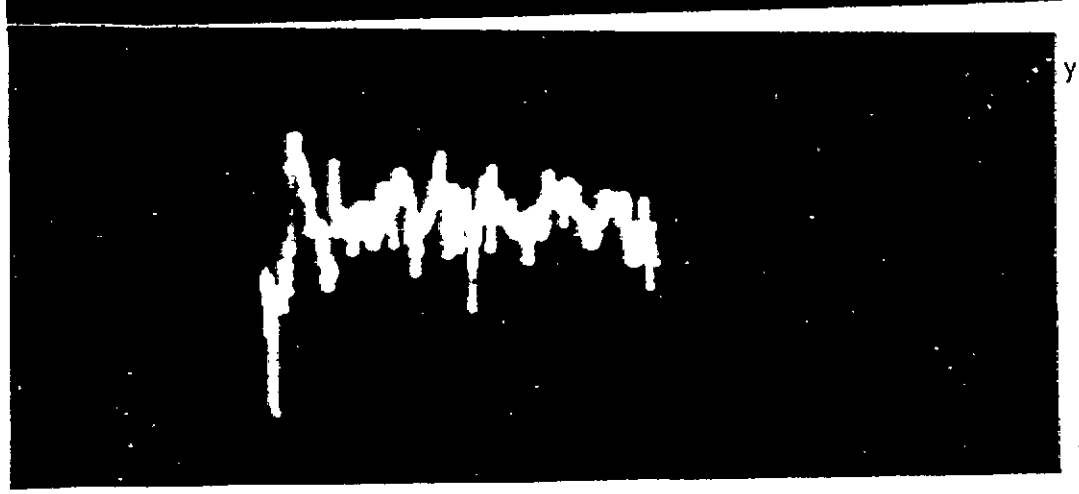

y -0·625=1·0 in

PLATE 5·1 CONTINUED

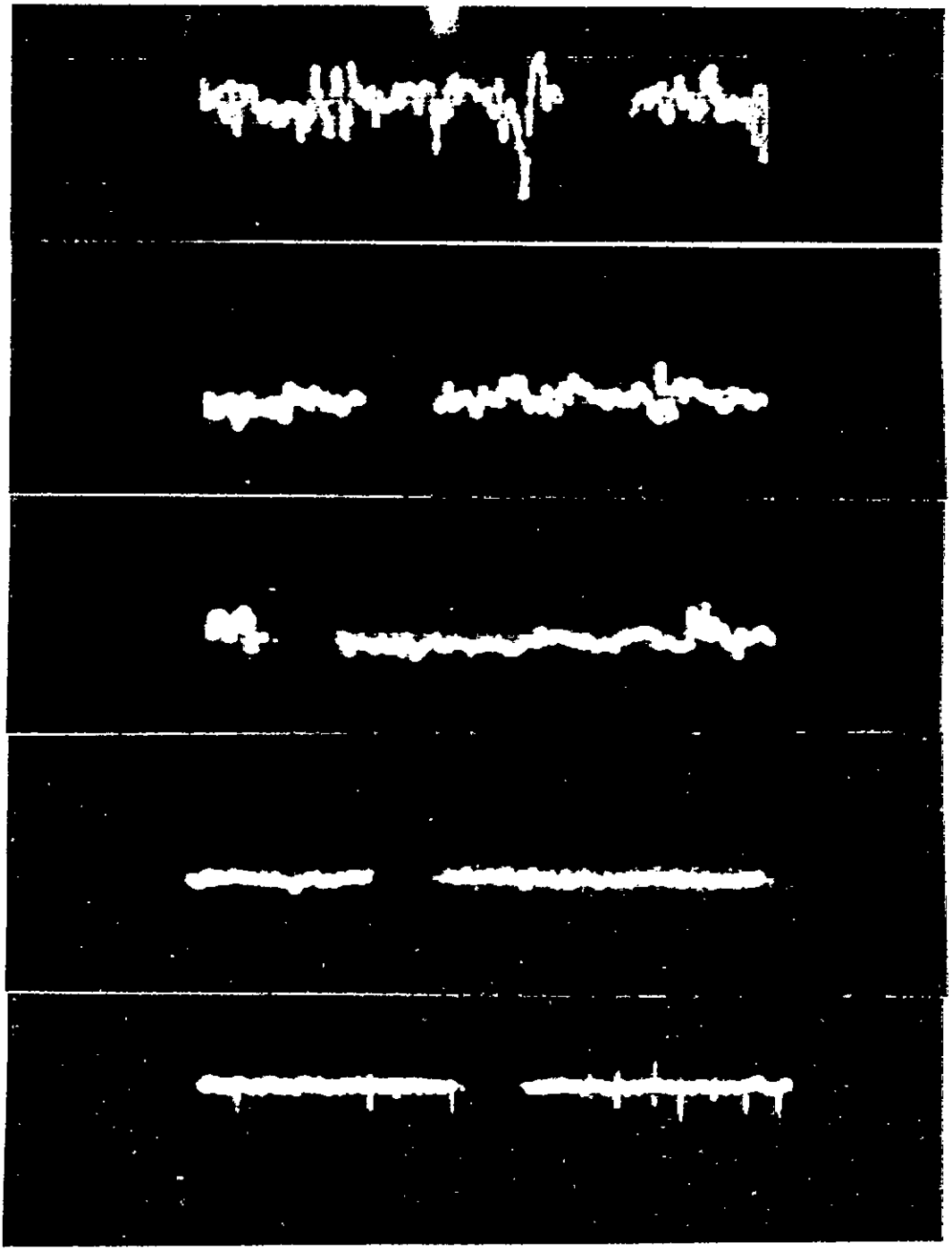

PLATE 5·1 CONTINUED